An analysis of ionospheric response to geomagnetic disturbances over South Africa and Antarctica

A thesis submitted in fulfilment of the
requirements for the degree of

DOCTOR OF PHILOSOPHY

of

RHODES UNIVERSITY

by

CHIGOMEZYO MUDALA NGWIRA

7 December 2011

Abstract

The ionosphere is of practical importance for satellite-based communication and navigation systems due to its variable refractive nature which affects the propagation of trans-ionospheric radio signals. This thesis reports on the first attempt to investigate the mechanisms responsible for the generation of positive ionospheric storm effects over mid-latitude South Africa. The storm response on 15 May 2005 was associated with equatorward neutral winds and the passage of travelling ionospheric disturbances (TIDs). The two TIDs reported in this thesis propagated with average velocities of ∼438 m/s and ∼515 m/s respectively. The velocity of the first TID (i.e. 438 m/s) is consistent with the velocities calculated in other studies for the same storm event. In a second case study, the positive storm enhancement on both 25 and 27 July 2004 lasted for more than 7 hours, and were classified as long-duration positive ionospheric storm effects. It has been suggested that the long-duration positive storm effects could have been caused by large-scale thermospheric wind circulation and enhanced equatorward neutral winds. These processes were in turn most likely to have been driven by enhanced and sustained energy input in the high-latitude ionosphere due to Joule heating and particle energy injection. This is evident by the prolonged high-level geomagnetic activity on both 25 and 27 July.

This thesis also reports on the phase scintillation investigation at the South African Antarctic polar research station during solar minimum conditions. The multi-instrument approach that was used shows that the scintillation events were associated with auroral electron precipitation and that substorms play an essential role in the production of scintillation in the high latitudes. Furthermore, the investigation reveals that external energy injection into the ionosphere is necessary for the development of high-latitude irregularities which produce scintillation.

Finally, this thesis highlights inadequate data resources as one of the major shortcomings to be addressed in order to fully understand and distinguish between the various ionospheric storm drivers over the Southern Africa mid-latitude region. The results presented in this thesis on the ionospheric response during geomagnetic storms provide essential information to direct further investigation aimed at developing this emerging field of study in South Africa.

Acknowledgements

Firstly, I would like to thank my supervisors, Dr. Lee-Anne McKinnell and Dr. Pierre Cilliers, for their invaluable contributions. The successful completion of this work would not have been possible without their guidance and encouragement. To Lee-Anne, a special thanks for providing support and motherly care. I thank Pierre whose vast MatLab knowledge was extensively utilised in this work.

I am grateful to the South African National Space Agency (SANSA) Space Science in Hermanus (formerly the Hermanus Magnetic Observatory) for hosting and supporting me during my studies. I wish to thank Dr. John-Bosco Habarulema and Dr. Ben Opperman for their support, especially during the initial phase of my research. Thank you to the National Astrophysics and Space Science Programme (NASSP) committee for providing the financial support in the form of a NASSP scholarship from 2009 to 2011.

I wish to specially acknowledgement Dr. Endawoke Yizengaw and Dr. Anthea Coster for the fruitful collaboration. My message of gratitude extends to all the people, mostly my student colleagues, who supported this work in one way or another. I acknowledge Elda Saunderson for her assistance in editing this thesis.

I thank my family and friends for their love and support. I would like to express my gratitude to my aunt, Mrs H. N. Abdulla, the “unsung heroine”, who has given me immense support throughout most of my academic journey. A special word of thanks to my wife, Chomba, for her encouragement and support. She has been so patient and understanding in the most difficult circumstances.

And finally, I thank the Lord Almighty for being with me throughout this journey. The grace of the Lord has taken me through many difficult challenges. To God be the glory for this milestone in my academic endeavours.

Chigomezyo Mudala “Makaranga” Ngwira
Hermanus, South Africa
7 December 2011

The world today has become increasingly dependent on the use of radio waves for many purposes, such as satellite communication and navigation. The ionosphere plays an important role in the propagation of radio waves, since its refractive property affects tran-ionospheric radio signals.

The work submitted for this thesis has been published in three papers in international peer-reviewed journals. These papers are:

1. Ngwira C. M., McKinnell L. A., Cilliers P. J. "GPS phase scintillation observed over a high-latitude Antarctic station during solar minimum". Journal of Atmospheric and Solar-Terrestrial Physics, 72(9-10), pp. 718-725, 2010.

2. Ngwira C. M., McKinnell L. A., Cilliers P. J. and Yizengaw E. "An investigation of ionospheric disturbances over South Africa during the magnetic storm on 15 May 2005". Journal of Advances in Space Research, 49, pp. 327-335, 2012.

3. Ngwira C. M., McKinnell L. A., Cilliers P. J. and Coster A. J. "Ionospheric observations during the geomagnetic storm events on 24-27 July 2004: Long-duration positive storm effects". Journal of Geophysical Research, in press, 2011. doi:10.1029/2011JA016990.

Acronyms

ACE	Advanced Composition Explorer
AE	Auroral electrojet
AGW	Atmospheric gravity wave
ASHA	Adjusted spherical harmonic algorithm
CME	Coronal mass ejection
DDM	Diurnal double maximum
DMSP	Defense Meteorological Satellite Program
EEJ	Equatorial electrojet
EIA	Equatorial ionisation anomaly
GLAT	Geographical latitude
GLON	Geographical longitude
GISTM	GPS Ionospheric Scintillation and TEC Monitor
GNSS	Global Navigation Satellite System
GPS	Global Positioning System
HF	High frequency
IEF	Interplanetary electric field
IMF	Interplanetary magnetic field
LSTID	Large-scale TID
LT	Local time
MCM	Master control station
MLAT	Magnetic latitude
MLON	Magnetic longitude
MLT	Magnetic local time
MSTID	Medium-scale TID
NGDC	National Geophysical Data Centre
Riometer	Relative ionospheric opacity meter
SANAE	South African National Antarctic Expedition
SANSA	South African National Space Agency
SED	Storm enhanced density
SSC	Storm sudden commencement
SSI/E	Special sensor for ions and electrons
TAD	Travelling atmospheric disturbance
TEC	Total electron content
TECU	TEC unit
TOI	Tongue of ionisation
TOPEX	TOPographic EXplorer
TID	Travelling ionospheric disturbance
UT	Universal time

Contents

List of Tables

List of Figures

Chapter 1

Introduction

This thesis is concerned with the response of the middle- and high-latitude ionosphere during ionospheric disturbances that result from geomagnetic storm events. Specifically, this thesis presents the first investigation of travelling ionospheric disturbances and long-duration ionospheric storm response over mid-latitude South Africa, and also presents an investigation of ionospheric scintillation at the southern high-latitude region (Antarctic) during the extended solar cycle 23 minimum period.

1.1 Space weather and ionospheric research

The Sun is a medium-sized star and the Earth's primary source of energy. Without this energy, life on Earth would not be sustainable. However, the Earth's space environment is also tremendously influenced by the Sun, which discharges vast amounts of energy in the form of electromagnetic and particle radiation that can adversely impact the integrity and performance of man-made technological systems (see Lanzerotti, 2001; Moldwin, 2008). Therefore, our Sun is the primary source of "space weather", which is an emerging field of Space Science focused on developing our understanding of societal and technological impacts of the solar-terrestrial relationship (Moldwin, 2008).

The term "space weather" typically refers to the conditions on the Sun and in the solar wind, magnetosphere, ionosphere, and thermosphere that can impact the performance and integrity of space-borne and ground-based technological systems, and can endanger human life or health (National Space Weather program strategic plan, 1995. Office of the Federal Coordinator for Meteorological Services and Supporting Research, FCM-P30-1995, Washington, D.C.).

Ionospheric storms represent an extreme form of space weather, which can have significant adverse effects on increasingly sophisticated space- and ground-based technological systems which have become important to governments, corporations, and the general public (see e.g. Buonsanto, 1999; Boteler, 2001; Goodman, 2005). These effects include among others: damage to satellites due to high energy particles (e.g. Fuller-Rowell *et al.*, 1994), damage to electric power transformers caused by geomagnetically induced currents (e.g. Boteler, 2001; Pirjola, 2005; Gaunt and Coetzee, 2007), increased atmospheric drag on satellites, degradation of the accuracy of Global Navigation Satellite System (GNSS) applications, high frequency (HF) communication black-outs (e.g. Goodman, 2005; Warnant *et al.*, 2007), and increased danger of radiation exposure to humans in space and in high-altitude aircrafts (e.g. Prölss *et al.*, 1991; Prölss, 1997). Severe ionospheric disturbances are also known to cause disruption of UHF satellite links and are a serious concern for satellite navigation and communication systems, and HF radio communication (Doherty *et al.*, 2000; De Paula *et al.*, 2004; Kintner and Ledvina, 2005). These effects are due to ionospheric electron density irregularities, which occur as a result of plasma density instabilities, including ionospheric scintillation and plasma bubbles (Kelley, 1989; Aarons *et al.*, 1995; Kintner *et al.*, 2007). In addition to the space weather effects mentioned above, the economic losses associated with some severe geomagnetic storms are extensive (Boteler, 2001; Yizengaw *et al.*, 2005a).

The world today has become increasingly dependent on the use of radio waves for many purposes such as HF communication, navigation and land surveying. The ionosphere, which is the ionised region of the Earth's upper atmosphere, plays an important role in the propagation of these radio waves. The ionosphere is of practical importance for satellite based communications and navigation systems because its variable refractivity affects the propagation of trans-ionospheric radio signals, effects which increase during geomagnetic storm events. Many international efforts aimed at monitoring and predicting space weather effects are on-going as a step to reduce the risk of economic losses. Nevertheless, our ability to predict ionospheric storm effects in great detail is limited by our incomplete earth-space system knowledge (see Buonsanto, 1999; Yizengaw *et al.*, 2005a; Burns *et al.*, 2007). This is one of the motivations for carrying out the research presented in this thesis, which is aimed at furthering our understanding of the ionospheric response during geomagnetic disturbances, particularly at mid- and high-latitude locations.

1.2 Motivation for this study

The characteristics of the mid-latitude ionosphere are generally regular, however, during large geomagnetic disturbances this predictable variability can be dramatically overturned as the forces which drive the high-latitude region expand equatorward (see reviews by Buonsanto, 1999; Mendillo, 2006). Currently there are still some major challenges facing the ionospheric community: understanding the development of geomagnetic storms and the impact that storms have on ionospheric behaviour, development and evolution of ionospheric irregularities, development of methods for ionospheric predictions, and other challenges (e.g. Goodman, 2005; Yizengaw *et al.*, 2005a).

Initially, the major goal of this research was to investigate ionospheric irregularities over the Southern Africa mid-latitude region, since very little is known about irregularities in this region. Irregularities have generally been assumed to occur less often in mid-latitude regions (Ledvina and Kintner, 2004; Kintner *et al.*, 2007, and references therein). Studies have shown that the mid-latitude is more complicated than initially thought, and that many different scales of structuring are possible, especially during geomagnetic storms (Fuller-Rowell *et al.*, 1994; Buonsanto, 1999; Ledvina *et al.*, 2002; Mendillo, 2006). However, due to unforeseen problems encountered during the preliminary investigation, the intended primary data recorded on two (out of three) of the instruments could not be used, as will be discussed later. This prompted a modification of the original research focus to include the ionospheric response over the Southern Africa mid-latitude region during geomagnetic storm events. Nevertheless, successful ionospheric scintillation studies were performed for a high-latitude Antarctic station and these results are presented in Chapter 7 of this thesis.

Even more than 80 years after discovery, ionospheric storms are still a fascinating and challenging topic of upper atmospheric physics since many aspects of this striking phenomenon are still not well understood (Prölss, 1995; Burns *et al.*, 2007; Pedatella *et al.*, 2009). This is especially true for long-duration positive ionospheric storms, which are tabled as one of the major unresolved problems of ionospheric storms in reviews by Prölss (1997) and Buonsanto (1999), and even more recently by Burns *et al.* (2007). Furthermore, this thesis presents ionospheric scintillation measurements observed at the South African Antarctic polar research station during solar minimum conditions. In addition, this work also highlights some of the major challenges that need to be addressed in order to fully understand the ionospheric storm drivers over this region. Therefore, the results presented in this thesis on the ionospheric response during geomagnetic storms and ionospheric scintillation at high latitudes will provide essential information needed to direct further investigations aimed at developing these emerging fields of study in South Africa.

1.3 Structure of the thesis

Chapter 2 reviews some of the theories relating to the physical processes that control the ionosphere. A significant amount of this material is focused on those processes that are fundamental for the research presented in this thesis.

The focus of Chapter 3 is on the instrumentation and sources from which data used in this thesis were derived. This chapter deals with a variety of measurements and modelling techniques employed in the data analysis.

A discussion of some of the phenomena associated with the disturbed solar-terrestrial environment is presented in Chapter 4. This chapter also discusses ionospheric irregularity phenomena in general.

In Chapters 5 and 6 the details of the investigations on ionospheric response during geomagnetic storms are presented, and the possible primary driving mechanisms are discussed. These chapters (5 and 6) deal with two kinds of ionospheric responses, i.e., short-duration and long-duration positive ionospheric storm effects, respectively.

The investigation on ionospheric scintillation observed over a high-latitude Antarctic station during solar minimum is presented in Chapter 7. Some of the challenges encountered during the initial investigation are also discussed.

Chapter 8 concludes this thesis with a summary of the major findings and conclusions drawn from the investigations.

Chapter 2

The ionosphere

2.1 Introduction

This chapter considers some of the theories that explain the physical processes that control the ionosphere. The emphasis here is on the basic processes that are fundamental to understanding the work presented in this thesis. A major reference for the work presented in the first two sections is the book published by Rishbeth and Garriott (1969).

2.1.1 A brief history of the ionosphere

The ionosphere is the ionised gas region extending from about 60-1000 km above the Earth's neutral atmosphere. The ionosphere plays an important role in the propagation of electromagnetic signals such as radio waves (Rishbeth and Garriott, 1969; White, 1970; Kelley, 1989). The discovery of the ionosphere in 1901 followed Marconi's successful transmission of wireless radio signal across the Atlantic between Poldhu in Cornwall, UK and St John's in Newfoundland, Canada. Marconi's accomplishing experiment meant that radio waves were deflected around the Earth's surface, to a much larger extent than could be explained by the diffraction theory (Rishbeth and Garriott, 1969). The first suggestion of a conducting layer in the upper atmosphere to explain small daily variations in the Earth's magnetic field dates back to the nineteenth century. In 1902, A. E. Kennelly and O. Heaviside independently suggested that a layer of free electrons in the upper atmosphere could reflect radio waves to great distances. Their names (*Kennelly-*

Heaviside) have been associated with the ionised layer since then (Rishbeth and Garriott, 1969; White, 1970, and references therein).

In 1903 J. E. Taylor first pointed out solar ultra-violet radiation as the primary source of the ions and electrons. This was later confirmed by J. A. Fleming in 1906. The first pioneering evidence of the existence of a conducting layer followed the experimental work by Appleton and Barnett published in 1925, that not only demonstrated the downward passage of reflected waves, but also gave an estimate of the angle of arrival of the waves (Rishbeth and Garriott, 1969; White, 1970, and references therein). The work by Appleton and Barnet was subsequently confirmed by Breit and Tuve in 1926, using a different method, which involved amplitude modulation of the carrier frequency (Rishbeth and Garriott, 1969). Since then, ionospheric radio sounding techniques have widely been employed as a primary tool for taking measurements for the purpose of studying the ionosphere.

2.2 Photochemical processes in the ionosphere

It is widely accepted that the absorption of solar extreme ultra-violet (EUV) and X-ray radiation are the primary production mechanisms for the creation of ions and electrons at the low and mid-latitudes (e.g. Rishbeth and Garriott, 1969; White, 1970; Kelley, 1989; Davies, 1990; Maruyama, 2001). By contrast, at high latitudes and during magnetic storms, collisions between energetic charged particles precipitated into the atmosphere and the neutral molecules are responsible for the production of ions and electrons. On the other hand, the different loss mechanisms in the ionosphere can be grouped as ion and electron (radiative) recombination; molecular ion and electron (dissociative) recombination; and the attachment of electrons to neutral molecules in the lower ionosphere (e.g. Rishbeth and Garriott, 1969).

The physical processes which control the ionosphere can effectively be classed down into two general categories: those that give rise to production or loss of ionisation, and those that lead to the movement of ionisation (e.g. Rishbeth and Garriott, 1969; Maruyama, 2001). The terms “photochemical” and “transport” have often been used as convenient labels to describe the two categories, but are not necessarily the ideal terms. The various processes which can potentially change the electron density concentration (N_e) can be summarised in terms of the continuity equation as

[Change in density] = [Gain by production] − [loss] − [change due to transport]

The continuity equation expresses the net effect of either the positive or negative ions, or, any constituent elements whose concentration is subject to change. If the transport processes result in a net drift velocity $\mathbf{V}$, then the changes due to transport can be defined in terms of the divergence of the flux $N_e\mathbf{V}$. The term $N_e\mathbf{V}$ represents the flux of electrons (or ions) resulting from transport, and its divergence reflects the rate of loss per unit volume and unit time. Therefore, the continuity equation for the electron density expressed as a function of time t using symbols is:

$$\frac{\partial N_e}{\partial t} = q - l(N_e) - \mathsf{div}(N_e\mathbf{V}), \tag{2.1}$$

where q and l represent the production and loss rates, respectively, the values of which are primarily determined by the solar ionising radiation and the ion recombination reactions. Equation (2.1) effectively describes the increase and decrease of electrons entering and exiting the boundary surrounding a unit volume space, and the quantity of electrons produced and lost within that space (Maruyama, 2001).

Since transport processes are not very important in the ionosphere below 200 km, they can be neglected entirely (Rishbeth and Garriott, 1969). Thus, a photochemical equation containing only the derivative term $\partial N_e/\partial t$ remains. Furthermore, the "time constant" associated with the loss term $l(N_e)$ can be so short that $\partial N_e/\partial t$ becomes much smaller than the other terms, so that the photochemical equilibrium equation $q = l(N_e)$ is sufficient (Rishbeth and Garriott, 1969). By contrast, above about 250 km, the continuity equation (2.1) is no longer dominated by the "photochemical" terms q and l. This leads to a "transport regime" at these heights. Therefore, the transport term compensates for the large imbalance between production and loss, and becomes more important (Rishbeth, 1986). It should be noted that although quite rapid horizontal motions may exist, generally they do not contribute significantly to the term $N_e\mathbf{V}$, given that the horizontal gradients of N_e and $\mathbf{V}$ are normally much smaller in comparison to the vertical gradients. Horizontal variations usually occur at distance scales of hundreds or thousands of kilometres, while vertical scales are only tens of kilometres (Rishbeth and Garriott, 1969). However, exceptions to this norm may develop either when horizontal gradients are specifically large (such as close to sunrise) or when there are special conditions to restrain the significance of vertical motions (for example in the equatorial ionosphere).

2.2.1 Photoionisation theory

The photoionisation theory takes into account the attenuation of solar radiation as it propagates through the atmosphere. Here, the production of ionisation in a horizontally stratified region by a monochromatic beam of solar ionising radiation is considered such that the photon flux is $I(h)$. A general formula for the ionisation rate, q, as a function of height h and the solar zenith angle χ can thus be derived.

If σ is the cross section for the absorption in a gas, and η is the ionising efficiency (i.e. the number of photoelectrons produced per photon absorbed), then the probability per unit time that a photon is absorbed by a given molecule is $I\sigma$, and the probability per unit time for the production of an ion pair is therefore $\eta I\sigma$. Hence, the essential equation for the rate of production per unit volume can be given as

$$q = I\eta\sigma n \tag{2.2}$$

where n is the gas concentration.
The decrease of radiation along the path relies on the absorption coefficient per unit length, σn. If ds is an element along the radiation path, an increment of optical depth τ can be defined by the equation

$$-dI/I = d\tau = \sigma n \, ds \tag{2.3}$$

with the intensity varying as

$$I = I_\infty e^{-\tau} \tag{2.4}$$

where I_∞ is the unattenuated flux at the top of the atmosphere. According to equations (2.2) and (2.3), $q = -\eta\, dI/ds$, which implies that the rate of production is proportional to the rate of attenuation of the radiation.

The altitude variation along the path of the radiation can be described using geometry as $ds = -dh \sec\chi$. Then equation (2.3) can be expressed in terms of ds as

$$-d(\ln I)/dh = d\tau/dh = -\sigma n \sec\chi \tag{2.5}$$

for a horizontally stratified atmosphere. Since $\sec\chi$ does not vary along the path for a plane Earth, then the intergrated content of a column of gas, of unit cross section, above any height h is $n(h)H(h)$. Therefore, integrating equation (2.5) yields

$$\tau(h,\chi) = \int_h^\infty \sigma n \sec\chi\, dh = \sigma n(h)H(h) \sec\chi \tag{2.6}$$

here $n(h)H(h)$ is the integrated content of a column of gas per unit cross section above any height h, where H is the scale height. Combining equations (2.2), (2.4) and (2.6) leads to the expression

$$q(h,\chi) = I_\infty \eta\sigma n(h) e^{-\tau(h,\chi)} \tag{2.7}$$

By integrating equation (2.7) with respect to τ from the top of the atmosphere ($\tau = 0$) to the bottom ($\tau \to \infty$), the integrated production rate per unit column, Q, can easily be obtained. So using equation (2.5), we have

$$Q = \int_0^\infty q\, dh = \int_\infty^0 q \frac{dh}{d\tau}\, d\tau = \frac{I_\infty \eta\sigma n}{\sigma n \sec\chi} \int_0^\infty e^{-\tau}\, d\tau = I_\infty \eta \cos\chi \tag{2.8}$$

The peak production rate q can be located by simply taking the logarithms in equation (2.7) and setting $d(\ln q)/dh = 0$. Given that $I_\infty\eta\sigma$ is a constant, it follows from equation (2.5) that the peak occurs where

$$\frac{1}{n}\frac{dn}{dh} = \frac{d\tau}{dh} = -\sigma n \sec\chi \tag{2.9}$$

This indicates that q is highest at the point where the downward increase of the gas concentration n just offsets the increasing attenuation of the radiation, as measured by τ.

The production function in equation (2.7) can be written in terms of the "reduced height" $z = \int (dh/H) = (h - h_0)/H$, where the reference height h_0, from which z is measured, is the level of unit optical depth ($\tau = 1 = \sigma n_0 H_0$) when the Sun is overhead. At this level, vertically incident radiation will be attenuated to a fraction e^{-1} of the initial intensity. Furthermore, this level relies on the absorption cross section $\sigma_i(\lambda)$ for the different atmospheric gasses, and at any given wavelength is determined by the condition

$$\sum_i \sigma_i(\lambda)\, n_i H_i = 1 \tag{2.10}$$

Therefore we have

$$q(z,\chi) = \frac{\eta I_\infty}{eH(z)} \exp[1 - z - e^{-z} \sec\chi] \tag{2.11}$$

where $\tau = e^{-z} \sec\chi = (p/p_o) \sec\chi$, $e^{-z} = p/p_0 = nH/n_0H_0$ and $p = nkT$ (p is the pressure according to the perfect gas law), assuming that $H \propto T$.

2.2.2 The Chapman production function

In order to get the classical Chapman formula for the production function, it has to be assumed that the scale height H is independent of height (Rishbeth and Garriott, 1969). In this case the level of unit optical depth coincides with the production peak, so that z takes the form

$$z_m = \ln \sec\chi \tag{2.12}$$

with subscript 'm' indicating quantities evaluated at the "peak" or "maximum". Thus the peak production rate is

$$q_m = q_0 \cos\chi \tag{2.13}$$

where the peak rate (q_0) for an overhead Sun is expressed as

$$q_0 = \eta I_\infty / eH \tag{2.14}$$

Note that changing the intensity of the solar flux alters the peak value q, but essentially does not affect the height of peak production (e.g. Davies, 1990). Then the production function can be defined by

$$q(z,\chi) = q_0 \exp\left[1 - z - e^{-z} \sec\chi\right] \tag{2.15}$$

$$q(z,\chi) = q_m \exp\left[1 - (z - z_m) - e^{z_m - z}\right] \tag{2.16}$$

The two sets of equations (2.15) and (2.16) show that the production function keeps the same shape as χ changes, but its amplitude is scaled by a factor $\cos\chi$ and its peak is shifted to $z = z_m$, as illustrated in Figure 2.1.

However, if H is now taken to be height dependent with a constant gradient Γ, but still consider g (acceleration due to gravity) to be constant, this leads to

$$H(h) = H_0 + \Gamma(h - h_0) \tag{2.17}$$

$$H/H_0 = T/T_0 = e^{\Gamma z} \tag{2.18}$$

The gas concentration then varies according to the equation

$$n/n_0 = e^{-z(1+\Gamma)} \tag{2.19}$$

Considering the formulae for the production function $q(z)$, given in equations (2.15) and (2.16), the "photochemical equilibrium" electron density distribution, which is the solution of the continuity equation with the transport term neglected and $\partial n/\partial t = 0$, can then be formulated. Assuming the electrons to be lost at a rate αn^2, where α is the mean dissociative recombination coefficient (Rishbeth and Garriott, 1969; Davies, 1990), then the electron density distribution conforming to the production formula in equation (2.15) is

$$N(z) = (q_0/\alpha)^{1/2} \exp\frac{1}{2}(1 - z - e^{-z} \sec\chi) \tag{2.20}$$

This distribution is referred to as the "alpha-Chapman" or simply "Chapman" layer.

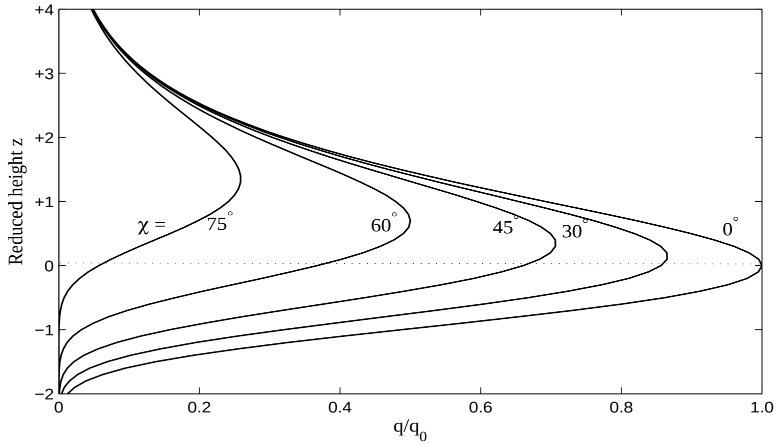

(a)

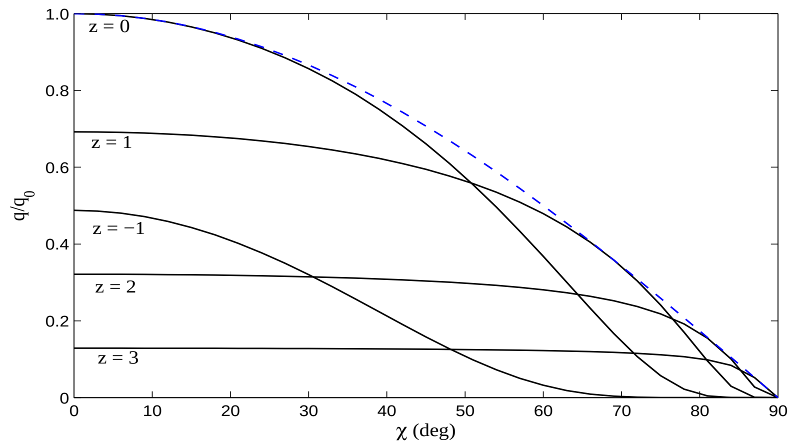

(b)

Figure 2.1: (a) The normalised Chapman production function plotted against the reduced height z, at a given solar zenith angle χ. (b) Normalised Chapman production function plotted against solar zenith angle χ, for different values of reduced height z. Both plots are according to equation (2.15). The dashed line is the envelope defined by $q_1/q_0 = \cos\chi$.

It should be noted that in the ideal atmosphere the production function $q(h, \chi)$ is more complex than has been assumed here because the fundamental assumptions (monochromatic radiation and a single ionisable gas) do not hold (Rishbeth and Garriott, 1969). Therefore, one has to consider the variation of η_i and σ_i with ultra-violet wavelength λ_i.

2.3 Stratification in the ionosphere

In order to understand the formation of the ionosphere, one must first understand how the plasma production and loss processes vary with altitude within the ionosphere (Maruyama, 2001). Photons of differing energies are able to penetrate and interact with atoms and molecules in the Earth's atmosphere. The penetration can be specified in terms of the level of unit optical depth, h_0, at which vertically incident radiation is attenuated to a fraction e^{-1} of its intensity above the atmosphere, as highlighted earlier. Densities of atmospheric constituents (e.g. molecular nitrogen and hydrogen) also vary with height, and therefore the ionosphere forms a number of different regions at various altitudes above the surface of the Earth (Rishbeth and Garriott, 1969; Davies, 1990), as depicted in Figure 2.2. Each region is characterised by a local maximum in the number density of ions.

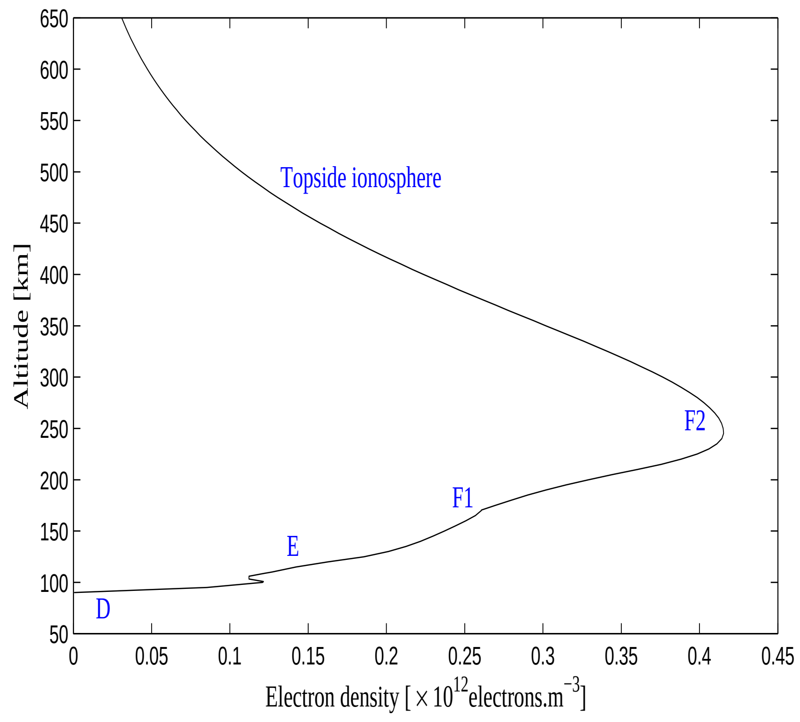

Figure 2.2: A typical ionospheric electron density versus height profile as derived from ionosonde data. The various ionospheric regions are labelled on the figure. The bottom side profile is obtained from measured ionogram data and the topside profile is obtained by fitting a Chapman model to the peak electron density value.

2.3.1 D-region

The D-region is the lowest layer in the ionosphere that extends from approximately 60 to 90 km. The major source of ionisation in the D-region is solar UV photons ionising nitric oxide (NO) molecules. Solar X-rays are considered to be the principal ionising source for air molecules (N_2 and O_2), particularly during solar maximum conditions when X-ray flux is dominant (Moldwin, 2008). In addition, cosmic rays also play an important part in the ionisation of particles at D-region altitudes, especially at sunspot minimum when the flux of galactic cosmic rays reaching the Earth's upper atmosphere is higher. This is related to the reduced shielding effect of the Earth's magnetic field. The main loss mechanism for electrons is dissociative recombination of the electrons on the positive ions. Because the neutral density is relatively high in the D-region, the rate of recombination is also significantly high due to the high collision rate between the electrons, the neutral atoms and molecules (Rishbeth and Garriott, 1969; White, 1970; Moldwin, 2008). For this reason the D-layer is only present during the daytime (though cosmic rays produce a residual level of ionisation at night), and the level of ionisation in the D-region is the lowest of the different ionospheric regions. The D-layer plays a major role with regards to HF radio communication because it absorbs radio waves, which results in degradation of long-distance HF communication. During sudden ionospheric disturbances, auroral absorption and intense polar cap precipitation of solar energetic particles, D-region ionisation can become so severe (may increase by 2 orders of magnitude) that it causes "blackouts" for HF communication (Stauning, 1996; Goodman, 2005; Moldwin, 2008).

2.3.2 E-region

Immediately above the D-region is the E-region, which extends from about 90 to 150 km. Both low energy (or soft) X-rays and solar UV radiation are the major sources of ionisation. The primary ionised ions are O_2^+, N_2^+, and O^+, however, as the photochemical equilibrium between production and loss is attained, NO^+ and O_2^+ become the dominant ions (Maruyama, 2001). The maximum (peak) density in the E-layer is more than a 100 times higher than the peak density in the D-layer, as recombination is lower at these high altitudes (Moldwin, 2008). However, similarly to the D-layer, the E-layer also fades away during the night, which effectively raises it's height, as the faster recombination times decay the E-region away much faster at low altitudes than at higher altitudes. It would suffice here to emphasise that in the D- and E-regions, transport of ionisation is insignificant and may be neglected all together, thereby leaving only the photochemical terms in the continuity equation as earlier mentioned in Section 2.1. Apart from solar photons, ionisation in the E-region also occurs due to energetic particles precipitating into the atmosphere. Particle precipitation effects are particularly important and most common at the high latitudes (see Stauning, 1996; Ngwira *et al.*, 2010, and references therein). Furthermore, ionisation in the E-region is substantially increased through particle precipitation, particularly at night when photon production is absent. Impact ionisation gives rise to the visible aurora, which appear as ovals in the southern and northern hemisphere high-latitudes.

Other short-lived sources of ionisation at E-region heights exist, which include complex dynamics resulting from the effects of the neutral atmosphere motion, auroral electric fields, and meteors entering the upper atmosphere that burn up and impact the surrounding neutral gas with sufficient energy to produce an ionised trail (Moldwin, 2008). Such sources produce narrow, short-lived regions of dense layers or patches of ionisation at E-region altitudes, collectively referred to as sporadic E (Rishbeth and Garriott, 1969; Moldwin, 2008). Sporadic E is latitude dependent, has a random time of occurrence and can last from a few minutes to several hours. Because ionisation can be very dense locally, HF radio waves may be reflected off these trails for long-distance communications.

2.3.3 F-region

The F-region is the densest region of the ionosphere that lies in the height range above 150 km. Production in the F-region is by solar EUV radiation, which ionises atomic oxygen (O). F-region ionisation is low at night, but not as low as in the D- and E-regions, therefore, the F-layer is always present. Recombination rates are lower at this higher altitude, and furthermore the region is composed of O rather than the molecular ions that are more prevalent in the D- and E-regions (Rishbeth and Garriott, 1969; Moldwin, 2008). Atomic ions have much lower recombination rates in general than molecular ions.

The peak electron density of the ionosphere occurs within the F-region near 300 km. Above the peak is a region commonly referred to as the topside ionosphere, where the density gradually decreases and merges into the plasmasphere. The topside ionosphere and the plasmasphere transition occurs around 1000 km. This region is marked by the transition from O as the dominant ion in the ionosphere to hydrogen as the most dominant ion in the plasmasphere (Moldwin, 2008).

2.4 Electron distribution in the F2-layer

The density distribution of ionisation in the F2-layer of the ionosphere is controlled by various processes, which include production, loss, vertical plasma motion and ambipolar (plasma) diffusion. If we assume equilibrium conditions (Rishbeth and Barron, 1960), which is justified on the basis that the F-region is in a state of quasi-equilibrium during most of the day in the temperate latitudes, the rate of change of electron concentration in the continuity equation is much smaller than other terms, therefore it may be neglected as an approximation.

Thus, the continuity equation for electron density N_e in the F2-layer takes the well known form

$$q - \beta N_e - M = 0 \tag{2.21}$$

where q is the production rate, β is the linear loss coefficient, and M is the transport factor for ionisation. Considering only the vertical motion, M can be expressed as

$$M = \frac{d}{dh} N_e(W + W_D) \tag{2.22}$$

where W is the upward component of the drift velocity due to electromagnetic motion, and is considered independent of height; W_D is the vertical component due to plasma diffusion (Rishbeth and Barron, 1960). It should be noted that by assuming equilibrium conditions, motions caused by thermal expansion and contraction of the atmosphere are neglected.

It is widely accepted that atomic oxygen is the ionisable constituent at F-region heights (Rishbeth and Barron, 1960; Rishbeth and Garriott, 1969; White, 1970;

Rishbeth, 1986; Maruyama, 2001). Furthermore, molecular nitrogen absorbs part of the ionising radiation, but the N_2^+ ions created decay rapidly through dissociative recombination and do not account for the observed ionisation. Thus, the loss rate in the F2-layer is proportional to the electron density N_e, and the loss coefficient β depends on the concentration $n(M)$ of molecular gasses, therefore,

$$\beta = Kn(M) \tag{2.23}$$

Taking the rate coefficient K to be independent of temperature and considering the scale height gradient to be constant, this equation leads to an essentially useful formula. If the molecular gasses and the ionisable constituent scale height are in the ratio 1:k (Rishbeth and Barron, 1960), we have

$$\beta = \beta_0 \exp[-z(k+\gamma)] \tag{2.24}$$

For a fully mixed ionosphere (i.e. atomic oxygen and molecular gasses) $k = 1$ in equation (2.24). If diffusive equilibrium is present $k = 1.75$ for N_2 or 2 for O_2. The two-stage process yields a non-linear loss function in the lower F-region which is expressed as

$$l(N_e) = \frac{Kn(M)\alpha N_e^2}{Kn(M) + \alpha N_e} \tag{2.25}$$

(Rishbeth and Barron, 1960, and references therein). A transition from the βN_e loss law in the F2-layer to the N_e^2 law applicable in the F1-layer exists, and occurs at the level where $Kn(M) \sim \alpha N_e$.

2.4.1 Plasma diffusion

For a horizontally stratified atmosphere, plasma diffusion formulations are based on the equation for the relative velocity of the diffusion of a binary gas mixture (Rishbeth and Barron, 1960), and can be written as

$$\begin{aligned} c_1 - c_2 = -\frac{n^2}{n_1 n_2} D_{12} \Bigg[& \frac{\partial(n_1/n)}{\partial h} + \frac{n_1 n_2 (m_2 - m_1)}{np\rho} \frac{\partial p}{\partial h} \\ & - \frac{p_1 p_2}{p\rho}(F_1 - F_2) + \frac{k_T}{T}\frac{\partial T}{\partial h} \Bigg] \end{aligned} \tag{2.26}$$

where p, ρ, n and m denote pressure, density, concentration (or number density), and molecular mass, respectively. The suffixes represent single constituent gas, and those without suffixes stand for the gas as a whole. T is the temperature and F the force per unit mass owing to external factors.

The coefficient D_{12} is the ambipolar diffusion coefficient $D(h)$, and the plasma is treated as one of the constituents for the case at hand (Rishbeth and Barron, 1960). Diffusion rate is high in the F-region but much less in the lower ionosphere where particle collisions are more prevalent (Rishbeth and Garriott, 1969). Since the number density N_e of the plasma is much smaller than that of the neutral atmosphere (n), the thermal diffusion term (last term) can be neglected. Therefore, the left-hand side of equation (2.26) is the plasma diffusion velocity, W_D, which leads to

$$-W_D = D(h)\left[\frac{1}{N_e}\frac{dN_e}{dh} + \frac{1}{T}\frac{dT}{dh} + \frac{\mu}{H}\right] \tag{2.27}$$

In equation (2.27), μ represents the ratio of the mean molecular weight of the plasma and the ionised gas, which takes the value $\mu = \frac{1}{2}$ for two chemically similar constituents (Rishbeth and Barron, 1960). The diffusion coefficient D is roughly estimated by

$$D = \frac{b\sqrt{T}}{n}\sin^2 I_{dip} \tag{2.28}$$

where $\boldsymbol{I}_{dip}$ is the magnetic dip angle. Note that in the F-region the plasma can only diffuse along magnetic field lines in the direction where the component of gravity takes the form $g \sin \boldsymbol{I}_{dip}$, as explained by Rishbeth and Garriott (1969). Further, these authors explain that at mid- and high-latitude regions, $\sin \boldsymbol{I}_{dip}$ can be considered as a constant along any particular field line throughout the vertical extent of the F-region. However, at low-latitudes $\boldsymbol{I}_{dip}$ varies significantly along field lines, a case which leads to complex expressions for the differential operator in which the coefficients become functions of magnetic latitude.

Combining equations (2.22), (2.27) and (2.28) the contribution M_D of the diffusion to the term M in the continuity equation (2.21) can be determined. To simplify these equations, the scale height gradient and the composition must be independent of height, with the result that γ and μ do not vary (Rishbeth and Barron, 1960). Therefore, $H/H_0 = T/T_0 = \exp(\gamma z)$ and $n/n_0 = \exp[-z(1+\gamma)]$, thus the diffusion rate, $d = D/H^2$ (per unit time) is

$$d(z) = d_0 \exp\left[z(1 - \frac{1}{2}\gamma)\right] \tag{2.29}$$

Hence, the contribution of diffusion to the transport term in equation (2.21) is

$$M_D = d(z)\left[\frac{d^2N_e}{dz^2} + (\phi + \psi)\frac{dN_e}{dz} + \phi\psi N_e\right] \tag{2.30}$$

where $\phi = \gamma + \mu$ and $\psi = 1 + \frac{1}{2}\gamma$. Considering the simplest case of an isothermal atmosphere with $\gamma = 0$ and $\mu = \frac{1}{2}$ (Rishbeth and Barron, 1960), the diffusion term can then be defined by

$$M_D = d_0 \exp(z)\left[\frac{d^2N_e}{dz^2} + \frac{3}{2}\frac{dN_e}{dz} + \frac{N_e}{2}\right] \tag{2.31}$$

Then it is determined empirically that the characteristics of the peak can be obtained by the relationship

$$q_m \simeq \beta_m N_{e,m} \tag{2.32}$$

$$\beta_m \simeq d_m \tag{2.33}$$

Thus, the F2-layer peak occurs at a height where both diffusion and loss are significantly important (i.e. where $\beta_m \sim D_m/H^2$), and the electron concentration at this level is given by $N_{e,m} \sim q_m/\beta_m$, which is similar to the expression obtained in the absence of diffusion (Rishbeth and Garriott, 1969). Therefore, a height independent gradient of scale height of the magnitude similar to that which exists in the F2-region, does not have a significant effect upon the form of the electron density distribution.

2.4.2 Vertical drift velocity effects

Rishbeth and Barron (1960) have shown qualitatively that an upward drift motion tends to push ionisation from the lower altitudes towards higher altitude levels where the loss rate is less, and thereby the average lifetime of the ion pairs is sustained and the peak electron density increased. Furthermore, they have also shown that an upward drift motion has a greater effect on the ionisation than a downward drift of the same magnitude. The changes which develop at the peak as a result of drift W can be summarised by the equations

$$\Delta(\log N_{e,m}) \simeq \frac{W}{Hd_m} \tag{2.34}$$

$$\Delta z_m \simeq \frac{W}{Hd_m} \tag{2.35}$$

so that d_m is the diffusion rate at the peak height z_m, when $W = 0$.

It has been reported by Rishbeth and Barron (1960) that rocket experiments suggested that O^+ is the most abundant positive ion above about 240 km. Then for a "mixed" atmosphere (i.e. O and N_2 completely mixed at all heights, so that $H(O) = H(N_2)$ and $k = 1$), the parameter μ in the diffusion velocity equation (2.27) relies on the relative abundances of N_2 and O. Whereas, in the "separated" atmosphere (i.e. O and N_2 are diffusely separated at heights above 150 km, so that $H(O) = 1.75(N_2)$, $k = 1.75$), μ increases with height and attains a limiting value of 0.5 at a level where the ratio of N_2 is small. At altitudes below 240 km, μ depends on the ion and the neutral atmosphere compositions. The term involving μ is not significant below the F2-peak in this region.

2.4.3 The thermosphere and neutral air winds

The ionosphere consists of plasma which is created from neutral gasses as a result of absorbing solar ionising radiation, and is converted back to neutral gasses through recombination of ions and electrons. However, even at the height of highest plasma density, the concentration is only about 10^{12} particles/m^3, while the neutral gas density is about 10^{15} particles/m^3 at the same height (Maruyama, 2001; Fuller-Rowell *et al.*, 2008). Therefore, the composition and the motion of the neutral gas particles are primarily responsible for the chemical reactions and interparticle collisions that have a dominating influence over the structure of the ionosphere (see Rishbeth, 1986; Fuller-Rowell *et al.*, 1997; Maruyama, 2001, and references therein).

At ionospheric altitudes, the cooling effect attained by infrared radiation is small compared with heating through solar UV and EUV absorption, thus creating a net rise in the neutral gas temperature in a region commonly referred to as the thermosphere (Rishbeth and Garriott, 1969; Maruyama, 2001). This height region is characterised by two important features: it is viewed as the thermosphere when emphasising the importance of the temperature of the neutral gasses present there, but referred to as the ionosphere when the density of the ionised gasses at a given altitude are of major concern (Maruyama, 2001).

The thermosphere can be considered to be a huge heat engine driven by energy from solar, high-latitude and interplanetary sources, with tidal and wave contributions from the underlying middle atmosphere (Rishbeth, 1998). The heat contributions from the various sources cause horizontal gradients of temperature and pressure. The pressure gradients then drive horizontal winds at F-layer heights, which together with the associated vertical up-currents and down-currents, form a global circulation that carries energy away from the heat sources and liberates it elsewhere (Jones and Rishbeth, 1971; Fuller-Rowell *et al.*, 1994, 1996; Rishbeth, 1998).

The height of the peak electron density in the ionosphere can be altered by an electric field or a neutral air wind (see reviews by Buonsanto, 1999; Mendillo, 2006). Vertical plasma drift can lead to the development of a zonal electric field $\mathbf{E}$ in the ionospheric E-region by day, and from the F-region after sunset. The electric field is directed to the east (eastward) during the day, producing an upward $\mathbf{E} \times \mathbf{B}/\mathbf{B}^2$ vertical drift velocity. The westward electric field produces a downward drift (Kelley, 1989; Rishbeth, 1998). The vertical drift is more pronounced at the equatorial latitudes, because at mid-latitudes the vertical drift speed is largely damped by the reaction of the neutral air ("ion-drag effect") (Rishbeth, 1998).

Thermospheric neutral air winds blowing in the neutral atmosphere of the thermosphere can alter the ionospheric structure through collisions between neutral particles and ions (Rishbeth, 1986; Fuller-Rowell *et al.*, 1994; Rishbeth, 1998). According to Rishbeth (1998), a horizontal wind U blowing from the auroral region to the magnetic equator will drive the ions and electrons up geomagnetic field lines (with dip angle $\boldsymbol{I}_{dip}$) at speed $U \cos \boldsymbol{I}_{dip}$, with a vertical component

$W = U \sin \boldsymbol{I}_{dip} \cos \boldsymbol{I}_{dip}$ as illustrated in Figure 2.3. The resulting upward drift raises the peak and enhances the peak electron density NmF2, which changes approximately in line with the values of the ratio q/β.

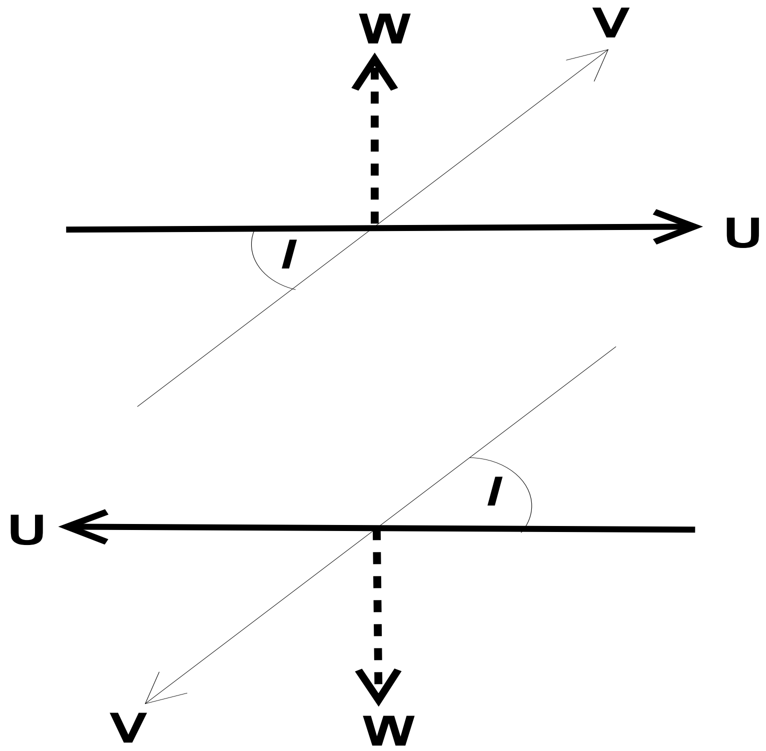

Figure 2.3: Sketches illustrating how a horizontal wind U blowing equatorward (top) or poleward (bottom) produces a field-aligned ion drift $V = U \cos \boldsymbol{I}_{dip}$ the vertical component of which is given by $W = V \sin \boldsymbol{I}_{dip} = U \cos \boldsymbol{I}_{dip} \sin \boldsymbol{I}_{dip}$. The thin sloping lines depict the direction of the geomagnetic field. Figure adapted from Rishbeth (1998).

The resultant wind velocity **U** produced by the horizontal pressure gradients relies on the Coriolis force due to the Earth's rotation, on the molecular viscosity of the air, and on the ion-drag due to collisions between air molecules and the ions (Fuller-Rowell *et al.*, 1994; Rishbeth, 1998). The "ion-drag effect" is produced because the ions are constrained by the geomagnetic field and can not move freely with the wind (Rishbeth, 1998). Then the equation of motion for the horizontal wind **U** at F2-layer heights is

$$d\mathbf{U}/dt = \mathbf{F} - 2\boldsymbol{\Omega} \times \mathbf{U} - KN_e(\mathbf{U} - \mathbf{V}) \tag{2.36}$$

where K is the collision parameter, KN_e is the neutral-ion collision frequency and $\boldsymbol{\Omega}$ is the Earth's angular velocity (Jones and Rishbeth, 1971; Rishbeth, 1998). The driving force $\mathbf{F}$ produced by the horizontal gradients of air pressure p (with density ρ), is given by the equation:

$$\mathbf{F} = -(1/\rho)\nabla_{horiz}p \tag{2.37}$$

In the F-region, molecular viscosity plays a significant role as it smooths out the vertical variation of the wind velocity, so that $d\mathbf{U}/dh \to 0$ at higher altitudes (Rishbeth, 1998). However, small-scale velocity gradients are not smoothed out lower down in the thermosphere.

The direction of the wind depends on the ratio of the Coriolis force to ion-drag, and can be visualised by considering special steady-state cases in equation (2.36) so that $d\mathbf{U}/dt = 0$ (Rishbeth, 1998). For a case were the Coriolis force is more dominant than the ion-drag, such as in the lower ionosphere, the wind blows perpendicular to the pressure gradients. However, a different case occurs in the daytime F-region, where ion-drag is large and the wind is almost parallel to the pressure gradient force. Nevertheless, both Coriolis force and ion-drag are important in general (Rishbeth, 1998). Since the direction of the driving force continually changes with local time, the wind direction also changes, but lags behind its steady-state direction due to inertia (Rishbeth, 1974).

The ion velocity $\mathbf{V}$ in equation (2.36) is strongly influenced by electrostatic fields. The air is accelerated horizontally through collisions with the drifting ions, and for a large value of $\mathbf{V}$, the ion-drag term in (equation 2.36) acts as a driving force for neutral air winds. This is more prevalent in the high-latitude regions, where strong electric fields of magnetospheric origin exist, which are in turn driven by the solar wind. The winds have a dominant day-to-night pattern in the high-latitudes, driven partly by the large-scale magnetospheric fields and partly by solar heating, which leads to the day-to-night pressure variations (Rishbeth, 1998). Further discussion on the neutral wind effects is given in Section 4 in relation to ionospheric disturbances.

2.5 Summary

This chapter presented some of the fundamental processes that are necessary for our understanding of the ionosphere and how its electron density concentration can be affected. The ionosphere plays an essential part in the propagation of radio waves because its variable refractivity affects the propagation of trans-ionospheric radio signals. The various physical processes that control the plasma variations in the ionosphere can be grouped into two general categories, i.e., those responsible for production or loss of ionisation, and those that lead to the movement of ionisation. These processes, which can potentially change the electron density concentration, can be written in terms of the continuity equation and are summarised in Table 2.1.

The F2-layer is normally in a "quasi-equilibrium" state given that the term $\partial N_e/\partial t$ is much smaller than other terms in the continuity equation. The behaviour of the F2-layer peak can be summarised by the following governing rules (Rishbeth, 1998):

- At heights below and up to the F2 peak, the production and loss terms are approximately in balance during the day: q is dependent on the atomic oxygen concentration [O], β is mainly dependent on the molecular nitrogen concentration $[N_2]$ with some contribution from molecular oxygen $[O_2]$. Both q and β reduce with the upward reduction of the gas concentration, however, the ratio q/β, which depends on the atomic/molecular ratio of the neutral air, increases upwards so that N_e also increases.

- At greater altitudes, gravity controls the plasma distribution and stops the upward increase of N_e. The F2 peak is established at the height where both the transport terms, and the production and loss terms are sufficiently comparable. This takes place where chemical control gives way to diffusive (gravitational) control.

- The height of the F2 peak usually occurs at a fixed pressure level in the atmosphere, thus at a fixed value of the reduced height z.

- At heights above the peak the plasma distribution is gravitationally controlled, and N_e decreases exponentially upwards with the plasma scale height.

- Changes in the height of the peak can be caused by neutral air winds or electric fields. Zonal electric fields produce vertical plasma drift motion. The drift velocity vertical component is upwards for eastward **E** and downwards for westward **E**, and is significantly important at equatorial latitudes.

- Thermospheric neutral air winds blowing from high to low latitudes in the neutral atmosphere can alter the ionospheric structure by moving plasma to higher altitudes where the recombination rate is low, thereby raising the peak height and increasing the peak electron density. These changes occur approximately in accordance with the value of the ratio q/β at the shifted level of the peak.

Besides the various ionisation sources already mentioned in this chapter, the enhancement of D-, E- and F-region ionisation observed during geomagnetic disturbances are probably due to high energy electrons and protons. The mechanisms by which this enhancement is attained is part of the general problem of geomagnetic storm phenomena, which will be discussed in later chapters. This problem forms part of the core on which this thesis is presented. The various data sources and analysis tools utilised during the course of this work will be dealt with in the next chapter.

Table 2.1: Summary of production and loss processes in the ionosphere as provided by Rishbeth and Garriott (1969).

Process	D-region ~60-90 km	E-region ~90-150 km	F-region ~150-600 km
Production		EUV 911-1027 Å	EUV 170-911 Å
Solar photoionisation (primary radiation shown [ ])	[Ly α 1216 Å] (ionises NO) X-ray 1-10 Å	[Ly β 1026 Å] O_2 ionised by $\lambda < 1027$ Å X-ray 10-170 Å	[HeII 304 Å, HeI 584 Å] O ionised by $\lambda < 911$ Å N_2 ionised by $\lambda < 796$ Å
Corpuscular ionisation (more important at high latitudes)	Electrons > 30 keV Protons > 1 MeV Cosmic rays	Electrons 1-30 keV cause some nighttime and sporadic E ionisation	Electron $\lesssim$ 1 keV (probably small; might be significant at night)
Loss			
Ion-ion recombination	Important	Few negative ions exist	Very few negative ions exist
Electron recombination			
Three-body recombination	Important	Gas densities too low	Gas densities too low
Radiative recombination	Insignificant	Not important	Not important
Dissociative recombination	Important	Principal loss mechanism	Principal loss mechanism
Ion-atom interchange (N_{A^+} = atomic ionisation concentration)	Not important because few atomic ions exist	Important	Important
Attachment Radiative Three-body	Three-body attachment is most important	Can maintain some negative ions at night	Radiative attachment provides a very weak source of negative ions
Collisional detachment, etc. Collisional detachment Associative detachment Detachment by meta-stable molecules	Important, especially at night	Fairly important	Insignificant
Photodetachment by solar visible and long UV radiation	Main cause of day/night change of N_-/N_e	Effective by day	Largely responsible for absence of negative ions

Chapter 3

Instrumentation and data sources

The coordinated analysis of geomagnetic disturbances presented in this thesis involves a wide range of observations from various ground- and space-based instrumentation. Different measurements recorded at geographically distributed locations, combined with satellite-based observations, frequently provide the necessary information needed to advance our understanding of the various processes occurring within the ionosphere. Therefore, in this study variations in the ionosphere were investigated using a variety of measurements and modelling techniques. The major instruments, data sources and analysis tools used for this thesis are discussed in this chapter.

3.1 Radio wave propagation in the ionosphere

The propagation of radio waves from one medium to another can essentially be treated like other electromagnetic waves, such as light (White, 1970). When a radio wave enters a medium with different refractive properties, it is refracted so that it changes the direction of propagation and the wave form bends. Similarly, in the ionosphere a radio wave will gradually bend under the influence of refraction until it reverses its direction and returns to the ground. Figure 3.1 illustrates the propagation of radio waves through the ionosphere. A radio wave transmitted at point A on the Earth's surface travels until it enters the ionosphere at point B and is refracted by the increasing electron density at higher altitudes. The incidence angle i at point B and the angle of refraction r at C are also shown in this figure. The angle of refraction at the peak O is 90°. The beam eventually

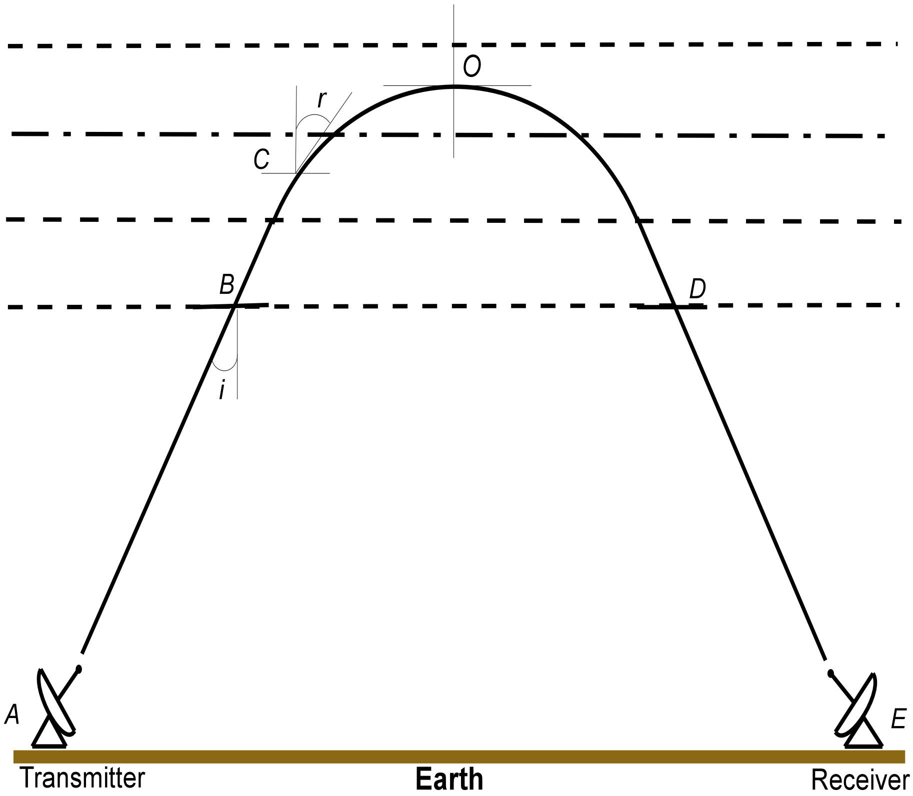

Figure 3.1: An illustration of the propagation of radio waves through the ionosphere along the path $ABCDE$. Figure adapted from White (1970).

exits the ionosphere at point D and returns to the surface at the receiver point E. At higher frequencies, the refraction may not be sufficient to return the wave to the Earth, and it passes through the ionosphere.

3.2 Ionosonde measurements

Much of the knowledge of the ionosphere is derived from remote sensing by radio waves. The traditional instrument for measuring the virtual height of the ionosphere is called an ionosonde (Rishbeth and Garriott, 1969; Davies, 1990). An ionosonde is a type of HF radar with frequency ranges between 3 and 30 MHz, and is the most commonly available ionospheric sounding equipment in use today. Ionosondes have been utilised extensively in remote sensing, both for monitoring long-term temporal and spatial variations of the ionosphere, and for scientific research. There are two types of modulation techniques that can be applied in an ionosonde (i.e. "pulse" or "chirp"), each with its own advantages and disadvantages. But in principle the chirp technique differs from that of a pulse-amplitude technique in that the radio signals are continuous waves in which the frequency is modulated (Davies, 1990, and references therein). However, details about these ionospheric sounding techniques are outside the scope of this thesis and interested readers should consult the relevant literature for details (e.g. Hunsucker, 1990).

So, for a radio wave of frequency f propagating through the ionosphere, the refractive index can be derived from the Appleton-Hartree equation, a simplified form of which is given by the expression (White, 1970):

$$\mu^2 = 1 - \frac{4\pi N_e e^2}{m_e \omega^2} \tag{3.1}$$

where e is the electron charge, m_e is the electron mass, and the angular frequency $\omega = 2\pi f$.

Now, if the refractive index outside the ionosphere is μ_0, and at point C (Figure 3.1) is μ_c, then as the wave penetrates deeper into the layers, the electron density increases and the wave normal changes according to Snell's law:

$$\mu_0 \sin i = \mu_c \sin r \tag{3.2}$$

The virtual (or group) height h' of ionospheric reflection can be determined when the flight time t from the transmitter to the receiver via the ionosphere is considered. A timing device (e.g. the time base of a cathode ray oscilloscope) is triggered when a pulse of radio waves is transmitted (Davies, 1990), and the position of the echo pulse on the time base of the cathode ray provides a measure of the flight time of the pulse, and thus, the virtual height. As the frequency increases, the pulse penetrates to higher altitudes in the ionosphere and the virtual height continues to increase until the signal penetrates the ionosphere.

Setting $\mu^2 = 0$ in equation (3.1) and letting $\omega_0 = 2\pi f_c$, it can be shown that

$$f_c = \sqrt{\frac{N_e e^2}{\pi m_e}} \tag{3.3}$$

which is the critical (cutoff) frequency of the ionosphere. Any frequencies below the cutoff f_c are reflected and eventually return to the ground. However, higher frequencies (above f_c) traverse the ionosphere into outer space. Therefore, the ionospheric electron density at the maximum height of reflection is

$$N_e(max) = \frac{\pi m_e}{e^2} f_c^2 = 1.24 \times 10^{10} f_c^2 \tag{3.4}$$

with $N_e(max)$ given in electrons/m^3 and f_c in megahertz (MHz). The virtual height is related to the flight time as follows:

$$h' = \frac{ct}{2} \tag{3.5}$$

where c is the velocity of light.

By applying different frequencies to cover the entire range of electron densities, a virtual height versus frequency record (an ionogram) is obtained. Short pulse application to the time base at selected frequencies provides a frequency calibration, whilst height calibration is done by applying short pulses from a pulse generator (Davies, 1990). Figure 3.2 presents some examples of ionograms for a mid-latitude location (Hermanus, South Africa) during the month of March 2011. The green and red traces are the X- and O-mode reflections, respectively. The frequencies at which the two traces become asymptotic to the height axis correspond to the frequencies at which the X- and O-mode rays penetrate the ionosphere. The daytime ionogram (Figure 3.2a) shows wave traces with reflections from the E, F1, and F2 layers, whereas, in the nighttime ionogram (Figure 3.2b), only the F2-layer echoes are present. However, in both ionograms, the virtual height gradually increases with frequency until the signal penetrates the ionosphere at a frequency higher than the F2-layer critical frequency (foF2). One of the distinguishing features in the two ionograms is the difference in the foF2 values, which is associated with ionisation levels in the ionosphere.

3.2.1 Ionogram interpretation

To interpret radio signals propagating through and reflected from the ionosphere, it is important to understand the radio refractive index of the ionosphere (Davies, 1990). If the refractive index of the ionosphere is independent of the influences of positive and negative ions on wave propagation (Rishbeth and Garriott, 1969;

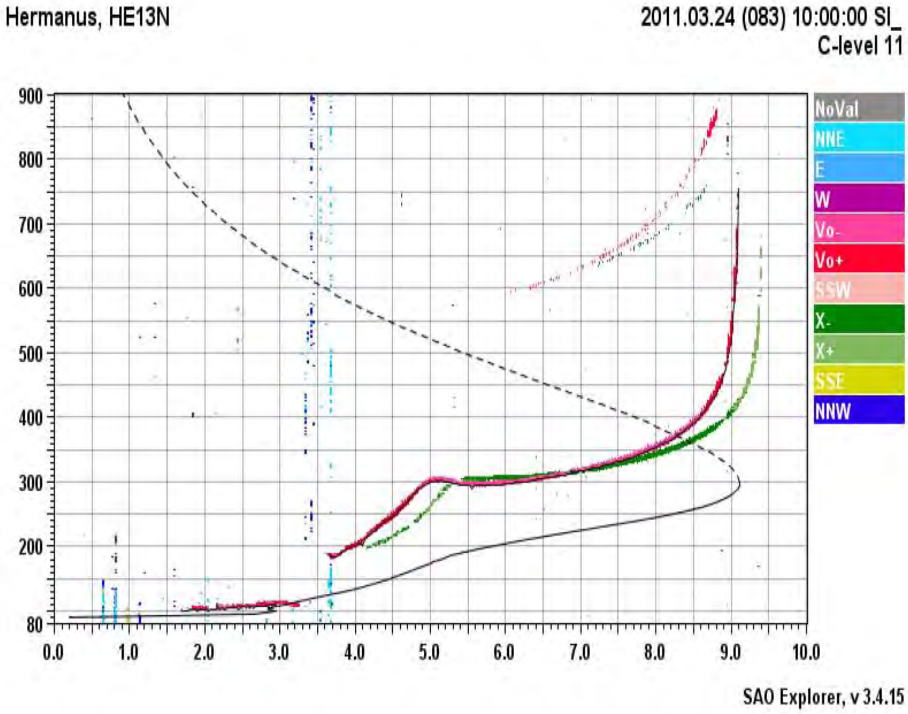

(a)

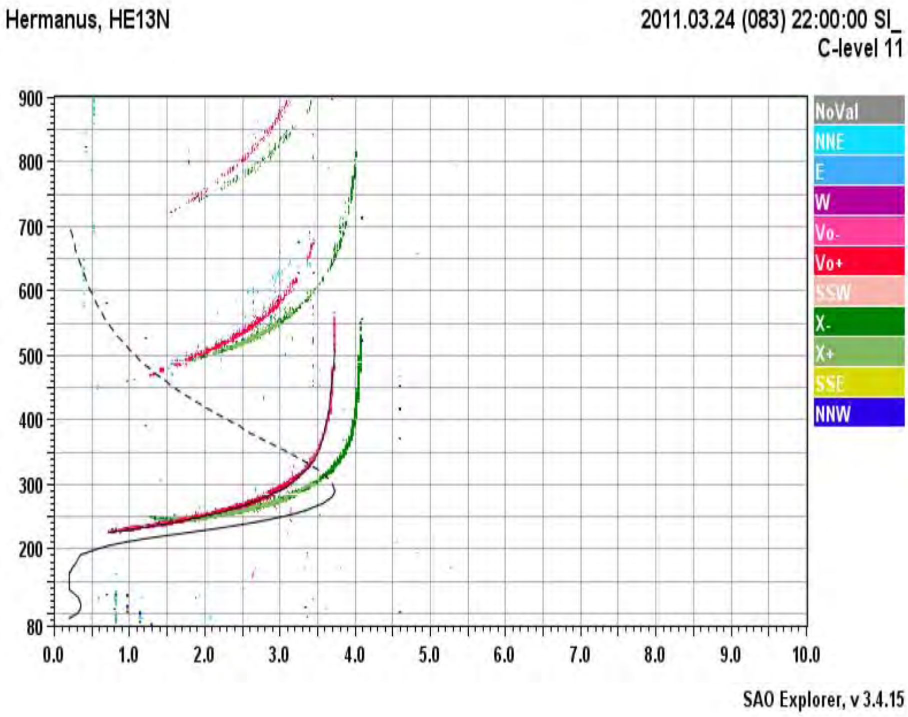

(b)

Figure 3.2: Sample daytime (a) and nighttime (b) ionograms for Hermanus field station during the month of March 2011.

Davies, 1990), two frequencies can be defined:

$$Plasma\ frequency : (2\pi f_{pe})^2 = \omega_{pe}^2 = N_e e^2/m_e \epsilon_0 \tag{3.6}$$

$$Gyrofrequency : \ 2\pi f_{ce} = \omega = \mathbf{B}e/m_e \tag{3.7}$$

where ϵ_0 is the electric permittivity of free space and $\mathbf{B}$ is the geomagnetic field flux density. Now, let θ be the angle between the direction of the wave normal and the magnetic field, so that $Y_L = Y \cos\theta$ and $Y_T = Y \sin\theta$. The subscripts T and L respectively denote the transverse and longitudinal components of the imposed magnetic field, with reference based on the direction of the wave normal. Then, the magnetoionic parameters can be expressed as

$$X = \omega_{pe}, \quad Y_L = e\mathbf{B}_L/m_e\omega, \quad Y_T = e\mathbf{B}_T/m_e\omega, \quad Z = \upsilon/\omega \tag{3.8}$$

Here, υ is the collision frequency of the electrons with heavy ions. The ionosphere is a doubly refracting medium in the presence of the Earth's magnetic field, with two characteristic modes of propagation termed the "*ordinary*" and "*extraordinary*" waves (see Davies, 1990; White, 1970). When collisions are negligible (e.g. in the F-region) so that $Z \approx 0$ (Rishbeth and Garriott, 1969; Davies, 1990), then the refractive index can be expressed in terms of the Appleton-Hartee equation:

$$\mu^2 = 1 - \frac{X(1-X)}{(1-X) - \frac{1}{2}Y_T^2 \pm [\frac{1}{4}Y_L^4 + (1-X)^2\, Y_L^2]^{1/2}} \tag{3.9}$$

The plus sign refers to the *ordinary* wave and the minus sign to the *extraordinary* wave. For a horizontally stratified ionosphere, a vertically incident wave is reflected at a level where $\mu^2 = 0$. This occurs where $X = 1$ for the *ordinary* wave, which is similar to having no magnetic field. As for the *extraordinary* wave, reflection occurs at a point where $X = 1 - Y$ if $Y < 1$ ($f = f_{ce}$), and where $X = 1 + Y$ if $Y > 1$ ($f < f_{ce}$).

With parallel propagation (i.e. wave normal in direction of geomagnetic field, e.g. at a geomagnetic pole) so that $\theta = 0$, then $Y_L = Y$ and $Y_T = 0$ (Davies, 1990). This reduces the Appleton-Hartee equation (3.9), so that the refractive index is now expressed as

$$\mu^2 = 1 - \frac{X}{1 \pm Y_L} \tag{3.10}$$

Since the two characteristic wave modes are elliptically polarised in the opposite sense, any plane polarised wave propagating through the ionosphere can be considered the sum of the *ordinary* and *extraordinary* components. The plane of polarisation continually rotates along the path of the wave, because the two components possess different phase velocities (Rishbeth and Garriott, 1969).

The relationships between the critical frequencies (o and x) are determined from the reflection conditions $X = 1 + Y$, $X = 1$, $\mu = 0$ and $X = 1 - Y$. If f_m is the frequency at the level of maximum electron density occurring in the F2-layer, and the plasma density at the peak is same for both wave modes, then we have

$$f_m^2 = f_{om}^2 = f_{xm}^2 - f_{xm} f_{ce} \tag{3.11}$$

Therefore,

$$f_{ce} = \frac{(f_{xm}^2 - f_{om}^2)}{f_{xm}} \tag{3.12}$$

This quadratic equation can be solved by considering the condition $f_{om} \gg f_{ce}$, which then reduces it to the form:

$$f_{xm} \cong \frac{f_{ce} + 2f_{om}}{2} \cong f_{om} + \frac{f_{ce}}{2} \tag{3.13}$$

This formulation is important in ionogram interpretation, in that it helps to distinguish the critical frequency of penetration of a particular layer, thus the *ordinary* ray from the *extraordinary* ray, and vice versa.

3.3 The Global Positioning System

The use of GNSS has become an integral part of the world's infrastructure, and today's society has become increasingly dependent on this technology. Systems such as the Global Positioning System or GPS (USA), GLONASS (Russia), Galileo (Europe), and Compass (China), are either fully operational or are being developed. These systems were planned as separate GNSS units, but are expected to be mutually compatible, thus providing improved, robust performance and capabilities than any of the individual systems. Since all these systems operate on the same basic principle, the discussion here focuses only on GPS.

The NAVSTAR GPS, the first fully operational (as of 1995) GNSS system, was conceived (mid-1970s) as a ranging system using known positions of the orbiting satellites in space to locations on land, sea, in the air and space (Hofmann-Wellenhof *et al.*, 1992; Trimble, 2007). The GPS is an all-weather, space-based navigation system developed by the US Department of Defense to meet the need of the military forces to precisely determine their position, velocity, and time in a common reference system, anywhere on or near the Earth on a continuous basis (Kintner and Ledvina, 2005; Misra and Enge, 2007). The GPS configuration can be divided into 3 categories: the space segment, consisting of satellites, their signals and codes, and the navigation message containing the information necessary for the receivers to determine the satellite positions; the control segment, dealing with the management of the whole system; and the user segment which includes all activities related to the development of both military and civilian receiver equipment.

The GPS baseline constellation (space segment) comprises a minimum of 24 active satellites in near circular orbits at an altitude of 20 200 km above the surface of the Earth, and have orbital periods of roughly 12 sidereal hours, with stationary ground tracks. The satellites are deployed in six orbital planes each inclined at 55° relative to the equatorial plane, with four primary satellite positions distributed unevenly in each orbit. There is a designated spare satellite in each orbital plane, to be used as a replacement in the event of failure or planned maintenance. Each satellite orbits the Earth twice a day so that at least four satellites are in view at any one time, from anywhere on or near the Earth's surface for users with a clear view of the sky. The GPS orbits place the satellites well above the ionospheric F-region and at an Earth-centred distance of $\sim$4 Earth radii, which is mostly above the plasmasphere depending on the location of the plasmapause and the satellite distance from the magnetic equator (Kintner and Ledvina, 2005).

The control segment consists of 12 ground stations, which have three core functions (Misra and Enge, 2007; Trimble, 2007). At the centre of this segment is the master control station (MCM), which operates the system and coordinates command and control functions. The monitor stations track the navigation signals from all the individual satellites and continuously feed the data to the MCM for processing. The MCM is responsible for computing orbit projections for each satellite, and also for the correction of the satellites' on-board clocks. This updated orbit and clock information is then sent to the four ground antenna sites, from which the data is uploaded to each satellite about three times per day for system accuracy maintenance. Commands for routine maintenance, software updates, and satellite orbit adjustment are also transmitted through the ground antenna stations.

Generally, the user segment has two primary user groups, namely military and civilian. The segment is further characterised by a wide rage of receiver types depending on the application. They vary from the handheld GPS receiver with accuracy within about 15 m, slightly more expensive receivers with about 1 m accuracy, and the advanced receivers used by surveyors and other professionals which are precise to less than a centimetre. However, GPS receivers have a common core operation: collection of the data broadcast by the satellites, analysis of the navigation message to find the satellite position, velocity, and clock parameters, and then finally, the estimation of the user position, velocity, and time (Misra and Enge, 2007).

3.3.1 GPS signal

Currently, each GPS satellite continuously broadcasts radio signals using two L-band carrier frequencies:

$$\text{L1: } f_{\text{L1}} = 1575.42 \text{ MHz, and L2: } f_{\text{L2}} = 1227.60 \text{ MHz}$$

However, under the GPS modernisation programme, additional navigation signals, such as the L5 (1176.45 MHz), will be broadcast by Block IIF satellites using a protected aviation frequency band for safety-of-life applications (Kintner and Ledvina, 2005; Misra and Enge, 2007).

The ranges, based on the transmission time of a signal from satellite to receiver, use two pseudo-random noise (PRN) codes that are modulated onto the two base carriers: the Coarse/Acquisition-code (C/A-code) and the Precision-code or P-code (Hofmann-Wellenhof *et al.*, 1992; Misra and Enge, 2007). Each satellite is identified by a unique code. The C/A-code is available for civil use, but access to the system capabilities available on the P-code is restricted (encrypted) to the US military and other authorised users. Civilian use was previously limited by using selective availability (S/A) to purposefully degrade system accuracy. However, this feature (S/A) was discontinued in 2000 following a US Presidential Decision Directive, because of the system's importance in other critical applications, and also because of the growing use of differential GPS techniques which essentially removed S/A-induced errors.

The carriers L1 and L2 are modulated by codes to enable satellite clock reading by the receiver and to broadcast information such as the orbital parameters (Hofmann-Wellenhof *et al.*, 1992; Misra and Enge, 2007). The broadcast signal is effectively continually marked by its own transmission time so that the received signal's transmission period is recorded with a synchronised receiver. The total code length is divided into 37 unique one-week segments, with each segment assigned to a specific satellite, defining its PRN number. These codes are reset at the beginning of every GPS week, i.e. at midnight each Saturday. GPS satellites also broadcast a navigation message which essentially contains information about the satellite's health status, the clock bias parameters, ephemeris (satellite position and velocity), and almanac information (giving reduced-precision ephemeris data on all satellites in the constellation) (Misra and Enge, 2007).

GPS receivers acquire their signals by generating a replica of the known C/A-code, and attempting to align it with the satellite transmitted signal by shifting the replica in time and calculating the correlation. Code tracking is performed as a feedback control loop, known as the delay lock loop, which continuously adjusts the replica code to keep it aligned with the code in the incoming signal (Misra and Enge, 2007). The PRN code is removed from the signal after alignment has been achieved, leaving the carrier modulated by the navigation message. This signal is then tracked by another feedback control loop, referred to as the phase lock loop.

3.3.2 Position estimation using GPS

In principle, position estimation using the GPS radio-navigation system is based on measurement of distances from known locations, an idea commonly referred to as trilateration (Misra and Enge, 2007). If the transmission time of a radio signal is measured, then the distance between the transmitter and observer can be computed, since radio waves travel at a known speed. Therefore, given the distances from an observer to three transmitting stations at known locations, the observer can determine his/her position precisely.

Basically in GPS systems, the receiver generates a sinusoidal signal to match the frequency and phase of the incoming signal, and extracts the navigation message in the process. Since GPS uses two synchronised clocks (i.e. one on the satellite and the other on the receiver), the receiver knows precisely the instant when the PRN code chips are generated in accordance with the satellite clock (Misra and Enge, 2007). Therefore, the measured ranges are biased by satellite and receiver clock errors, and are referred to as pseudoranges (Hofmann-Wellenhof *et al.*, 1992; Misra and Enge, 2007).

Now let t_s be the satellite clock reading and t_r the receiver clock reading, so that δ_s and δ_r are the respective clock biases, with respect to the GPS system time. Then, the propagation time of the signal is equivalent to the time shift Δt required to align the receiver-generated code replica and the signal received from the satellite. This is expressed as

$$\Delta t = t_r - t_s = [t_r(GPS) - \delta_r] - [t_s(GPS) - \delta_s] = \Delta t(GPS) + \Delta\delta \tag{3.14}$$

where $\Delta t(GPS) = t_r(GPS) - t_s(GPS)$ and $\Delta\delta = \delta_s - \delta_r$ (Hofmann-Wellenhof *et al.*, 1992).

Multiplying the time interval Δt by the speed of light c gives the pseudorange R, which is defined as

$$R = c\Delta t = c\Delta t + c\Delta\delta + \Delta\rho_{ion} + \Delta\rho_{trop} + \varepsilon_R \tag{3.15}$$

where $\Delta\rho_{ion}$ and $\Delta\rho_{trop}$ are the ionospheric and tropospheric propagation delays respectively, and ε_R accounts for other errors, e.g. receiver noise, multipath, orbit prediction error, etc (Misra and Enge, 2007). These error sources can be classified as satellite-related errors, propagation medium-related errors, and receiver-related errors. Known errors can be corrected using parameters in the navigation message from the satellite (Hofmann-Wellenhof *et al.*, 1992; Misra and Enge, 2007). However, details on the implementation of the correction measures are not discussed here. They have been widely documented (Hofmann-Wellenhof *et al.*, 1992; Klobuchar, 1996; Misra and Enge, 2007, and references therein).

3.3.3 GPS-derived total electron content

The propagation of electromagnetic waves in a medium depends on the refractive index n, as mentioned earlier. The ionosphere, being a dispersive medium relative to the radio wave signals, has a phase and group refractive index which can approximately be expressed as

$$n_{ph} = 1 + \frac{c_2}{f^2} \qquad\qquad n_{gr} = 1 - \frac{c_2}{f^2} \tag{3.16}$$

respectively. The coefficient c_2 is estimated to be $c_2 = -40.3\ N_e\,\mathrm{Hz}^2$ (Hofmann-Wellenhof *et al.*, 1992, and references therein). As a result of the dispersion of the ionosphere, a group delay and a carrier phase advance is introduced (Hofmann-Wellenhof *et al.*, 1992). Therefore, the measured code pseudoranges are too long and the measured carrier phase pseudoranges are too short compared to the geometric range between the satellite and the receiver.

The measured range s is expressed in terms of Fermat's principle (Hofmann-Wellenhof *et al.*, 1992), according to the equation

$$s = \int ds \tag{3.17}$$

The geometric range s_0 along the straight line between the satellite and receiver can be derived by setting $n = 1$, so that

$$s_0 = \int ds_0 \tag{3.18}$$

where the integral is taken along the signal ray path.

The ionospheric delay (Δ^{Iono}) is the difference between the measured and geometric range:

$$\Delta^{Iono} = \int ds - \int ds_0 \tag{3.19}$$

Taking the case of the group refractive index, this can be expressed as

$$\Delta^{Iono}_{gr} = \int (1 - \frac{c_2}{f^2})\, ds - \int ds_0 \tag{3.20}$$

Then, by considering the integration along the geometric path, so that ds becomes ds_0, equation (3.20) reduces to

$$\Delta^{Iono}_{gr} = -\int \frac{c_2}{f^2}\, ds_0 \tag{3.21}$$

Replacing c_2 ($-40.3\ N_e\,\mathrm{Hz}^2$) leads to

$$\Delta^{Iono}_{gr} = \frac{40.3}{f^2} \int N_e ds_0 \tag{3.22}$$

The propagation speed of radio waves in the ionosphere depends upon the integrated number of electrons along the line-of-sight path of the radio signal extending between the satellite in space to the receiver on the ground. The latter is commonly defined as the total electron content (TEC). TEC, which is measured in units of 10^{16} electrons/m^2, can be expressed mathematically as

$$\mathrm{TEC} = \int N_e ds_0 \tag{3.23}$$

Now, from equations (3.22) and (3.23) it follows according to Hofmann-Wellenhof *et al.* (1992) that:

$$\Delta^{Iono}_{gr} = \frac{40.3}{f^2}\,\mathrm{TEC} \tag{3.24}$$

So the ionospheric group delay (in metres) is proportional to TEC, and inversely proportional to the square of the frequency. A linear combination of the measured pseudorange and phase observables recorded by the receiver on the two L-band carrier frequencies is used to quantify GPS-derived TEC measurements. A similar expression can be derived for the phase delay, but a negative sign is introduced in accordance with equation (3.16). TEC is usually expressed in TEC Units (TECU), where 1TECU $= 1 \times 10^{16}$ electrons/m^2.

The slant TEC (sTEC) which is determined along the line-of-sight of the signal path can be mapped to vertical TEC (vTEC) by using a single layer ionospheric model. The mapping is done by applying a cosec transform considering the geometry in Figure 3.3 (Hofmann-Wellenhof *et al.*, 1992):

$$\text{sTEC} = \frac{\text{vTEC}}{\cos z'}, \qquad \sin z' = \frac{R_e}{R_e + H} \sin z \tag{3.25}$$

where R_e is the Earth's radius (6 378.13 km), H is the assumed single layer ionospheric shell height of 350 km, and z and z' are the zenith angles at the observation site and sub-ionospheric pierce points (IPPs) respectively.

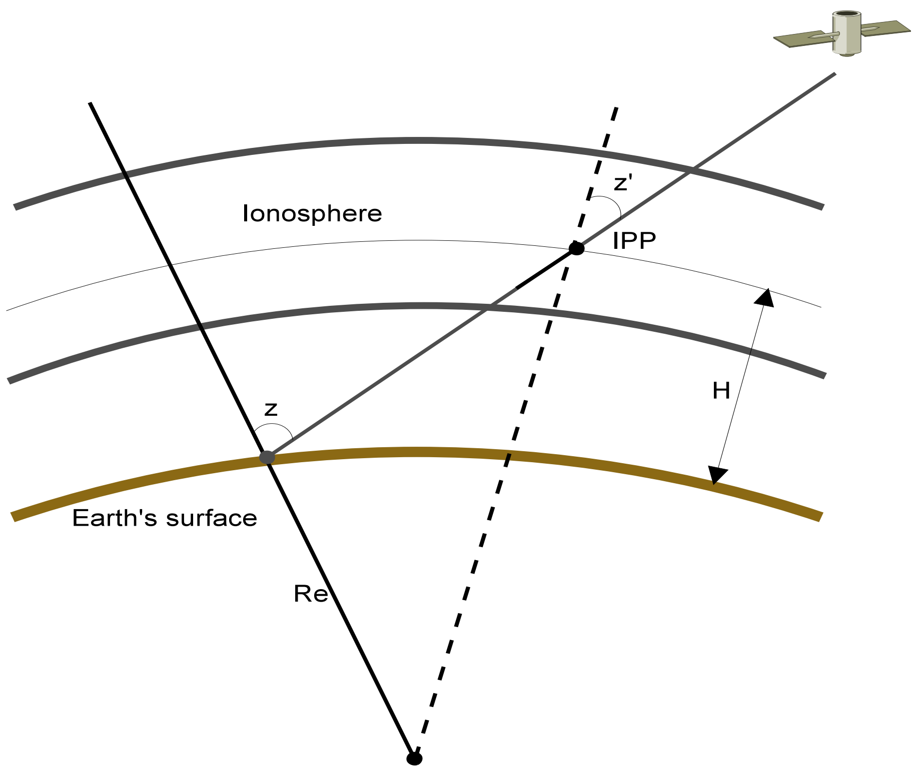

Figure 3.3: The geometry for a signal propagating through the ionosphere.

3.3.4 The ASHA regional TEC algorithm

This study employed GPS-derived TEC measurements obtained by using the Adjusted Spherical Harmonic (ASHA) regional algorithm for South Africa (Opperman *et al.*, 2007). The ASHA algorithm is based on the Schaer (1999) Global Spherical Harmonic Analysis (GSHA) method which is used by the Centre for Orbit Determination in Europe.

Both ASHA and GSHA use observed ionospheric delay measurements along the line-of-sight of the signal path and apply a single-layer mapping function to map computed sTEC to vTEC at the IPPs. Also, both approaches estimate the TEC as a spherical harmonic expansion given by the equation (Opperman *et al.*, 2007):

$$\mathrm{TEC}(\lambda,\phi) = \sum_{n=0}^{N}\sum_{m=0}^{n}\overline{P}_{nm}[cos(\phi)]\{a_{nm}sin(m\lambda) + b_{bm}cos(m\lambda)\} \tag{3.26}$$

where λ and ϕ are the IPP Sun-fixed longitude and co-latitude respectively, $\overline{P}_{nm}$ are the normalised associated Legendre functions, a_{nm} and b_{bm} are the spherical harmonic coefficients, and n and m are the degree and order of the spherical expansion, respectively.

Furthermore, the Sun-fixed longitude used in both AHSA and GSHA has the advantage that it conveniently condenses the IPPs time and longitude parameters into a single angular observation coverage of 360° over a 24 hour period, and thus the spatial and temporal changes of the ionosphere with respect to GPS receivers are taken into account (Opperman *et al.*, 2007). However, the polar angle measured from the North pole (co-latitude) is dealt with differently in the two algorithms.

The GSHA approach does not require a change to the co-latitude as the n wavelengths of the Legendre polynomial are defined over the 180° latitude coverage of a sphere, which is well covered by the IPP observations derived from the International GNSS Services (IGS) global network of GPS ground receivers with a latitude coverage of approximately 175°. However, the latitude coverage of the IPPs from the South African regional GPS network was ∼30° in 2007. This mapped the regionally confined IPPs onto a relatively narrow latitude band on a sphere when combined with the Sun-fixed longitude (Opperman *et al.*, 2007). Thus, to fit the same number of latitude wavelengths into this narrow latitude band would require a sufficiently higher degree spherical harmonic expansion when using the traditional GSHA.

By contrast, the ASHA algorithm applies an approach similar to De Santis *et al.* (1991), which requires transforming and scaling the narrow co-latitude band of the IPPs to a hemisphere using the minimum co-latitude of IPPs, ϕ_0 and the latitude span, θ, of the observations (Opperman *et al.*, 2007):

$$\phi' = \frac{90°}{\theta} \cdot [\phi - \phi_0] \tag{3.27}$$

Therefore, the IPP co-latitude in the equation (3.26) is substituted with the scaled co-latitude, ϕ', which is defined on a hemisphere [0°, +90°]. The slant ionospheric delay (including the biases δ_r, δ_s) then follows from equation (3.15):

$$\Delta\tau_{Iono} = \frac{40.3}{cf_1^2} \cdot \frac{\text{vTEC}}{\cos\varphi} + (\delta_r + \delta_s) \tag{3.28}$$

The separated spherical harmonic representation of the vTEC is then defined as

$$\begin{aligned} \text{vTEC}(\lambda, \phi) = & \sum_{n=0}^{N} \sum_{m=0}^{n} \overline{P}_{nm}[cos(\phi)] \cdot a_{nm} sin(m\lambda) \\ & + \sum_{n=0}^{N} \sum_{m=0}^{n} \overline{P}_{nm}[cos(\phi)] \cdot b_{bm} cos(m\lambda) \end{aligned} \tag{3.29}$$

Making a substitution into equation (3.28) yields

$$\begin{aligned} \Delta\tau_{Iono} = & \frac{40.3}{cf_1^2} \cdot \left(\sum_{n=0}^{N} \sum_{m=0}^{n} \overline{P}_{nm}[cos(\phi)] \cdot a_{nm} sin(m\lambda) \right. \\ & \left. + \sum_{n=0}^{N} \sum_{m=0}^{n} \overline{P}_{nm}[cos(\phi)] \cdot b_{bm} cos(m\lambda) \right) + (\delta_r + \delta_s) \end{aligned} \tag{3.30}$$

The ASHA algorithm estimates vTEC, and compensates for the differential clock and satellite biases. The clock biases from both satellite transmitters and GPS receivers, along with the spherical harmonic coefficients, are determined by a weighted least squares solution.

3.4 Ionospheric scintillation parameters

Fluctuations in the amplitude and phase of radio wave signals are one of the earliest known space weather effects (Yeh and Liu, 1982, and references therein). The fluctuations are commonly referred to as scintillations, which at sufficiently intense levels will degrade the GPS signal quality, reduce its information content or, in some cases, cause failure of the signal reception (Yeh and Liu, 1982; Kintner and Ledvina, 2005; Meggs *et al.*, 2006; Kintner *et al.*, 2007). Understanding the magnetosphere-ionosphere-thermosphere interaction that controls the development of random ionisation density irregularities that cause ionospheric scintillation is one of the top priorities of international space weather programmes (Wernik *et al.*, 2003, 2004). This is due to the significant impact of scintillation on the performance of satellite radio communication and navigation (Doherty *et al.*, 2000; De Paula *et al.*, 2004; Ledvina and Kintner, 2004; Dubey *et al.*, 2005; Kintner *et al.*, 2007).

The term "scintillation" typically implies rapid, random fluctuations of the amplitude and phase of a radio wave signal propagating through the ionosphere (Yeh and Liu, 1982; Wernik *et al.*, 2004). Ionospheric scintillation is characterised by significant spatial and temporal variability. It depends on many factors, that include: the transmission frequency, local time, the season, solar activity, the satellite zenith angle and on the angle between the ray path and the Earth's magnetic field (Wernik *et al.*, 2004).

3.4.1 Ionospheric scintillation theory

One of the most widely used scintillation theories is based on the phase screen approach (Rino, 1979a,b; Yeh and Liu, 1982; Wernik *et al.*, 2004, and references therein). Assume an incident plane wave with a uniform amplitude. For a wave propagating through an irregularity layer, the ionosphere is modelled as an infinitely thin layer (phase-changing screen) which alters only the phase of the wave (Yeh and Liu, 1982), as depicted in Figure 3.4. Therefore, a wave emerging from the irregularity layer (screen) with induced phase perturbations, will manifest amplitude and phase scintillations.

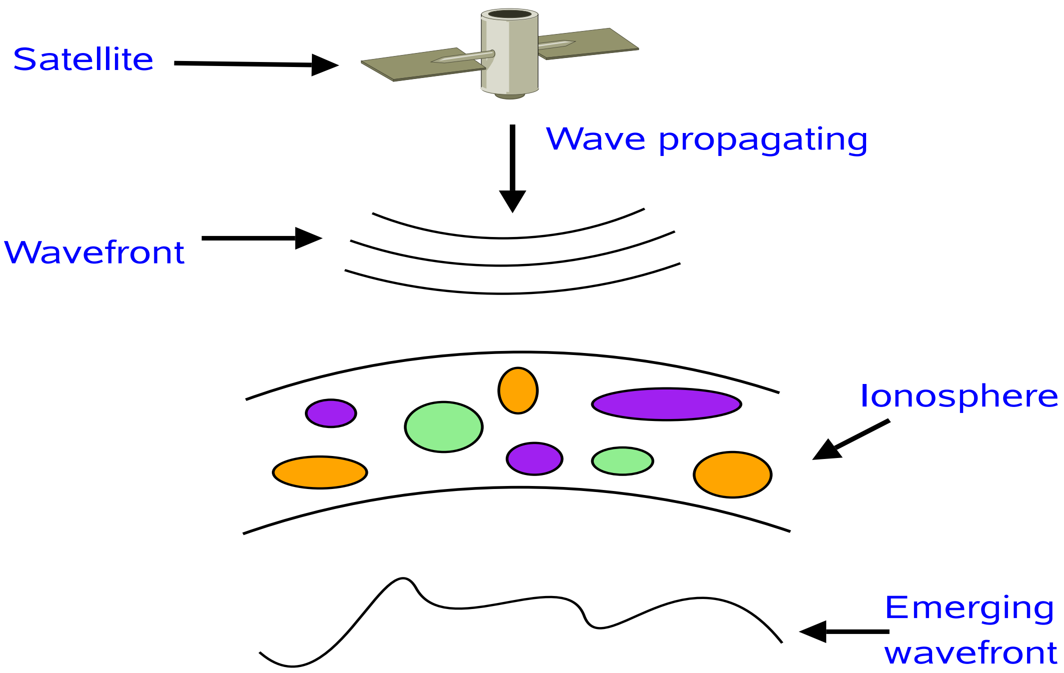

Figure 3.4: A schematic illustrating how ionospheric irregularities impact the propagation of radio waves.

To elaborate on this further, consider a region of randomly distributed electron density located at $z = 0$ to $z = L$, where z is the height of the upper boundary of the irregular layer, and L is the layer thickness. An incident plane wave enters the irregular layer at point $z = 0$, before it is received on the ground. For this wave propagating through the irregular layer, to first order, only the phase will be affected by the random variations in the refractive index (Yeh and Liu, 1982). As the wave emerges from the irregularity layer and propagates towards the receiver, further phase mixing occurs, which randomly modulates the phase front and eventually produces a complex diffraction pattern on the ground that leads to amplitude scintillation. This interference (diffraction) pattern will depend on the random deviations of the curvature of the phase front, which in turn is dependent on the size and strength of irregularity distributions.

According to Yeh and Liu (1982), geometric calculations show that the most significant contribution to amplitude scintillation on the ground is from phase front deviations caused by irregularities with a scale-size of the order of the first Fresnel zone $d_F = \sqrt{\lambda(z - L/2)}$, where λ is the incident signal's wavelength. The description above basically explains the amplitude scintillation phenomenon under small phase deviations and a coherent wave front across each irregularity acting to focus or defocus the rays. In contrast, in the presence of strong irregularities, the phase deviations may become so large that the phase front is distorted across irregularities greater than a certain size. For such a case, the irregularities no longer have the potential to focus or defocus the rays, and the amplitude fluctuation argument above is rendered invalid. In this case, the original plane wave will not be distorted, but the observed phase at the receiver will change as the integrated phase shifts across the medium changes.

Therefore, the scintillation theory attempts to quantitatively investigate the various aspects of this phenomenon. Basically, the starting point for radio wave propagation through a random scattering medium is effectively Maxwell's equations. This process begins by deriving the scalar wave equation, which represents wave propagation in an irregularly scattering medium where it is assumed that the temporal fluctuations of the irregularities are much slower than the wave period and have scale-sizes much greater than the wavelength of the wave (Yeh and Liu, 1982). This can be expressed in terms of the scalar Helmholtz wave equation:

$$\nabla^2 \mathbf{E} + k^2[1 + \epsilon_1(\vec{r})]\mathbf{E} = 0, \qquad 0 < z < L \tag{3.31}$$

where $\mathbf{E}$ is the electric field component, ϵ_1 is the dielectric permittivity defined by a field of density irregularities, k is the electric field wave vector, and $\vec{r}$ is the vector representing the location of the irregularities. It is important to note that since the solutions to equation (3.31) are a function of the wave number, which is inversely proportional to the wave frequency, the ionospheric scintillations of the signals at two unique frequencies broadcast from the same satellite will be affected differently by the irregularities (Kintner *et al.*, 2007).

So, the phase screen model helps to greatly simplify the general problem of wave propagation in a randomly scattering medium, and is a very useful practical tool which provides a means of computing unique, equivalent statistical parameters to characterise irregularity structure along the propagation path (Rino, 1979a; Kintner *et al.*, 2007).

3.4.2 Amplitude and phase scintillation

The intensity of the amplitude scintillation activity is usually quantified in terms of the S_4 index. The S_4 index is defined as the normalised standard deviation of the signal intensity or power determined over a period of time, and can be expressed as (Yeh and Liu, 1982):

$$S_4 = \sqrt{\frac{< I^2 > - < I >^2}{< I >^2}} \tag{3.32}$$

where I is the signal intensity and $<>$ indicate the mean value of the quantity taken over a given interval.

Ionospheric phase scintillation is produced by ionospheric irregularities with small wave numbers and close to the first Fresnel radius. Irregularities with small wave numbers are regarded as being refractive. Scintillation associated with refractive irregularities is produced by fluctuations in the integrated electron density (TEC) along the signal path, while scintillation caused by irregularity structures with size near the first Fresnel radius is produced through interference by different phases leaving the thin diffractive layer (Kintner *et al.*, 2007).

Phase scintillation levels are measured using the σ_ϕ index, which is defined as the standard deviation of the signal phase, ϕ, in radians. This is expressed mathematically in the form (Beach, 2006):

$$\sigma_\phi^2 = < \phi^2 > - < \phi >^2 \tag{3.33}$$

When processing the σ_ϕ index, it is crucial to take into account that the index is sensitive to data detrending approaches, which may introduce receiver clock noise or GPS satellite motion, as discussed by Forte and Radicella (2002). Also, Forte (2005) and Beach (2006) show that failure to adequately take irregularity dynamics into account may result in false conclusions. Furthermore, Beach (2006) recommends the development of suitable alternative measures, a process which needs careful consideration of the elements of scintillation and their impact.

Theoretically, the S_4 index for amplitude scintillation saturates at unity, while σ_ϕ can increase indefinitely, because there is no defined upper limit. However, both S_4 and σ_ϕ are normally computed from raw data over a 1-minute interval. This time interval could be arbitrarily larger or smaller, bearing in mind that the time interval must be long compared to the Fresnel length divided by the irregularity drift speed (Kintner *et al.*, 2007). Intense S_4 levels can cause signal power fades below threshold limits, which lead to receiver loss of lock on signal and cycle slips. Strong σ_ϕ levels could also cause loss of lock when the Doppler shift exceeds the phase lock loop bandwidth. During such times, GNSS positioning can be impaired (Basu *et al.*, 2002).

3.5 Ionosonde and GPS infrastructure in South Africa

Currently, South Africa has a GPS reference station network comprising a Trignet network of fifty-five Trimble NetRS receivers operated by the Chief Directorate: National GEO-Spatial Information (formerly the Chief Directorate: Surveys and Mapping, www.trignet.co.za), and three IGS receivers maintained by the Geodesy group at the Hartebeesthoek Radio Astronomy Observatory. The Trignet GPS receivers record dual-frequency observables at 1-second intervals and the IGS receivers at 30-second intervals, thus making it possible to monitor rapid variations in the ionospheric TEC.

South Africa also operates four ionosonde field stations, located at Hermanus, Grahamstown, Louisvale and Madimbo. Each of these field stations has a Digisonde, which continuously records the ionospheric behaviour, and a co-located GPS dual frequency receiver. The Digisondes are pulse ionospheric sounders developed and manufactured by the University of Massachusetts Lowell Centre for Atmospheric Research (UMLCAR). Figure 3.5 shows the locations of the four ionosonde sta-

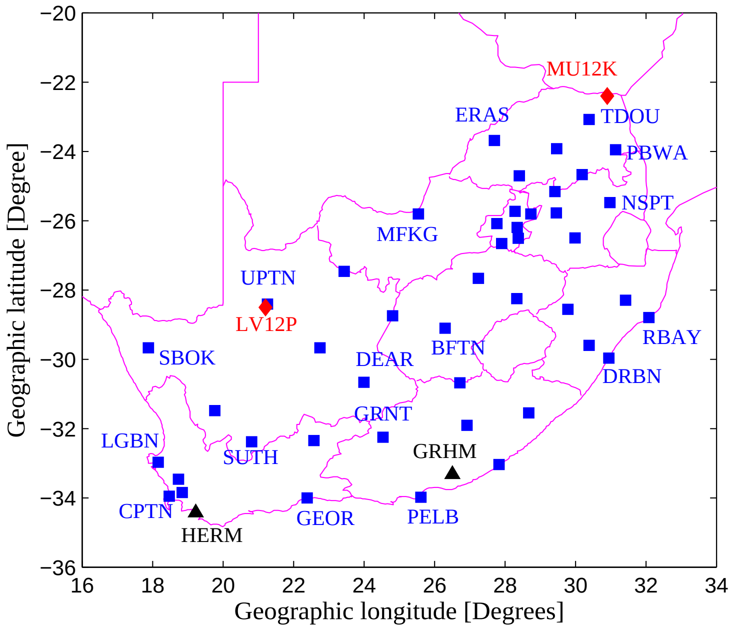

Figure 3.5: Location of GPS and ionosonde stations across South Africa. Red diamonds are ionosondes stations, blue squares are GPS reference stations, and black triangles are stations with co-located ionosondes and GPS receivers.

tions and part of the GPS network of receivers.

Furthermore, South Africa has a network of four GPS Ionospheric Scintillation and TEC Monitors (GISTM) located on Marion Island and Gough Island, at SANAE-IV Antarctic research station, and at the Hermanus field station (installed May 2010). However, data from the Hermanus station is not part of the present study. The SANAE-IV receiver was installed as a project of the International Polar Year (IPY 2007-2009). One focus of the IPY was to conduct multi-instrument investigations of the high-latitude ionosphere (Alfonsi *et al.*, 2008). The receivers, which are maintained by the SANSA Space Science Directorate (formerly Hermanus Magnetic Observatory), have been operational since December 2006 (SANAE-IV), April 2007 (Marion Island) and September 2008 (Gough Island). The geographical longitudes (GLON) and latitudes (GLAT), and the magnetic longitudes (MLON) and latitudes (MLAT) of the GPS, GISTM and ionosonde sites that were used in this study are listed in Table 3.1.

Table 3.1: GPS, GISTM and ionosonde stations that provided data for this study.

Location	Code	Geo. Lat	MLAT	Geo. Lon	MLON
GPS stations					
Bloemfontein	BFTN	29.1°S	38.9°S	26.3°E	91.9°E
Cape Town	CPTN	34.0°S	42.7°S	18.5°E	81.7°E
George	GEOR	34.0°S	43.0°S	22.4°E	85.7°E
Graaff Reinet	GRNT	32.3°S	42.0°S	24.5°E	88.7°E
Kimberley	KLEY	28.7°S	39.6°S	24.8°E	90.5°E
Langebaan	LGBN	33.0°S	42.1°S	18.1°E	81.8°E
Mafikeng	MFKG	25.8°S	37.6°S	25.5°E	92.4°E
Nelspruit	NSPT	25.5°S	37.1°S	30.9°E	98.1°E
Port Elizabeth	PELB	34.0°S	42.4°S	25.6°E	90.0°E
Pretoria	PRET	25.7°S	37.4°S	28.3°E	95.3°E
Richards Bay	RBAY	28.8°S	39.7°S	32.1°E	97.9°E
Springbok	SBOK	29.7°S	39.9°S	17.9°E	82.9°E
Ionosonde stations					
Grahamstown	GR13L	33.3°S	42.8°S	26.5°E	90.2°E
Hermanus	HE13N	34.4°S	43.1°S	19.2°E	82.2°E
Louisvale	LV12P	28.5°S	39.4°S	21.2°E	86.7°E
Madimbo	MU12K	22.4°S	34.5°S	30.9°E	99.1°E
GISTM stations					
Gough Island	GOUGST1	40.3°S	42.2°S	09.9°W	49.9°E
Marion Island	MARGST1	46.9°S	52.8°S	37.9°E	93.3°E
SANAE-IV	SANGST1	71.7°S	66.0°S	02.8°W	43.1°E

The GISTMs are modified Novatel GSV4004 GPS receivers that can simultaneously track up to 11 satellites at L1 and L2 frequencies, at a 50 Hz sampling rate. All the GISTM receivers record both L1 amplitude and phase scintillation indices at 1-minute intervals, in the form of S_4 and σ_ϕ respectively (see Van Dierendonck *et al.*, 1996). These receivers were initially set to log TEC, S_4 and σ_ϕ derived from 50 Hz data at 1-minute intervals, but have also been logging raw 50 Hz data since January 2009. To minimise multipath effects on the GPS data, only scintillation and TEC values for satellites above a 30° elevation angle cut-off were used for the present study.

A riometer (Relative Ionospheric Opacity Meter) was installed in the vicinity of the GISTM system at the SANAE-IV station in Antarctica, by the Space Physics group of the NorthWest University in South Africa, and is currently maintained by SANSA Space Science. Beamforming riometers are a valuable and powerful tool for remote sensing of the ionosphere (Rodger and Jarvis, 2000, and references therein) and are well suited for observing the smaller-scale structures and dynamics of polar cap absorption events, substorms and the ionospheric footprint of the interplanetary magnetic field (IMF) (Stauning, 1996; Wilson, 2000).

3.6 Satellite-based instrumentation

3.6.1 The DMSP instruments and data

The Defense Meteorological Satellite Program (DMSP) of the US Air Force was approved in August 1961 for the purpose of providing weather observations by satellite. Since then, a number of DMSP satellites have been launched to investigate the Earth's environment at an altitude of 830 km in sun-synchronous (inclination ~99 degrees) near-polar orbits, with a period of 101 minutes. DMSP satellites fly in one of two local time configurations: approximately dawn-dusk and roughly 0930-2130 LT. Basically DMSP satellites have a variety of on-board sensors, but only two of these sensors (SSJ/4 and SSI/ES) are of interest for the present study.

DMSP SSJ/4 data covers a complete energy spectrum of the low energy particles that are responsible for the aurora and other high-latitude phenomena. The data comprises electron and ion particle fluxes between 30 eV and 30 keV, recorded by using four electrostatic analysers at 1-second resolution and also comprises satellite ephemeris and magnetic coordinates where the particles are likely to be absorbed by the atmosphere. The SSJ/4 instruments were designed to measure the flux of charged particles entering the Earth's upper atmosphere from the near-Earth space environment. The SSJ/4 archive data is processed on-board the satellite and at the National Geophysical Data Center (NGDC). The DMSP particle detectors were designed by Dave Hardy of the Air Force Research Laboratory in USA.

DMSP SSJ/4 data is used extensively in space physics research, monitoring of the space environment and space weather forecasting. The data sets have been used to investigate the electron and ion features of the aurora, and to characterise or model the polar cap, the polar cusp, and the auroral zone (e.g. Hardy *et al.*, 1985). The data has also been used to mapout the equatorward boundary of the auroral zone, to specify the structure of the high-latitude ionosphere and neutral atmosphere, and in investigations dealing with the cause of satellite anomalies.

The SSI/ES instrument is a modified version of the Special Sensor for Ions and Electrons (SSI/E). The SSI/E instruments took measurements of the ambient electron density and temperatures, the ambient ion density, and the mean ion temperature and molecular weight at the DMSP orbital height. The instrument comprises an electron sensor (Langmuir probe) and an ion sensor secured on a 2.5 metre platform. The ion sensor is a planar aperture and planar collector sensor and is always positioned along the spacecraft velocity vector. The DMSP SSI/ES sensor coordinates are such that the x vector is in line with the satellite velocity, y lies in the horizontal direction ($\sim$ east-west), and z lies in the vertical direction. The SSI/ES instrument includes a plasma drift meter and a scintillation meter, in addition to the Langmuir probe and planar collector which make up the SSI/E. Improved versions of the SSI/ES (SSI/ES-2) are planned for flights on vehicles through S-20. Further details on all the DMSP instrumentation can be found on the DMSP websites (http://www.ngdc.noaa.gov/dmsp/ or http://cindispace.utdallas.edu/DMSP/faq.htm#2).

3.6.2 TOPEX and JASON-1 satellite data

The TOPEX (TOPographic EXplorer) and JASON-1 satellites were designed to take measurements of the changing topography of the ocean, and therefore, do not provide data over landmasses. They were designed as a collaborative project of NASA Jet Propulsion Laboratory (JPL) in the United States and Centre National d'Etudes Spatiales (CNES) in France. The TOPEX/JASON-1 satellites have an orbital period of about 112.42 minutes, with a 66° inclination circular orbit at an altitude of 1336 km and provide about 95% full geographic coverage of the Earth's oceans roughly every 10 days.

TOPEX/JASON-1 operate in the Ku-band (13.6 GHz) and the C-band (5.3 GHz) using a dual-frequency altimeter. The measured range delay difference between the two frequencies is used to estimate the ionospheric vertical TEC from the satellite to the surface of the ocean. The reader should refer to Imel (1994) for detailed information about the TOPEX/JASON-1 satellites.

3.6.3 The Advanced Composition Explorer (ACE)

The ACE satellite was launched in August 1997 and contains six high resolution spectrometers and three monitoring instruments that together measure the low-energy particles of the solar wind and high-energy galactic particles (Stone *et al.*, 1998). The ACE orbits the Earth-Sun L1 libration point which is ∼1.5 million km sunward of Earth and ∼148.5 million km from the Sun. ACE is in direct view of the higher energy particles originating from the Sun, as well as heliospheric, galactic and extra-galactic particles. Therefore, the ACE satellite provides near-real-time 24/7 continuous coverage of solar wind parameters and solar energetic particle intensities (space weather), and provides an advance warning (about one hour) of geomagnetic storms that can severely impact the performance and integrity of space-borne and ground-based technological systems, and can endanger human life or health.

The ACE satellite was lauched with the primary objective of analysing and comparing the elemental and isotopic composition of a number of distinct samples of matter, including the solar corona, the interplanetary medium, the local interstellar medium, and galactic matter. Matter from the Sun is examined by determining the composition of the solar wind, of the coronal mass ejections (CMEs), and of solar energetic particles (for more details see Stone *et al.*, 1998). The ACE data used in this study includes: solar wind speed and ram pressure, proton density, proton temperature and the solar wind total magnetic field and Bz-component.

3.7 Summary

The various instruments and data sources for this thesis were highlighted in this chapter. Both space- and ground-based observations can be used to study the effects of space weather events on the TEC and plasma density of the ionosphere. Dense networks of ground-based GPS receivers across the world have been used in the investigation of GPS ionospheric TEC. Table (3.2) provides a list of the instruments discussed in this chapter, and also provides a useful reference for each instrument and an important URL or name of organisation responsible for managing the data.

The next chapter takes a look at some of the solar-terrestrial phenomena usually associated with geomagnetic disturbances, with more emphasis place on ionospheric and thermospheric phenomena. These phenomena are important for understanding the discussions in later chapters of this thesis.

Table 3.2: List of instruments, including the name, useful reference and the URL of or name of organisation responsible for data management.

Name of instrument	Useful reference	Data management
Ionosondes	McKinnell (2008)	SANSA Space Science
GPS receivers	Ngwira *et al.* (2011b)	www.trignet.co.za or www.hartrao.ac.za/geodesy
GISTM receivers	Van Dierendonck *et al.* (1996)	SANSA Space Science
Riometers	Wilson (2000)	SANSA Space Science
DMSP	Hardy *et al.* (1985)	www.ngdc.noaa.gov/dmsp
TOPEX/JASON-1	Imel (1994)	www.altimetry.info/
ACE	Stone *et al.* (1998)	http://cdaweb.gsfc.nasa.gov/

Chapter 4

Solar-Terrestrial disturbance phenomena

4.1 Introduction

This chapter looks at a number of solar-terrestrial phenomena which contribute to the deviation of the ionospheric electron density from the background conditions in association with geomagnetic disturbances. Some knowledge of these fundamental processes and driving mechanisms is necessary to understand the results of this research, their interpretation and discussion.

4.2 The Sun, solar wind and IMF

The Sun, a primary source of space weather, has a magnetic field which varies approximately with the 22-year solar cycle that is characterised by a reversal of the magnetic polarity. This magnetic field is associated with a number of observable phenomena that occur on the solar surface such as sunspots, solar flares, CMEs, prominences and filaments.

Sunspots are regions on the Sun's surface which have lower temperatures than their surroundings and thus appear as dark spots relative to their surroundings (Kivelson and Russell, 1995). The number of sunspots visible on the solar surface varies with an 11-year sunspot cycle, which is marked by increased (solar maximum) or decreased (solar minimum) solar activity. Figure 4.1 shows the monthly

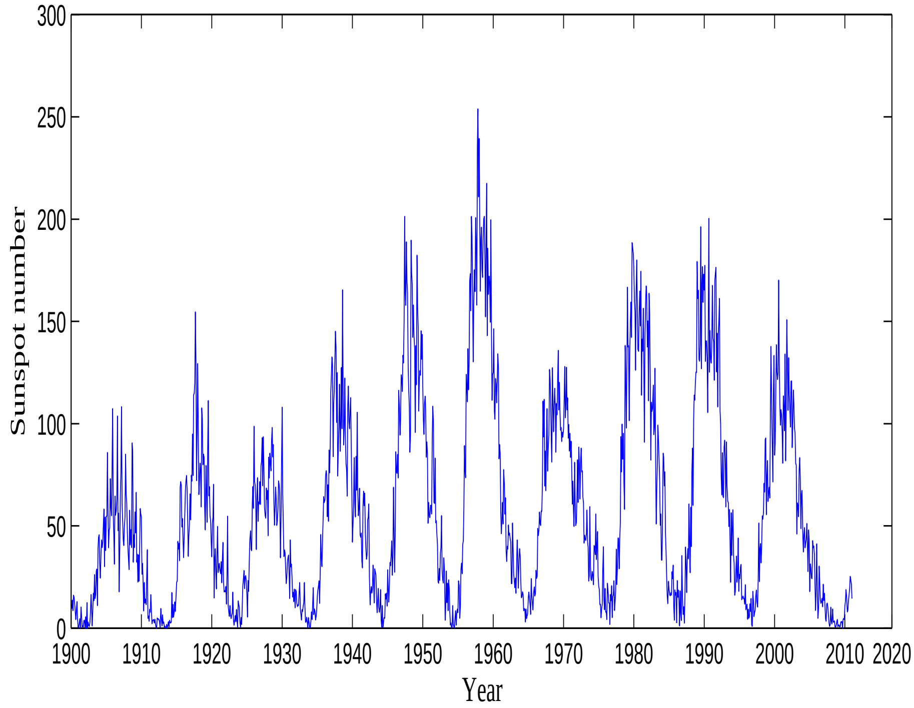

Figure 4.1: Monthly sunspot number from January 1900 to December 2010. Data available on the NOAA ftp site: ftp://ftp.ngdc.noaa.gov.

sunspot numbers from 1900 to 2010, with clearly defined cycles.

The solar wind is the outflow of plasma from the Sun's surface into interplanetary space. High speed solar winds interacting with the Earth's magnetic field can produce large geomagnetic storms in the Earth's magnetosphere depending on the composition of the solar wind parameters (see Lopez *et al.*, 2004). Associated with the solar wind is the interplanetary magnetic field (IMF), which is part of the Sun's magnetic field. Due to the rotation of the Sun, the IMF travels outward in a spiral pattern originating from regions on the Sun where open magnetic field lines emerging from one region do not return to a conjugate region, but instead extend indefinitely into space.

The IMF is described by three orthogonal component directions Bx, By, and Bz. The directions of the IMF are important for the study of the coupling of the solar wind with the magnetosphere/ionosphere. Campbell (1997) reports that the accepted model of the IMF supposes that, when the southward-directed IMF ($-$Bz) encounters the northward-directed geomagnetic field, then the field lines interconnect, distorting the Earth's dipole field and providing entry of the solar wind particles into the magnetosphere through the process of magnetic reconnection. Therefore, a southward Bz-component (Bz < 0) becomes the requirement for the initiation of major magnetic disturbances on the Earth (Campbell, 1997; Richardson *et al.*, 2001; Rosenqvist *et al.*, 2005). During reconnection, there is an increased energy input into the magnetosphere which initialises the conditions for dynamic changes within the magnetospheric current systems.

CMEs are a discharge of huge amounts of plasma from the surface of the Sun into interplanetary space. The occurrence of CMEs is associated with solar magnetic field lines that open up into interplanetary space, and can take place at any time during the solar cycle (Campbell, 1997, Chapter 3). However, the rate of CME occurrence increases with increasing solar activity which tends to peak during solar maximum (Campbell, 1997; Richardson *et al.*, 2001). Observations reveal that Earth-directed CMEs that evolve into interplanetary CMEs (ICMEs) are the major cause of intense geomagnetic storms at the Earth (Richardson *et al.*, 2000; Srivastava and Venkatakrishnan, 2004; Gopalswamy *et al.*, 2005). However, it should be pointed out that not all Earth-directed CMEs are responsible for major geomagnetic storms. Srivastava and Venkatakrishnan (2004) have shown that the intensity of geomagnetic storms is strongly influenced by the southward component of the IMF, followed by the initial speed of the CME and the solar wind ram pressure. However, the main solar factors that determine the geoeffectiveness of CMEs are not fully understood, as there is no sufficient information to characterise the solar sources of strong geomagnetic storms and their interplanetary properties. This is a complex situation which has implications for space weather forecasting, i.e. a good understanding of such characteristics would help in forecasting the occurrence of strong geomagnetic storms well in advance.

4.2.1 Magnetospheric electrodynamics

The magnetosphere can be viewed as the region of space in which the Earth's magnetic field dominates the IMF. The dynamics of the plasma and energetic particles within the magnetospheric cavity are strongly influenced by the geomagnetic field. The magnetosphere extends away from the Earth for several Earth radii with the ionosphere as its lower boundary (Matsushita and Campbell, 1967; Walker, 2005). The formation and extent of the outer region of the magnetosphere are mostly determined by its interaction with the solar wind (Figure 4.2), which is its primary source of energy (Kelley, 2009). Therefore, solar activity has a strong influence on the shape and size of the magnetosphere on both the dayside (sunward) and nightside (anti-sunward), and is the main driver of phenomena such as the aurora, geomagnetic storms and substorms.

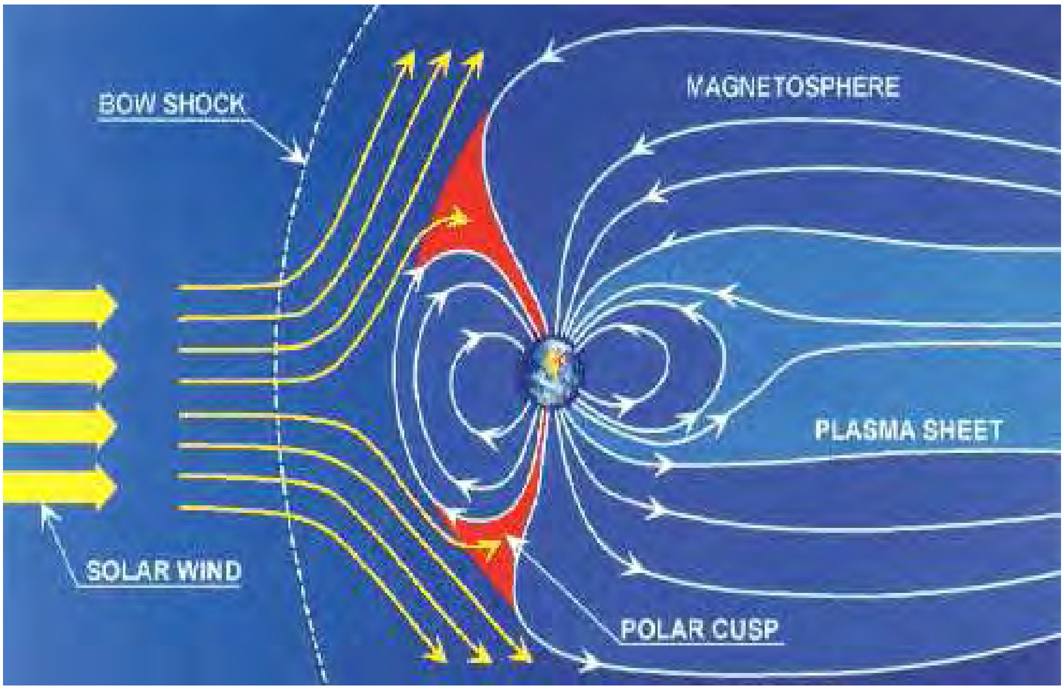

Figure 4.2: Solar wind and magnetosphere interaction. Image courtesy smsc.cnes.fr/OVH/

The coupling between the magnetosphere and the ionosphere is important because it allows for the transfer of a large amount of energy into the ionosphere and at the same time the ionosphere provides an inner boundary. For IMF −Bz the convection in the magnetosphere is largely driven by reconnection at the dayside magnetopause. The newly reconnected magnetic flux is convected over the polar caps and added to the magnetotail lobes (Walker, 2005). Reconnection in the magnetotail then closes the flux again and the closed magnetic flux is transported azimuthally around the Earth to the dayside to restart the cycle. However, this is a simplified model that is well suited to illustrate the coupling aspects.

Basically, traditional magnetosphere-ionosphere coupling models assume a stationary state. For such a case $\partial/\partial t = \nabla \times \mathbf{E}$ assumes that the F-region electric field ($\mathbf{E}$) can be derived from a potential $\mathbf{E} = -\nabla\,\phi$, whereas $\mathbf{E} \cdot \mathbf{B} = 0$ assumes that this potential is constant on geomagnetic field ($\mathbf{B}$) lines and maps into the ionosphere (Walker, 2005). Induction currents, which are caused by the solar wind's electric field ($\mathbf{E} = -v \times \mathbf{B}$) imposed onto the Earth's magnetosphere, are the physical origins of geomagnetic activity that results in a complex system of magnetospheric and ionospheric current systems (McPherron, 1979).

Enhanced energy injection at high latitudes, commonly associated with geomagnetic storms, can result in a significant modification of the quiet-time global ionospheric structure and composition, which in turn induces regional structuring and instability in ionospheric plasmas and neutral constituents. The source mechanisms for such dramatic restructuring of the mid- and low-latitude ionospheric plasma probably involve electrodynamic processes and transport, as well as chemical processes, and therefore, magnetospheric/ionospheric electrodynamics are of principal importance in understanding and interpreting such observations (Scherliess and Fejer, 1997; Fejer *et al.*, 2007; Maruyama *et al.*, 2007).

The two principal electric fields which cause ionospheric disturbances are: (1) the prompt-penetration electric fields associated with magnetospheric convection (Fejer and Scherliess, 1995; Foster and Rich, 1998; Kelley *et al.*, 2003; Tsurutani *et al.*, 2004), and/or (2) the ionospheric disturbance dynamo electric fields, driven by Joule heating at auroral latitudes which changes the global circulation pattern in the thermosphere and the ionosphere (Blanc and Richmond, 1980; Fejer and Scherliess, 1997). The extensive number of multi-instrument observations, put to use in first-principle modelling, has resulted in a good understanding of how, individually and together, these two sources regulate the mid- and low-latitude ionosphere.

Penetration of magnetospheric electric fields to low latitudes occurs in response to large and rapid IMF-driven changes in the strength of magnetospheric convection, when there is a momentary lapse of equilibrium between the convection-related charge density and the charge density in the Alfvén layer (Fejer *et al.*, 2007). These electric fields are attributed to changes in the strengths of the region 1 and region 2 Birkeland (field-aligned) current systems, which are required for shielding the inner magnetosphere and mid- and low-latitude ionosphere from the complete effect of the dawn-dusk magnetospheric convection electric field (Fejer *et al.*, 2007; Maruyama *et al.*, 2007). However, when convection suddenly increases/decreases, mainly caused by the southward turning of the IMF Bz-component, which in turn leads to an increase in the cross-polar cap potential drop, the shielding mechanism fails to protect the mid- and low-latitude ionosphere from the effects of the convection-driven electric field (Maruyama *et al.*, 2007). Therefore, these electric fields can perturb the ionosphere nearly simultaneously ("prompt-penetration") from middle to equatorial latitudes. Wolf *et al.* (2007) provide a comprehensive review of inner magnetospheric electrodynamics, including the effects of undershielding and overshielding.

By contrast, the disturbance dynamo electric field effects manifest in time scales of a few hours to days (Blanc and Richmond, 1980; Mazaudier and Venkateswaran, 1990), and can be distinguished from the prompt-penetration electric fields based on these long time scales (Scherliess and Fejer, 1997). However, it should be noted that long-lasting penetration of magnetospheric electric fields, which is associated with long-lived geomagnetic disturbances, was reported in some recent studies (Huang and Foster, 2005; Maruyama *et al.*, 2007). On the other hand, Scherliess and Fejer (1997) report of fast-occurring disturbance dynamo electric fields (about 2-3 hours after significant increase in convection), which are most likely driven by the dynamo action of high velocity equatorward wind surges (Fuller-Rowell *et al.*, 2002).

On the dayside, the prompt-penetration electric field moves eastward during dawn-dusk and the associated upward $\mathbf{E} \times \mathbf{B}$ plasma drift, where $\mathbf{E}$ is the F-region electric field, uplifts the ionospheric plasma to higher altitudes where chemical recombination is less prevalent. At the same time, increased solar radiation aids the formation of new electron-ion plasma at lower altitudes, thus leading to an overall increase in dayside ionospheric plasma (Foster and Rich, 1998; Tsurutani *et al.*, 2004; Heelis *et al.*, 2009). By contrast, model predictions by Blanc and Richmond (1980) revealed that the ionospheric disturbance dynamo electric field moves westward on the dayside and eastward on the nightside, i.e. opposite to the quiet-time dynamo electric field daily variations. The disturbance dynamo effects, through plasma transport, can cause depletion of ionospheric plasma on the dayside (Tsurutani *et al.*, 2004) and can also suppress the equatorial ionisation anomaly (EIA) peaks (Fuller-Rowell *et al.*, 2008), whilst on the nightside, strong local time dependence is reported with enhanced upward drifts in the postmidnight sector (Fuller-Rowell *et al.*, 2002, 2008).

4.3 Thermospheric storms and TIDs

During geomagnetic storms, two of the major drivers of ionospheric structures are the electric fields and energy deposits in the auroral ionosphere. In the previous section the electrodynamic effects were discussed, and this section will address the effects of energy deposition in the auroral ionosphere.

High energy deposition in the higher-latitude ionosphere, due to auroral currents and precipitating particles, may drive strong storm-time changes in the neutral air and its composition, which affect the rate of production and loss of ionisation (Fuller-Rowell *et al.*, 1994; Rishbeth, 1998; Buonsanto, 1999; Crowley and Meier, 2008). These storm-time perturbations alter the distribution of ionospheric plasma by producing an increase and/or a decrease in electron density, and constitute the positive or negative storm phases respectively (Fuller-Rowell *et al.*, 1994; Prölss, 1995; Buonsanto, 1999; Mendillo, 2006).

At high latitudes enhanced Joule and particle heating can produce thermal expansion of neutral air following geomagnetic disturbances. This leads to horizontal temperature and pressure gradients. It is followed by an upwelling (positive vertical velocity) across constant pressure surfaces and an increase in molecular constituents, i.e. reduction in the ratio of atomic oxygen density [O] to molecular nitrogen [N_2] and oxygen [O_2] densities. This modifies the neutral composition by increasing the chemical loss rates that in turn lead to a reduction in the ionospheric plasma density (Fuller-Rowell *et al.*, 1994, 1997; Buonsanto, 1999). In addition to the expansion of the neutral air, increased polar thermospheric temperatures create large-scale pressure gradients that drive a global thermospheric circulation (Fuller-Rowell *et al.*, 1994, 1997). The equatorward disturbance winds push plasma up along geomagnetic field lines to higher altitudes where the plasma loss rate is lower, because fewer molecular species are available, and subsequently plasma increases at F-region heights (Fuller-Rowell *et al.*, 1994; Prölss, 1993a, 1995). Conversely, Fuller-Rowell *et al.* (1997) demonstrated that winds and waves can propagate from one hemisphere and penetrate well into the opposite hemisphere. These become known as poleward winds. These poleward winds push plasma to lower altitudes where there are more molecular species. This accelerates the plasma decay by means of enhanced recombination rates, causing a negative storm effect. The dynamic effects of these processes are observed particularly at the F-region heights where the chemical effects are relatively low. They also give rise to the north-south asymmetry in the EIA peaks (Fuller-Rowell *et al.*, 1994).

Equatorward winds on the nightside longitude sector have the strongest response, because they then add to the background day-to-night circulation (Fuller-Rowell *et al.*, 1997; Buonsanto, 1999). Fuller-Rowell *et al.* (1997) identified two factors that strengthen the winds: the location of the longitude sector of the geomagnetic pole, and preference for wind and wave propagation on the nightside. They attributed the weak response on the dayside to the prevailing poleward wind, but also singled out ion-drag due to high plasma density as the most likely cause of rapid dissipation of the wind surge. Buonsanto (1999) associated equatorward winds with enhanced equatorward surges or travelling atmospheric disturbances (TADs) which are driven by impulsive heating events.

TADs are launched by large-scale atmospheric gravity waves (AGWs) driven by high-latitude phenomena such as Joule heating, Lorentz forces, or intense particle precipitations, and are manifested in the ionospheric plasma as travelling ionospheric disturbances (TIDs) (Hines, 1960; Hunsucker, 1982). TIDs play a significant role in the transport of energy and momentum in the ionosphere, as they propagate from the high latitudes to mid- and low-latitudes. TIDs can be categorised as medium-scale (MSTIDs) or large-scale (LSTIDs), depending on their wave parameters such as wavelength, velocity, and period (see review by Hocke and Schlegel, 1996). The LSTIDs are believed to propagate in the thermosphere with horizontal velocities between 400 and 1000 m/s and horizontal wavelengths greater than 1000 km, while, MSTIDs propagate in the lower atmosphere before they can be detected in the ionosphere and are believed to have horizontal velocities between 100 and 250 m/s, with wavelengths of several hundred kilometres (Hocke and Schlegel, 1996).

A number of recent studies were able to infer the physical properties of TIDs particularly using TEC maps derived using dense networks of ground-based GPS receivers (Nicolls *et al.*, 2004; Tsugawa *et al.*, 2007; Ding *et al.*, 2007). An investigation of geomagnetic conjugacy of LSTIDs using GPS networks in Japan and Australia by Tsugawa *et al.* (2006) found that LSTIDs were not associated electromagnetically through the geomagnetic field between the two hemispheres, but were rather generated by AGWs, which independently propagated to lower latitudes. They also concluded that the asymmetry of LSTID appearance at mid-latitudes in the two hemispheres was related to the asymmetry of the auroral energy input, rather than the ionospheric and atmospheric background conditions. Subsequently, Tsugawa *et al.* (2007) showed for the first time, using the North American GPS network that nighttime MSTIDs propagated southwestward with wavelengths of about 200-500 km and wavefronts longer than approximately 2 000 km, whilst daytime MSTIDs had wavelengths of ~300 to 1 000 km and propagated southeastward until mid-afternoon and southwestward in the late afternoon.

4.4 Ionospheric storms

Ionospheric storms are a manifestation of geomagnetic storm events. They represent an extreme form of space weather, which is a cause for concern when it comes to the safety and reliability of increasingly sophisticated space- and ground-based technological systems. As discussed previously, global electrodynamics, neutral winds and subsequent compositional changes in the plasma density following geomagnetic storm activity have a major impact on the quiet-time ionospheric F-region density, and can lead to positive or negative ionospheric storm effects.

At mid-latitudes positive storm effects are more prevalent in winter, and negative storm effects appear more frequently in summer (Fuller-Rowell *et al.*, 1996, 1997; Huang and Foster, 2005). This is attributed to the prevailing summer-to-winter circulation, where the poleward winds restrict the equatorward movement of the composition disturbance in the winter hemisphere (Fuller-Rowell *et al.*, 1996; Buonsanto, 1999). This leads to a decrease of molecular constituents and produces a positive storm effect. On the other hand, the modified neutral-chemical distribution in the summer hemisphere leads to an increase of molecular constituents, which subsequently reduces the F-region electron density in the mid-latitude ionosphere and generates a negative storm effect. The occurrence of positive and neg-

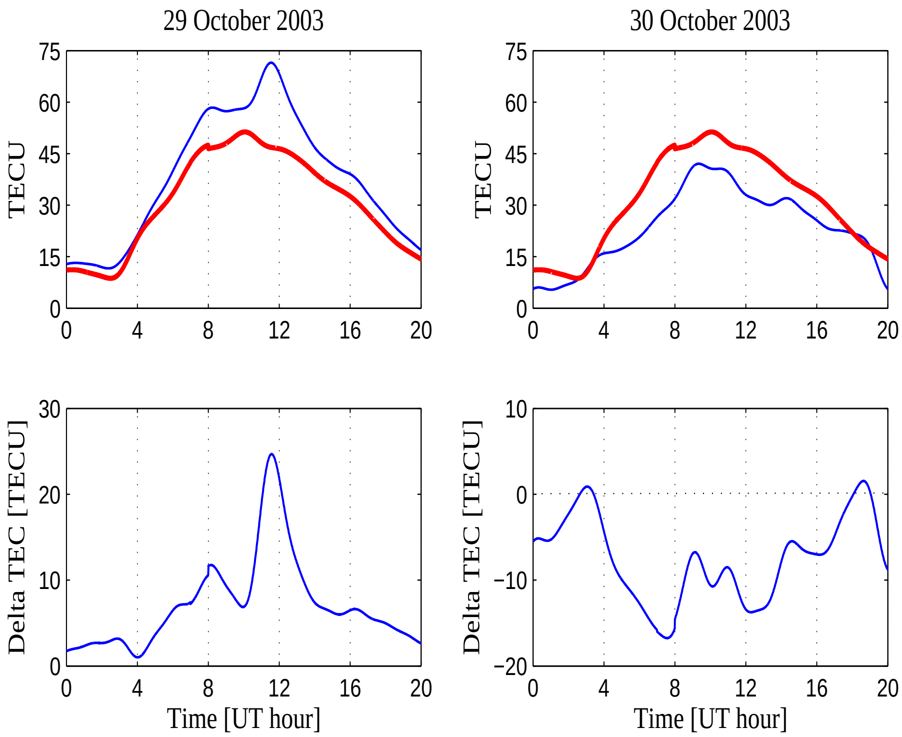

Figure 4.3: An example of a positive (left) and negative (right) ionospheric storm effect on the GPS-derived TEC for the storms on 29 and 30 October 2003, respectively. The top panels show the observed TEC (blue) and the quiet-day mean values (red), while the bottom panels show the relative TEC deviation on the two days, i.e. $\Delta\text{TEC} = \text{TEC}_{obs} - \text{TEC}_{mean}$.

ative storm effects is determined by the season, location of the station (magnetic latitude), local time of the geomagnetic storm onset and the phase of the storm (Fuller-Rowell *et al.*, 1994). Figure 4.3 displays a positive storm effect (left) and negative storm effect (right) on the GPS-derived TEC as observed at Nelspruit, South Africa. The observed TEC (blue) and the quiet-day mean values (red) are shown in the top panels, while the bottom panels show the relative TEC deviation on the two days.

4.4.1 Negative storm effects

The primary driving mechanisms that are thought to be responsible for positive and negative ionospheric storm effects have widely been investigated, helped by recent advances in observational and modelling techniques (Prölss, 1995; Fuller-Rowell *et al.*, 1994; Buonsanto, 1999; Mendillo, 2006; Burns *et al.*, 2007; Pedatella *et al.*, 2009). It is widely accepted that negative storms are generated by neutral composition changes (Prölss *et al.*, 1991; Rishbeth, 1991; Fuller-Rowell *et al.*, 1997; Buonsanto, 1999; Mendillo, 2006). During geomagnetic storms, the energy input from the magnetosphere to the atmosphere is increased, which enhances the Joule heating at high latitudes. This decreases the normal poleward wind on the dayside and strengthens the equatorward wind on the nightside, thereby creating a storm circulation that transports air with increased molecular species to mid-latitudes. Now, it is well established that the F2-layer electron density depends on the neutral air composition and the recombination rate depends on the molecular concentrations (Fuller-Rowell *et al.*, 1997; Rishbeth, 1998). Therefore, an increase in molecular species is associated with an increase in plasma loss rates, which reduces the F-region electron density, causing a negative storm effect.

Nowadays, it has become clear that the negative storm effects are due to a decrease in the [O/N_2] and [O/O_2] neutral density ratios (Rishbeth, 1991; Buonsanto, 1999). Much of the progress towards understanding these responses are due to the combination of *in situ* observations (Prölss *et al.*, 1991; Christensen *et al.*, 2003; Meier *et al.*, 2005; Crowley and Meier, 2008) and theoretical prediction models (Burns *et al.*, 1991; Fuller-Rowell *et al.*, 1996; Richmond *et al.*, 2003).

4.4.2 Positive storm effects

Unlike negative storms, the general understanding of positive storms is still incomplete, with several mechanisms being proposed to explain their generation (Foster, 1993; Buonsanto, 1999; Werner *et al.*, 1999; Huang and Foster, 2005; Pedatella *et al.*, 2009). Positive storms display many characteristics and can be grouped into several classes depending on the duration, local time and latitude. One frequently observed class of positive storm is the daytime short-duration enhancement of the mid-latitude ionospheric electron density. These are usually attributed to atmospheric disturbances resulting from AGWs, that are launched in the high latitudes during storms or substorms and travel to mid-latitudes (Prölss and Jung, 1978; Prölss, 1993a; Werner *et al.*, 1999). As explained earlier in Section 4.2, the equatorward disturbance winds push ionospheric plasma to greater altitudes, and consequently increase the F-region electron density.

In addition to equatorward winds, storm-enhanced eastward electric fields can uplift plasma to higher altitudes where molecular recombination rates are lower, resulting in increased ionospheric F-region electron density (Foster and Rich, 1998; Vlasov *et al.*, 2003; Tsurutani *et al.*, 2004). In the equatorial region such an electric field will lead to an enhanced "fountain effect". As a result, the F-region electron density decreases over the geomagnetic equator, and the electron density at the anomaly regions will be increased (Foster and Rich, 1998; Foster *et al.*, 2005). Since the latitudinal location of the anomaly peaks depends on the strength of the electric field, a strongly enhanced eastward electric field moves the anomaly peaks to higher latitudes (Mannucci *et al.*, 2005; Huang and Foster, 2005; Maruyama and Nakamura, 2007).

Following geomagnetic storms, large enhancements in F-region electron density are usually observed in the local afternoon and evening hours, and thus termed the "dusk effect". Observations by Millstone Hill incoherent scatter radar show that an evening storm enhancement is followed by the equatorward movement of the ionospheric trough (Buonsanto, 1999, and references therein). The dusk effect is believed to be associated with rapid sunward convection of high density plasma from the low latitudes (Foster, 1993). Such a storm-induced enhancement on the equatorward edge of the dusk sector ionospheric trough is commonly known as storm enhanced density (SED) (Foster *et al.*, 2002; Coster *et al.*, 2003). The SED plumes, which are associated with the erosion of the outer plasmasphere after a geomagnetic storm, are known to occur in close proximity to subauroral polarisation stream electric fields (Su *et al.*, 2001; Foster *et al.*, 2002). A study by Buonsanto (1995) suggests that both a wind-induced uplifting and a transfer of plasma originating in the low latitudes could also contribute to the dusk effect. Recently, investigations by Foster *et al.* (2005) revealed that the source of the SED plasma lies in the low latitudes, thus confirming the mechanism earlier suggested by Foster (1993).

It should be noted that earlier reports on SED plumes were all from the North American longitude sector, which led to the assumption that this was the preferential location because of the geomagnetic field layout at these longitudes (i.e. high geomagnetic latitude relative to its geographic location). However, a recent study by Yizengaw *et al.* (2006a), who employed a combination of ground-based GPS-derived TEC, EISCAT incoherent scatter radar, and DMSP F15 ion drift observations, demonstrated that SED features also occur over Europe, and more recently, Yizengaw *et al.* (2008) reported on SED features over other longitudinal sectors.

Another class of positive storms is the long-duration enhancement in the F-region electron density at low and mid-latitudes. The long-duration positive storm effects can occur on a continental scale and last for many hours or days. According to Buonsanto (1999) two primary mechanisms have been proposed to explain the long-duration storm effects: downwelling of neutral atomic oxygen (O) and uplifting of the F2-layer by enhanced equatorward winds. However, recent studies suggest that enhanced eastward electric fields could also play an important role in generating long-duration positive storm effects (Huang and Foster, 2005; Pedatella *et al.*, 2009). In any case, long-duration storm effects are still considered to be one of the major unresolved problems of ionospheric physics (Buonsanto, 1999; Burns *et al.*, 2007), and will be the subject of Chapter 6.

4.5 Ionospheric irregularities

Radio wave scintillation investigations have become one of the most commonly used approaches to sensing ionospheric irregularities, particularly in the E- and F-regions (Basu and Basu Su., 1981; Yeh and Liu, 1982; Basu *et al.*, 1993; Aarons *et al.*, 1997; Kintner and Ledvina, 2005). The ionosphere can generally be considered a continuous layer with a fairly smooth plasma density distribution. However, under disturbed conditions, localised structuring of electron density can develop. This kind of electron density structuring is what is commonly referred to as ionospheric irregularities. The presence of structured irregularities in the ionosphere, resulting from plasma density instabilities, cause scattering of radio waves in the frequency range of 0.1-4 GHz, giving rise to amplitude and phase scintillation (Basu *et al.*, 1988, 2002). Therefore, ionospheric scintillation can be regarded as wave propagation in a random media. Scintillation can severely impact radio signals such as those used by GNSS or HF systems (Yeh and Liu, 1982; Kintner *et al.*, 2001; De Paula *et al.*, 2004; Cervera and Thomas, 2006; Kintner *et al.*, 2007).

On the other hand, since ionospheric scintillation is caused by random electron density irregularities acting as a medium for scattering waves, research on the development and evolution of irregularities is closely related to scintillation studies (Yeh and Liu, 1982; Aarons *et al.*, 1996; Pi *et al.*, 1997; Wernik *et al.*, 2004). Therefore, interpretation of scintillation data is essential for strengthening the understanding of the physics and dynamics of the upper atmosphere. Scintillation effects are most severe in the equatorial region, moderate at high latitudes and generally weak at mid-latitudes (Basu *et al.*, 2002, and references therein). Generally, the levels of scintillation in all latitude regions are at a maximum and more frequent during the solar maximum period, when the F-region electron density increases and the irregularities occur against a background of enhanced ionisation density. However, intense scintillations at low latitudes are also observed during geomagnetically quiet periods (Basu *et al.*, 2002). Therefore, scintillation effects are expected during the upcoming solar maximum period, which is expected to occur between 2012-2014, and are of concern to GNSS applications. The lower frequencies in particular are more severely affected by scintillation, as discussed in Section 3.4.

4.5.1 Equatorial irregularities

The equatorial and low-latitude ionospheric region is one of the most extensively studied regions, as evidenced by widely documented literature (Kelley, 1989; Aarons, 1993; Abdu, 1997; Fejer *et al.*, 1999; De Paula *et al.*, 2003; Dubey *et al.*, 2005; Dashora *et al.*, 2009, and references therein). During the post-sunset period, large-scale irregularities with typical east-west dimensions of several hundred kilometres which contain small-scale irregularities of varying scale-sizes, ranging from tens of kilometres to tens of centimetres, are generated in the equatorial F-region due to plasma density instabilities. The major contributor to their development is the equatorial vertical plasma drift, when the eastward electric field is enhanced due to the action of the F-region dynamo (Fejer *et al.*, 1999; De Paula *et al.*, 2004; De Rezende *et al.*, 2007). The irregularities cause intense scintillation along two belts in the low-latitude region marked by the presence of the EIA with high electron density peaks observed around 13°-18° North and South of the geomagnetic equator. The cause of these equatorial irregularities is linked to the steep electron density gradients present on the edges of the EIA, which are associated with irregularity structures of a smaller scale.

Equatorial irregularities, which manifest on HF radar ionograms as spread F, are generated along the geomagnetic equator after sunset primarily due to the Rayleigh-Taylor plasma instability (Kelley, 1989; Aarons, 1993; Fejer *et al.*, 1999; De Paula *et al.*, 2003, and references therein). After sunset and at the geomagnetic equator, the ionospheric plasma is uplifted by the vertical $\mathbf{E} \times \mathbf{B}$ drift, where the electric field $\mathbf{E}$ during the daytime is mapped from the E-region to the F-region (De Paula *et al.*, 2003; De Rezende *et al.*, 2007). The zonal electric field in the equatorial ionosphere flows eastward during the daytime, producing an upward $\mathbf{E} \times \mathbf{B}/\mathrm{B}^2$ drift velocity. Immediately after sunset, this eastward flowing electric field is enhanced due to conductivity enhancement at the terminator, a process called the pre-reversal enhancement. The plasma from the F-region is then uplifted to higher altitudes, and at the same time the plasma in the low-latitude regions quickly diminishes due to the decreasing intensity of the solar radiation (Kelley, 1989). Following this, the plasma begins to descend (or diffuse) along geomagnetic field lines by the action of gravity (g) and the pressure gradient (∇p) forces. The phenomenon of plasma uplifting and subsequent descent along geomagnetic field lines is called the "fountain effect". This is the origin of the EIA and is illustrated in Figure 4.4.

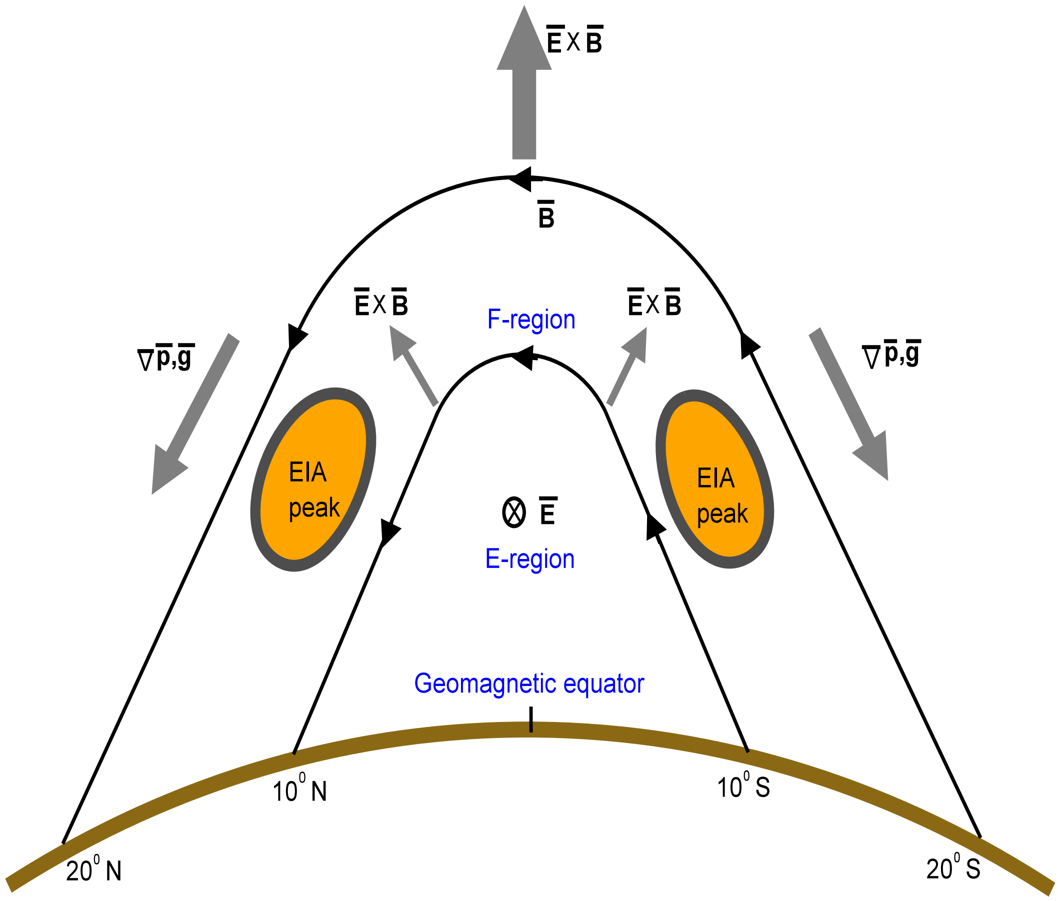

Figure 4.4: Illustration of the equatorial fountain effect and the development of the EIA in the electron density of the F2-layer.

The non-linear development of the Rayleigh-Taylor instability leads to a large spectrum of irregularities of different scale-sizes, which can be investigated by observational techniques that use different signal frequencies (Basu and Basu Su., 1981; De Paula *et al.*, 2004; Cervera and Thomas, 2006, and references therein). At the L1 GPS carrier frequency, it is possible to probe plasma irregularities with scale-sizes of about 400 m. Under favourable ionospheric conditions, these irregularities can grow along geomagnetic field lines reaching continental dimensions and become known as plasma bubbles (Basu and Basu Su., 1981; De Paula *et al.*, 2004; Nishioka *et al.*, 2008).

During geomagnetic storms, strong eastward (or westward) disturbance magnetospheric dynamo electric fields can penetrate to the equatorial region causing enhancement (or weakening) of the upward plasma drift, and thereby trigger (or inhibit) the generation of ionospheric irregularities (Aarons, 1991; De Rezende *et al.*, 2007). The driving mechanism behind the inhibition or generation of irregularities appears to be primarily the height of the F2-layer, with a possible contribution by the pre-reversal drift velocity and the rate of decrease of the layer. According to Aarons (1991), a negative ring current excursion during presunset period can directly or indirectly decrease the local eastward electric field thus reducing the F2-layer height and possibly the downward velocity in the postsunset generation period. Furthermore, Aarons (1991) using equatorial ionospheric data collected from two widely separated stations (i.e. Manila and Huancayo), was able to show that when the maximum ring current energy, as inferred from the Dst index, occurred during the midnight to postmidnight time sector, irregularities were generated. Aarons (1991) furthermore showed that with a minimum Dst in the early afternoon, the irregularities were inhibited, and when the minimum occurred during sunset or shortly after sunset, then there was no notable effect on the formation of irregularities that particular night. Therefore, geomagnetic activity plays a key role in the formation or inhibition of irregularities by changing the progression of events.

4.5.2 Mid-latitude irregularities

In contrast to the equatorial ionosphere, it was long believed that the mid-latitude ionosphere was a less active scintillation region. L-band frequencies were perceived to be devoid of scintillation, as the mid-latitude was assumed to lack the necessary mechanisms generally required for irregularity development (Ledvina and Kintner, 2004). However, studies have shown that the mid-latitude is more complicated than initially thought, and that many different scales of structuring are possible (Ledvina *et al.*, 2002, and references therein). Ledvina *et al.* (2002) explain that these developments suggest that the mid-latitude ionosphere is more active than previously assumed and that the ionospheric/magnetospheric processes responsible for the production of mid-latitude structures are not well understood. Several mechanisms could be the source of mid-latitude irregularities, working separately or in combination (Kelley, 1989; Basu *et al.*, 2005a).

The characteristics of the mid-latitude ionosphere are generally regular, however, during geomagnetic disturbances this predictable variability can be dramatically overturned as the forces which drive the high-latitude region expand equatorward (see reviews by Buonsanto, 1999; Mendillo, 2006). Therefore, the most intense mid-latitude space weather effects often occur after geomagnetic storm events. During such times, steep electron density gradients develop in these regions. The steep gradients are mainly associated with two factors, i.e. the southward movement of the ionospheric trough toward the higher density mid-latitude region, and abutment of plumes of greatly enhanced TEC and high ion flux values, or SED (Coster *et al.*, 2003; Doherty *et al.*, 2004; Foster *et al.*, 2005; Yizengaw *et al.*, 2008). The electron density gradients (as much as 50 TEC/degree) may be vulnerable to instabilities which lead to the development of irregularities. Some studies have shown that VHF and UHF scintillation is frequently observed on the trailing edges of the ionospheric trough and SED plumes, where density gradients are the largest (Bowman, 1991; Basu *et al.*, 2001; Skone *et al.*, 2003; Kintner *et al.*, 2007).

In addition, Basu *et al.* (2005a) have demonstrated that mid-latitude irregularities can also form in association with auroral plasma processes, which appear to take place when the auroral irregularity belt moves equatorward into the mid-latitudes. Furthermore, these authors (Basu *et al.*, 2005a) also observed that scintillation typically occurred at the equatorward edge of the auroral emission, a case strongly favouring an auroral process for the 0.1 to 10 km scale plasma structuring.

4.5.3 High-latitude irregularities

The high-latitude region is an environment of extremely complex and dynamic ionospheric phenomena, which result from the coupling of the solar wind to the Earth's magnetosphere and upper atmosphere. Therefore, the source mechanisms for high-latitude irregularities are not always easy to identify. During the last 40 years, these phenomena have been measured using numerous techniques, e.g. *in situ* satellite observations, rockets, balloons, incoherent scatter radars and many other radio sounding methods. Plasma in the high latitudes exhibits horizontal motions, because the geomagnetic field is nearly vertical in this region (Kelley, 2009).

Several known mechanisms which cause high latitude ionospheric irregularities are soft electron precipitation, $\mathbf{E} \times \mathbf{B}$ gradient drift instability, velocity shears, the current convective and the Kelvin-Helmholtz instability (Keskinen and Ossakow, 1983; Kersley *et al.*, 1988; Kelley, 1989; Aarons, 1997; De Franceschi *et al.*, 2008). For a more comprehensive discussion of the various source mechanisms responsible for high latitude E- and F-region irregularities, the reader is referred to the review paper by Keskinen and Ossakow (1983) and the book by Kelley (1989).

The auroral oval is a typical high latitude feature that results from the interaction between the solar wind and the geomagnetic field. In the auroral regions irregular precipitation of energetic electrons occurs following substorm activity, and during such events, structured depletion/enhancement of TEC are created in the auroral ionosphere, particularly at E-region altitudes of 110 km (Skone *et al.*, 2003). Particle precipitation effects at high latitudes are well documented (Basu *et al.*, 1993; Kersley *et al.*, 1995; Aarons, 1997; Aarons and Lin, 1999; Ngwira *et al.*, 2010). Kelley *et al.* (1982) provides evidence that structured soft electron precipitation is a major source of large-scale ($\lambda \gtrsim 10$ km) F-region irregularities in the high latitudes, and that convection acts to distribute the irregular plasma throughout the polar ionosphere. These large-scale structures become unstable and generate smaller-scale irregularities. Therefore, the resulting spectrum of irregularities generated in the F-region becomes a complex balance of instability growth and damping that depends on E-region events and magnetospheric activity. Furthermore, Kelley *et al.* (1982) proposes that the current convective instability driven by field-aligned currents or electric fields (or both), is an extremely significant process that injects wave energy at the intermediate scale, and that drift waves play a key role at smaller scales.

In the polar cap region, the auroral oval plays a significant role in the generation of large-scale ionospheric F-region structures called patches (Basu *et al.*, 1998). A wide range of studies reveal that during active geomagnetic events, the cross polar cap electric field on the dayside auroral oval imparts a "tongue of ionisation" (TOI), which extends from the subauroral region into the nightside polar cap ionosphere (Tsunoda, 1988; Basu *et al.*, 1998; Skone *et al.*, 2003; Mitchell *et al.*, 2005; De Franceschi *et al.*, 2008). The high plasma flows then cause the TOI to divide into discrete structures (or patches), and as these patches convect across the polar cap, they lead to the formation of intermediate scale irregularities (tens of km to tens of metres) by the action of the gradient drift instability mechanism. In another study Lockwood and Carlson Jr. (1992) put forward transient magnetopause reconnection as mechanism for the formation of polar cap patches, a case which was supported by Carlson Jr. *et al.* (2004).

Electron density irregularities causing scintillation at high latitudes have dimensions ranging from metres to kilometres and can affect GNSS signals propagating through the ionosphere (Doherty *et al.*, 2000; Skone *et al.*, 2003). High latitude scintillation has been under investigation for many years, with strong phase scintillation and weak amplitude scintillation typically associated with precipitating electrons (Doherty *et al.*, 2000; Skone *et al.*, 2003; Ngwira *et al.*, 2010; Prikryl *et al.*, 2011). Furthermore, high-latitude scintillation is observed mainly during the local nighttime. It will be discussed in Chapter 7.

4.6 Summary

This chapter attempted to summarise a highly complex geophysical system, i.e. the response of the ionospheric plasma to various forms of geomagnetic disturbance. Ionospheric currents responsible for geomagnetic disturbances that affect electron density distribution in the ionosphere at low to high latitude regions are linked to processes in the magnetosphere. During storm events, current systems in the magnetosphere and ionosphere are altered, and these in turn modify the distribution of ionospheric electron density. This leads to positive and/or negative ionospheric storm effects. When the photochemical processes are more significant than the electrodynamic processes, the ionospheric electron density will be proportional to the [O/N_2] density ratio (see review by Crowley and Meier, 2008). Negative storm effects are fairly well understood, but positive storm effects are still a major challenge for the ionospheric science community with many possible mechanisms having been proposed to account for their generation. A simplified picture of the ionospheric storm chain of processes is shown in Figure 4.5. The figure reveals that understanding the thermosphere is a critical step towards understanding the ionosphere.

The world today has become increasingly dependent on the use of radio waves for satellite communication and GPS navigation systems. The study of ionospheric irregularities is of major interest in the understanding of the physical processes governing the ionospheric plasma and, in addition, is of practical significance due to the effects of irregularities on radio systems using ionospheric or trans-ionospheric propagation channels (Kersley *et al.*, 1988). Ionospheric irregularities, which cause radio wave scintillations are a serious concern for users of such systems.

In the following two chapters, case studies of the ionospheric response during

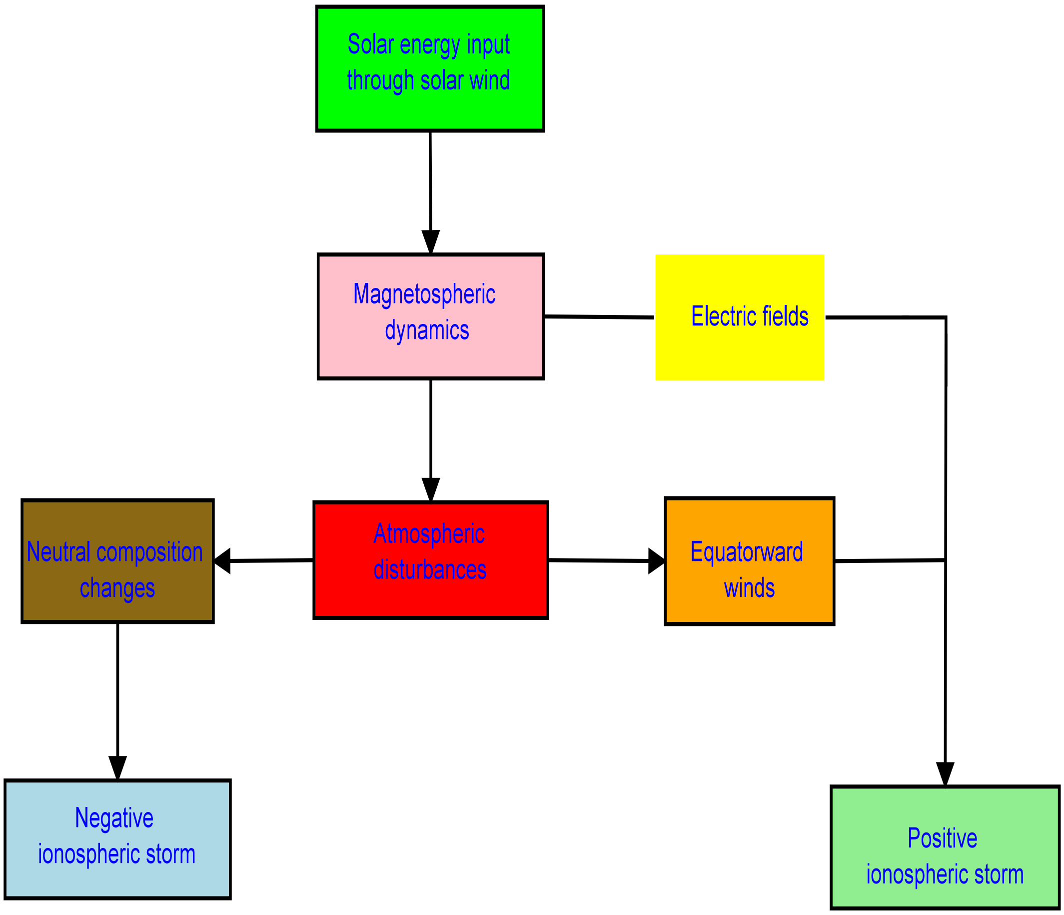

Figure 4.5: A summary of the ionospheric storm chain of events.

geomagnetic storm periods as observed over South Africa will be presented. This will be followed by a case study of ionospheric scintillation over the South African polar research station in Antarctica.

Chapter 5

Mid-latitude ionospheric storm response

5.1 Introduction

The objective of this chapter is to report on the investigation into the response of the ionosphere during the major magnetic storm event of 15 May 2005, with a focus on mid-latitude locations within South Africa. The effects of the severe geomagnetic storm were studied using both ground- and satellite-based observations. A number of studies have investigated the evolution and generation of ionospheric disturbances over mid-latitude regions, however, this chapter presents the first investigation of positive ionospheric storm effects and associated TIDs over South Africa.

In recent years the subject of the ionospheric effects of large geomagnetic storms has attracted wide interest (Basu *et al.*, 2005b; Lin *et al.*, 2005; Yizengaw *et al.*, 2006b; Dashora *et al.*, 2009; Ngwira *et al.*, 2011b,a, and references therein). Kelley *et al.* (2000) have shown that the mid-latitude ionosphere has its own unique physical processes which result in remarkable and important mesoscale ionospheric structures during geomagnetic storms. These changes in the plasma density distribution and the subsequent formation of plasma density irregularities in the ionosphere are known to affect trans-ionospheric radio signals, such as those used by the GNSS systems and may severely impact satellite communication and navigation systems, as well as HF radio communication.

Although many studies have been done on positive ionospheric storms and TIDs (Prölss and Jung, 1978; Fuller-Rowell *et al.*, 1997; Nicolls *et al.*, 2004; Ding *et al.*, 2007; Tsugawa *et al.*, 2007; Lynn *et al.*, 2008, and references therein), none have been done for South Africa. A number of ionospheric studies utilising GPS observational data from across South Africa have been done and are well documented (Cilliers *et al.*, 2004; Moeketsi *et al.*, 2007; Opperman *et al.*, 2007; McKinnell *et al.*, 2007). More recently, neural network techniques are being applied in the modelling of GPS-derived TEC over South Africa (Habarulema *et al.*, 2009, 2010, and references therein).

5.2 The 15 May 2005 geomagnetic storm

A CME was ejected from the solar surface into space on 13 May 2005 (16:50 UT) and reached the Earth on 15 May 2005, causing a major geomagnetic storm with a minimum Dst index of -263 nT, and sparking bright auroras over the high latitudes. The interplanetary conditions associated with this storm are shown in Figure 5.1. The top six panels display interplanetary parameters recorded by the ACE satellite. The panels display, from top to bottom, the solar wind speed (Vsw), proton density (Np), proton temperature (Tp), the solar wind total magnetic field magnitude (|B|), the interplanetary magnetic field (IMF) Bz-component in GSM coordinates and the solar wind ram pressure (Pram). The corresponding ring current activity as manifested by the Dst (blue curve) and the three-hourly Kp index (bars) are shown in the bottom panel of Figure 5.1. A solar wind propagation time delay of ∼31 minutes was estimated for the propagation from the ACE satellite location to the magnetosphere, using the measured solar wind speed of ∼800 km/s, at an assumed distance of 1.5×10^6 km. Therefore, the solar wind data in Figure 5.1 were shifted to match the Dst and Kp indices.

A storm sudden commencement (SSC) occurred at 02:40 UT on May 15, as indicated by the vertical dashed line. The ground magnetic field, as depicted by the Dst index, began to decrease rapidly after 06:00 UT. The shock arrival, identified by the abrupt increase of the solar wind speed from ∼ 480 km/s to about 800 km/s, occurred at about 02:40 UT on May 15. About 3 hours after the shock,

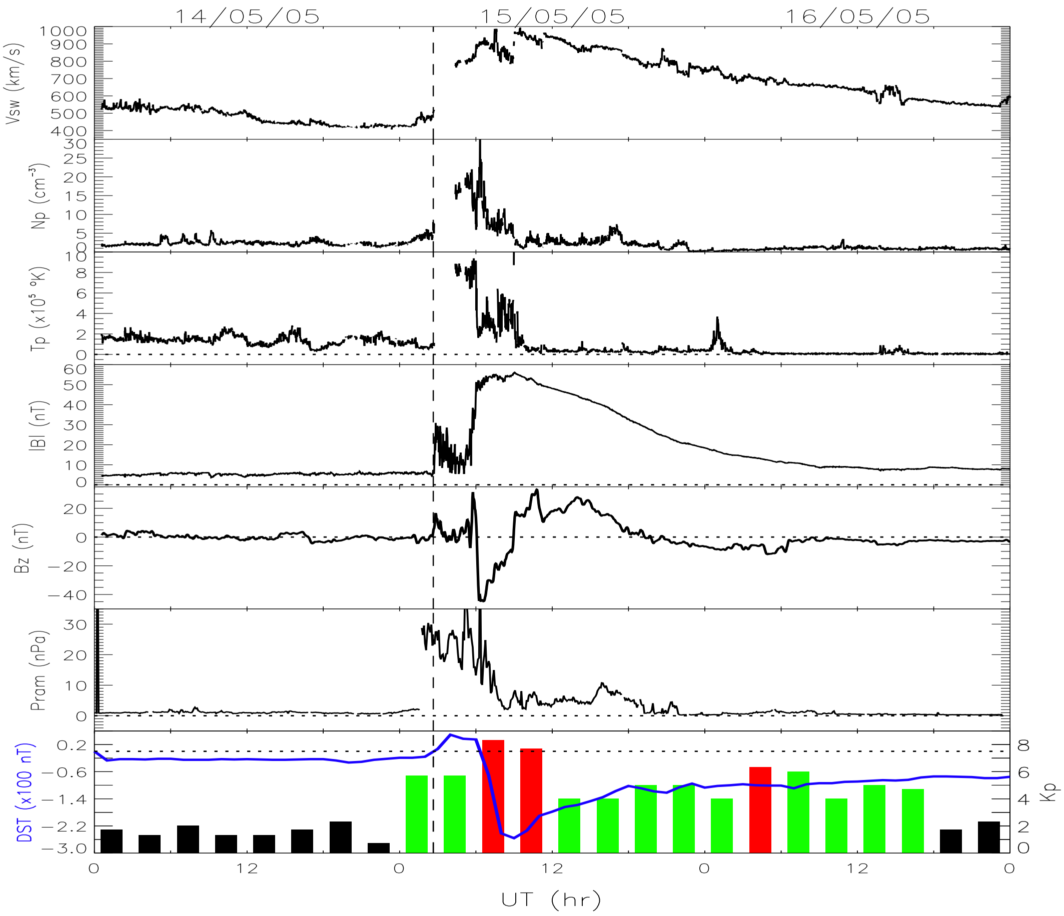

Figure 5.1: The interplanetary and geomagnetic variations on 14-15 May 2005. From top to bottom the panels represent the solar wind speed (Vsw), proton density (Np), proton temperature (Tp), the solar wind total magnetic field magnitude (|B|), the Bz-component, the solar wind ram pressure (Pram). The *Dst* (blue curve) and *Kp* indices are displayed in the bottom panel as overlay plots. The vertical dashed line indicates the time of the SSC.

the IMF Bz-component turned to the north for about 30 minutes and then turned sharply to the south (turning from about +39 to −43 nT in about 1 hour). The Bz then remained south with a major negative excursion for about three hours. Other solar wind parameters also showed a marked positive response to the shock. The variation of the Auroral Electrojet (*AE*) index (Figure 5.2), a measure of the energy deposited in the auroral regions, showed intense substorm activities between 02:00 and 10:00 UT on May 15, with the peak value of the *AE* index exceeding 1800 nT. Also shown in this figure is the interplanetary electric field (IEF), i.e. IEFy.

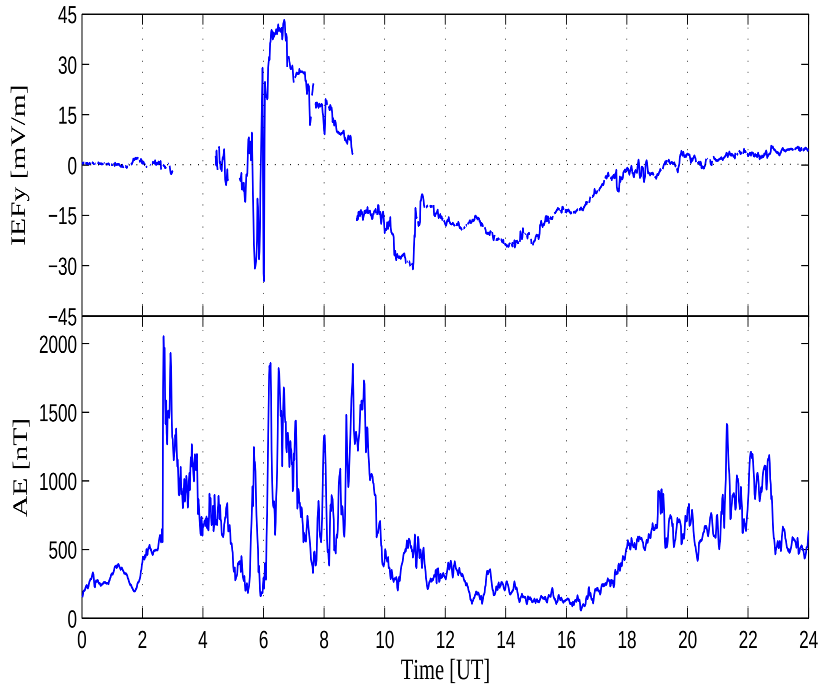

Figure 5.2: The *AE* index and the IEFy as derived for 15 May 2005.

The May 15 geomagnetic storm response, particularly in the equatorial region over the Indian sector has been a subject attracting great interest (Bagiya *et al.*, 2011; Dashora *et al.*, 2009; Malik *et al.*, 2010). Perhaps the interest stems from the highly unusual IEFy (Figure 5.2), which was determined by using the IMF Bz-component and the solar wind velocity component V_x (see report by Bagiya *et al.*, 2011). This enhanced IEFy produced strong penetrating electric fields in equatorial and low-latitude regions that resulted in large electron density perturbations in the dayside ionosphere. Dashora *et al.* (2009) performed the first ever investigation into the response of the equatorial and low-latitude ionosphere over the Indian sector using GPS-derived TEC measurements, a study which revealed a strong positive storm response. These authors explained the observed storm-time features in terms of the local low-latitude electrodynamic response produced by penetration electric fields and the occurrence of TIDs, which resulted in an altered fountain effect.

Malik *et al.* (2010) also concluded that the TEC increase during the May 15 storm could be explained by the action of a prompt-penetration electric field, and that the enhanced levels of TEC and long-lived storm effects could be attributed to the added influence of TIDs. Recently, Bagiya *et al.* (2011) conducted a detailed analysis on storm-time electrodynamical and neutral dynamical coupling and their effect on the equatorial and low-latitude ionosphere during the said storm period. They found that the daytime storm-induced increase in TEC was probably associated with prompt-penetration electric fields from high to low latitudes, in agreement with earlier findings by Dashora *et al.* (2009) and Malik *et al.* (2010). The penetration electric fields occurred shortly after the northward turning of the IMF Bz-component and subsequent intensification of the IEFy. This was followed by an enhancement of the equatorial electrojet (EEJ) and sudden rise in absolute horizontal geomagnetic field values for Tirunelveli, India.

5.3 Data and methods

Regional TEC data for South Africa were computed using the ASHA algorithm, which is discussed in Section 3.3.4. The ASHA algorithm estimates vertical TEC and also estimates and compensates for the differential clock and satellite biases. The contribution of multipath effects on the GPS data was minimised by considering only TEC values for satellites above a 30° elevation angle cut-off. To investigate the latitudinal response of TEC, three GPS receiver stations were chosen: Mafikeng (MFKG), Bloemfontein (BFTN) and Port Elizabeth (PELB). These observation points were selected so that they where nearest to the 26°E longitude, as shown by the vertical black line in Figure 5.3. This was done to separate latitudinal variation from time variation in the TEC. Furthermore, the longitudinal response of TEC was investigated at three selected latitudes. They are indicated by the three horizontal blue lines in Figure 5.3.

The temporal evolution of the different storm phenomena is easier to observe when the diurnal variation is removed from the ionospheric measurements. The residuals then allow one to see the accompanying storm-induced perturbations of the TEC. To achieve this, the deviation of TEC relative to the quiet-time median values (TEC_{med}) was calculated as defined by the equation:

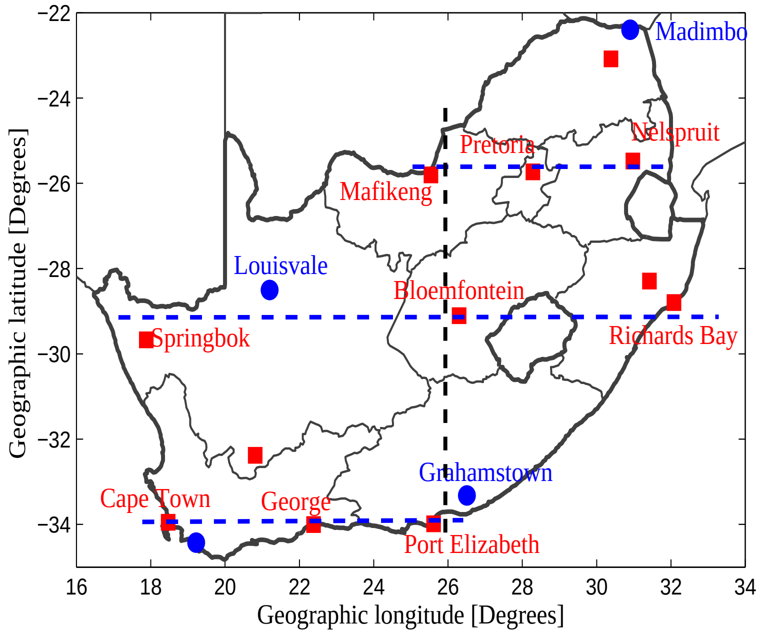

Figure 5.3: Distribution of GPS (red squares) and ionosonde (blue circles) stations used in the present study.

$$\Delta\text{TEC} = \text{TEC}_{obs} - \text{TEC}_{med} \tag{5.1}$$

The median values were determined using data for six quiet days close to the storm date.

5.4 Results

During the May 15 storm, the signature of the ionospheric TEC response to the interplanetary energy input in the magnetosphere was first observed at the southernmost latitudes of South Africa just after 07:30 UT (Figure 5.4). This occurred when Bz reached its minimum value, and is consistent with observations by Tsurutani *et al.* (2004) for previous storm events. The TEC values rapidly increased above the quiet-day values before reaching their peak values at about 08:40 and 09:10 UT (or at about 10:23 and 10:55 solar local time) at Port Elizabeth and Bloemfontein respectively. The positive ionospheric storm effects had a more dominant effect

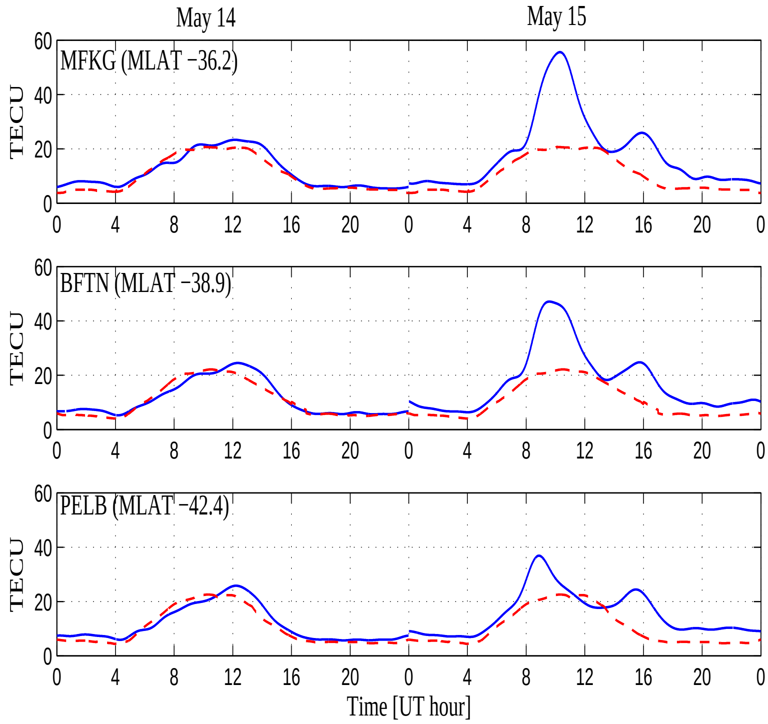

Figure 5.4: Temporal TEC variations during May 14-15, 2005 at three GPS reference stations along approximately the same longitude, but separated in latitude. The monthly median TEC values (red dashed lines) were used as quiet-day reference. At the three locations shown, standard time = UT + 2 hrs. The data are sampled at 30-second intervals and the jump in TEC at the end of the first day is a consequence of the data processing method.

at the northernmost station Mafikeng (36.2°S MLAT), where TEC levels reached values approximately twice as high as those on the preceding quiet-day, rising above 55 TECU. Usually during quiet periods, the daytime peak of TEC occurs at about noon and post noon solar local time. Contrary to this, on May 15 at Port Elizabeth and Bloemfontein, the TEC maximum was observed at pre-noon solar local time, with indications of a 1-3 hour time shift due to effects of the storm. The peak TEC occurred about 3 hours earlier at Port Elizabeth, and 2 hours earlier at Mafikeng compared to the peak of the preceding day. The ionospheric TEC responses in Figure 5.4 clearly show large TEC enhancements during the storm period on May 15, as compared to the quiet-day median values. A second TEC enhancement occurred about seven hours after the first event.

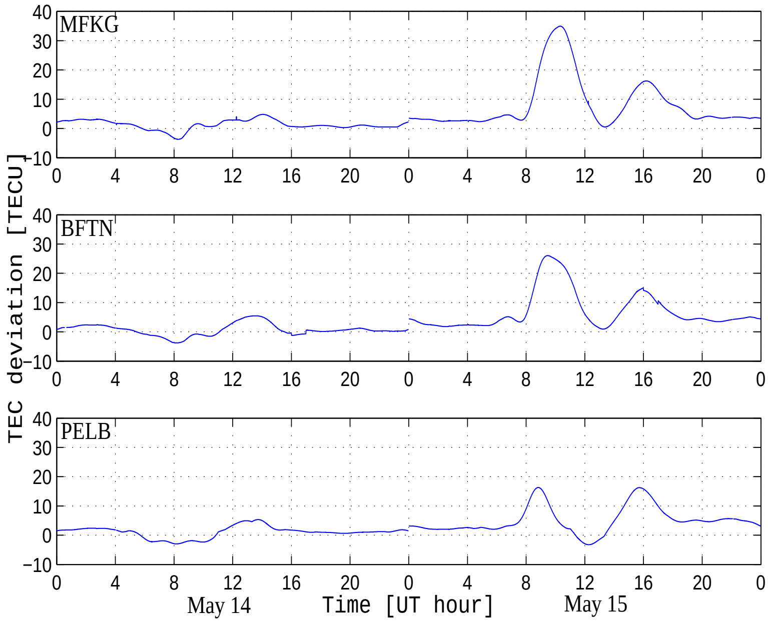

Figure 5.5: Deviation of ionospheric TEC relative to quiet-day median values for the same three locations as in Figure 5.4 during the period May 14-15, 2005.

Figure 5.5 displays the temporal TEC perturbations (ΔTEC) at the same locations as in Figure 5.4. The storm had a predominantly positive effect in comparison to the preceding quiet-day, except for a small negative phase visible at the Port Elizabeth station. The TEC enhancement varied between 16 and 35 TECU during the first enhancement and the maximum observed deviation had a characteristic latitudinal dependence. The highest TEC enhancement during the first event occurred at the station closest to the equator (Mafikeng) and reduced with increasing latitude towards the southernmost station (Port Elizabeth). By contrast, the second TEC enhancement does not show any latitudinal dependence in terms of the maximum levels of enhancement, with almost similar levels of enhancement at all stations.

Also, the GPS TEC perturbation series at different observation points in Figure 5.5 are similar in shape but shifted with time, thus indicating that the structure causing the perturbations was propagating northwards to mid-latitudes from the high latitudes. The daytime enhancement is a typical feature of TADs which manifest in the ionosphere as TIDs and will be discussed in the next section.

5.5 Discussion

Figure 5.6 displays the TOPEX and JASON-1 altimeter TEC values along the satellite ground tracks (top panel) and the altimeter TEC as a function of geographic latitude (bottom panel) observed on 15 May (DOY 135) 2005. The horizontal dashed line represents the geomagnetic equator. The satellites crossed the equator at 16:01 LT (approximately 09:20 UT) at 99.9°E and 101.3°E and at 11:10 UT at 73.0°E. In the bottom panel the different coloured curves show dif-

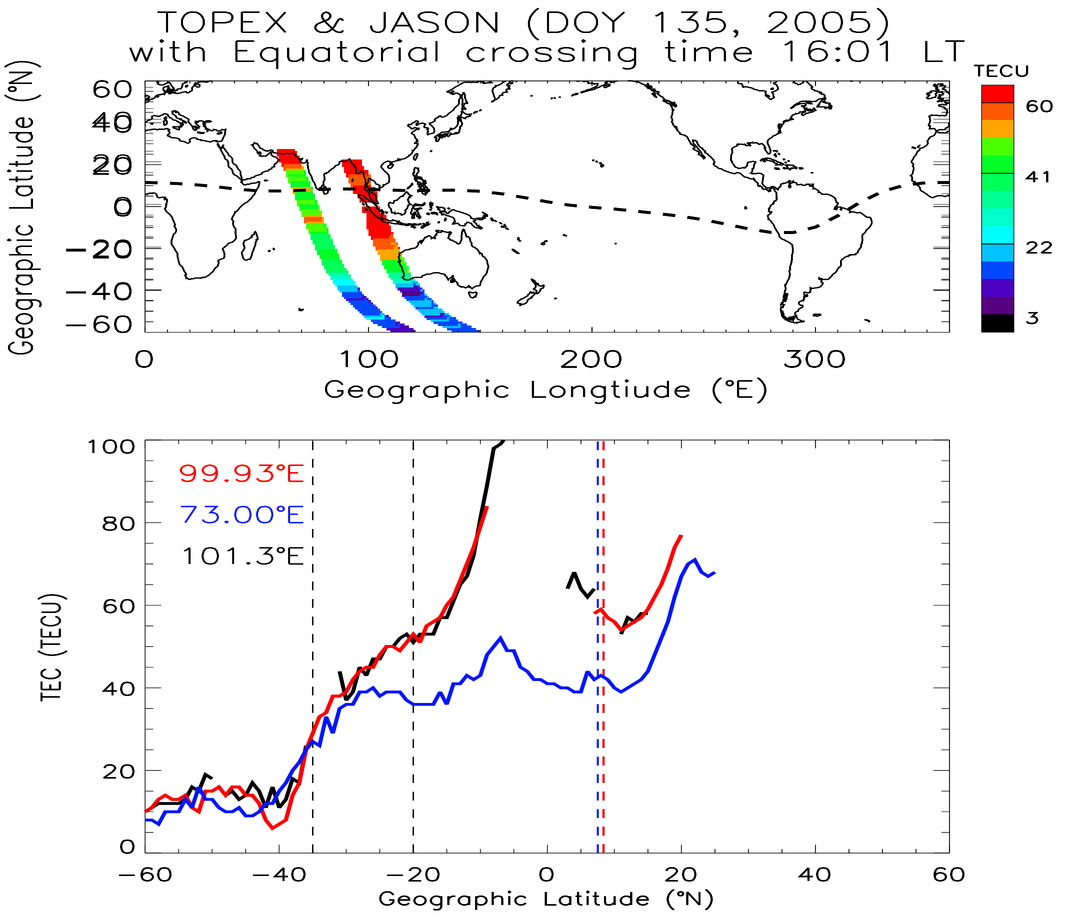

Figure 5.6: The top panel shows the TOPEX and JASON-1 ground tracks in the contour plot. The ground track shown on the right represents two passes (i.e., TOPEX and JASON-1), whereas the one shown on the left is only for the JASON pass. The bottom panel shows TOPEX (red) and JASON (blue and black) altimeter TEC values as a function of latitude for individual passes, and the corresponding coloured numbers depict the longitudes where the pass crossed the equator.

ferent TOPEX and JASON-1 passes and the corresponding longitudes where the crossed the equator are shown at the top left corner. The coloured vertical dashed lines represent the geomagnetic equator of the corresponding passes. The TEC enhancement observations displayed in Figure 5.5 are consistent with the TOPEX and JASON-1 altimeter TEC observations seen in Figure 5.6.

Between the vertical black dashed lines (in the bottom panel) of Figure 5.6, altimeter TEC for all three passes display a TEC increase in the southern hemisphere. The TEC increase is located between 22-38°S geographic (or 30-45°S geomagnetic), which is a region where the equatorward winds drive the plasma along the field lines to higher altitudes where recombination rates are much lower, leading to TEC enhancement. For all three passes, clear anomaly peaks occurred at about 7.0°S, and thus the TEC increase shown between the vertical black dashed lines may not be considered as the EIA peaks. However, the EIA asymmetry is clearly visible (blue trace) where the EIA peaks have shifted farther away from the geomagnetic equator in the northern hemisphere than in the southern and also have higher TEC values. Since the TOPEX and JASON-1 altimeters measure TEC only over the ocean, it was not possible to see the full TEC structure in the northern hemisphere as the satellites traversed over landmass in that hemisphere. The TOPEX/JASON-1 data not only reveal that the TEC increase seen at mid-latitudes was not related to the expansion of the EIA, but also show that the TEC increase was across the dayside sector. Although the TOPEX and JASON-1 data is not from the region of ground-based measurements, the altimeter observed TEC enhancement from both TOPEX and JASON-1 data demonstrate that the TEC-enhanced region was not localised, but that the enhancement expanded spatially to the region covered by ground-based observations.

The TADs features in Figure 5.5 are believed to be generated by auroral substorm activity which causes enhanced thermospheric pressure gradients, that launch the gravity waves which are responsible for large-scale ionospheric disturbances, propagating from high to mid-latitudes (Prölss, 1993a; Pi *et al.*, 1993; Mikhailov *et al.*, 1995; Ho *et al.*, 1998). As seen in Figure 5.2, the high-latitude region experienced intense substorm activity between 06:00 and 10:00 UT, which could have been responsible for the generation the TADs and subsequent equatorward winds.

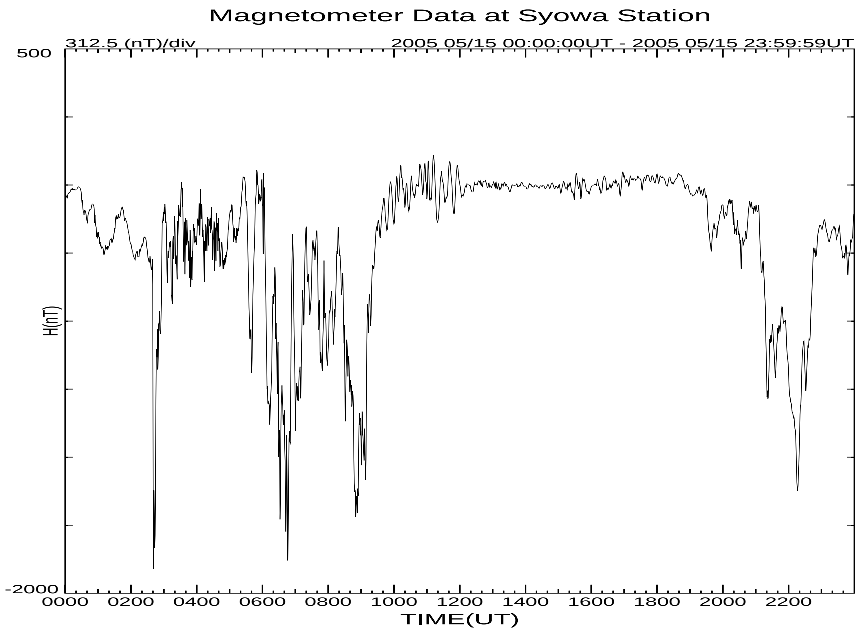

Figure 5.7: Horizontal component of the geomagnetic field as observed at Syowa station in Antarctica during the 15 May 2005 storm.

The *AE* index data is consistent with the H-component data observed at Syowa station in Antarctica as shown in Figure 5.7. The H-component shows strong perturbations, which further supports an auroral source for the TID mechanism. At daytime mid-latitude locations, equatorward propagating waves can cause an uplifting of the F2-layer by leading the ionospheric plasma along magnetic field lines to higher altitudes where chemical loss is much lower, at a time when solar ionisation is high. This in turn leads to plasma density enhancement (Prölss, 1993a; Ho *et al.*, 1998; Jakowski *et al.*, 1999). During nighttime, an uplifting of the F2-layer by a TID does not produce a significant increase in the electron density due to low ionisation levels and the absence of solar photo ionisation (Prölss, 1993a).

Furthermore, Figure 5.8 shows the longitudinal response of TEC at three selected latitudes. This was done in order to get a rough estimate of the TID propagation direction. The figure reveals that the TEC crests and troughs within each latitude sector occur almost at the same time, suggesting that the TID front moved due north towards the equator. Similar equatorward propagation was reported for the southern hemisphere over Australia by Lynn *et al.* (2008). In addition, an

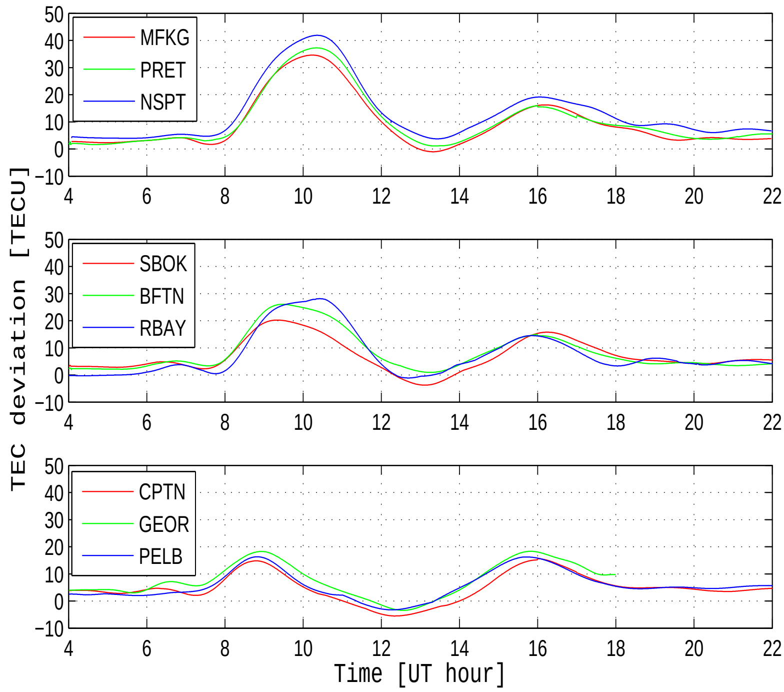

Figure 5.8: Differential TEC variations on May 15, 2005 at three latitude sectors. The plots show the longitudinal response of TEC at the selected latitude sectors.

analysis of the time delay between the peaks at the three different stations along the 26°E longitude indicates that the structures moved with average velocities of ∼438 and ∼515 m/s for the first and second TIDs respectively. These velocities are consistent with typical values for large-scale TIDs. In the literature they vary from some 300 to over 1200 m/s (Hocke and Schlegel, 1996; Ding *et al.*, 2007; Lynn *et al.*, 2008). The first TID velocity value (438 m/s) determined in this study is consistent with observations by Dashora *et al.* (2009), who studied the same storm event over equatorial stations in the Indian zone and calculated an average velocity of ∼485 m/s. Further analysis is required to determine other characteristics (such as wavelength and period) associated with the two TIDs discussed in this chapter, but such actions would require additional data sources which are not available for the period under consideration.

At this point, it should be noted that the TEC enhancement profiles presented in Figures 5.4 and 5.5 may be considered diurnal double maximum (DDM), as

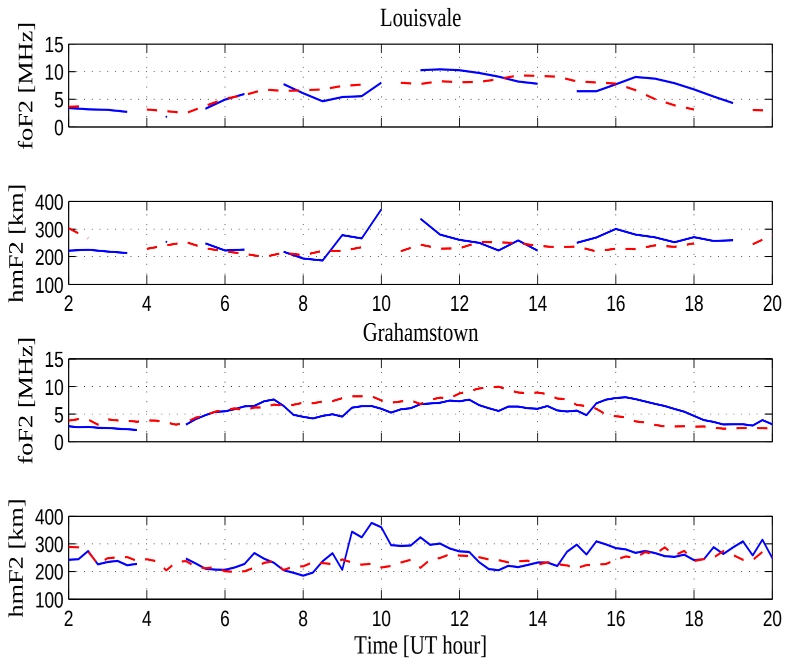

Figure 5.9: Ionospheric foF2 and hmF2 variations at Louisvale and Grahamstown ionosonde stations on May 15, 2005. The data obtained for May 14, 2005 are used as the quiet-day reference values (red dashed lines).

discussed by Pi *et al.* (1993). However, according to Pi *et al.* (1993), one of the common features of DDM is that they show almost no time delay from high to low latitudes in the TEC pattern. Also, Pi *et al.* (1993) point out that TIDs can explain the DDM only if the concerns about propagation speeds and the lack of observable time delays in effects at different latitudes are dealt with. Considering this, the observations presented in this chapter clearly show a time delay and thus it can be argued that the conclusion that TID effects are manifested is justified. Furthermore, long-lasting TEC enhancements (approximately 4 hours) can be attributed to the local time variation of winds and changes in the composition of neutrals at mid-latitudes. These can cause positive storm effects to last longer in winter if they occur while production of ionisation is still prevalent, as explained by Buonsanto (1999). This could account for the observations shown in Figure 5.5.

Unlike the TEC enhancements observed during the geomagnetic storm, the F2-layer critical frequency (foF2) values observed at Grahamstown and Louisvale did not show any obvious enhancement (see Figure 5.9). Actually, the foF2 descended below the quiet level (May 14) during the disturbance period except between 10:00 and 13:00 UT at Louisvale. Note that data were not available for the Madimbo ionosonde and the Hermanus ionosonde was not operational at the time. Maruyama and Nakamura (2007) suggest that the dissimilarity between the foF2 and TEC disturbances could be a consequence of two competing effects, i.e. the westward electric field and the equatorward neutral wind. They argue that the equatorward neutral wind effect could be a major cause of the positive storm effects, while the composition change may gradually become effective, resulting in a weak negative foF2 phase in spite of the large layer uplifting, as ionospheric TEC remains positive. The composition changes, which originate at high latitudes, can be transported by background and storm-induced circulation changes and spread to mid-latitudes (Fuller-Rowell *et al.*, 1994, 2002). However, during the second enhancement the foF2 values increased after 15:00 UT at both stations, and was preceded by an uplifting of the F2-layer as evidenced by the F2-layer peak height (hmF2). This response suggests that the effect may have been due to an equatorward neutral wind during a second TID event (Prölss, 1993a). It is important to note that foF2 is a local quantity at the F2-layer peak height and is more sensitive to the chemical recombination effect than TEC, which is a quantity integrated along the vertical height and includes contributions from the plasmasphere (Maruyama and Nakamura, 2007).

In contrast to the foF2 response, the hmF2 showed marked responses to the passage of the TIDs. Figure 5.9 illustrates that the hmF2 variability began to increase shortly before 08:00 UT on May 15. On May 14, the day preceding the storm, hmF2 had fairly low variability, but on the storm day, hmF2 steadily increased above the quiet-day height by several tens of kilometres within one hour, rising from an altitude of around 218 km to 370 km, between 09:00 and 10:00 UT. The F2-layer uplift and the subsequent TEC increase can be attributed to enhanced equatorward neutral winds, which lead plasma to higher altitudes where the recombination rate is low, as explained earlier.

Figure 5.10 shows ΔH (nT) values derived by detrending the observed horizontal geomagnetic field using the nighttime mean values of ground-based geomagnetic measurements at a single magnetometer station (Addis Ababa, 0.9°N geomagnetic) in the African sector. These values are used to estimate the equatorial electrojet (EEJ) current, which is proportional to the east-west electric current (Anderson *et al.*, 2004; Yizengaw *et al.*, 2011). A positive EEJ indicates an eastward current or eastward electric field. The ΔH data were included in order to examine whether the enhancement peaks that were observed could have been produced by prompt-penetration electric fields. The changes in the north-south component of the geomagnetic field reflect the east-west electric field. Figure 5.10 clearly shows that on the storm day (red curve), the eastward current was enhanced between 03:00 and 06:15 UT, it then sharply reversed to a strong westward current (negative ΔH) and was predominately westward for the next 8 hours. This indicates that the equatorial electric field, which is associated with the formation of a strong fountain effect that may transport plasma to higher latitudes, was actually westward, according to Figure 5.10, and could not have caused a strong fountain effect at the given longitudinal sector. These observations are consistent with the TOPEX/JASON observations in Figure 5.6, which showed that the EIA was not

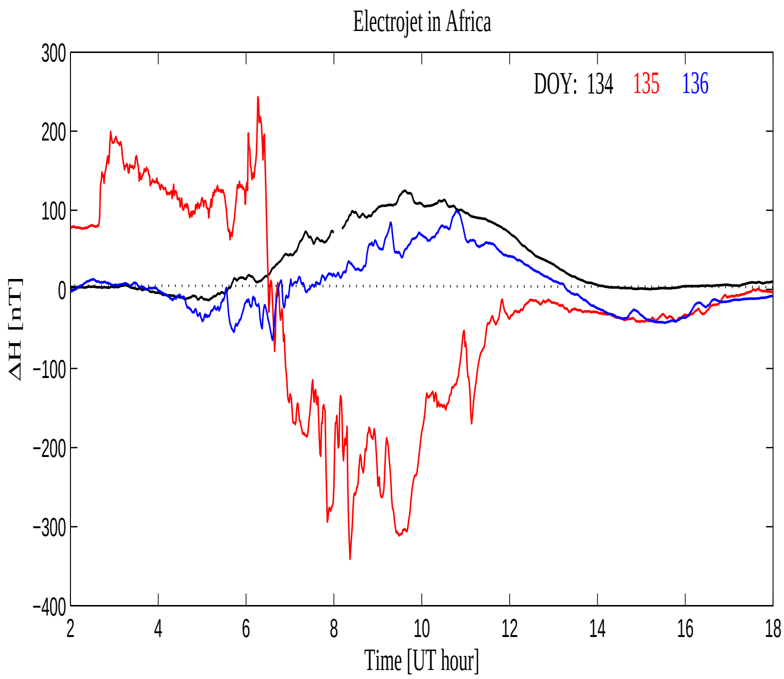

Figure 5.10: ΔH values as derived from the ground-based magnetometer observations at an equatorial station in the African sector (Ethiopia).

enhanced in the winter (southern) hemisphere. Therefore, the equatorial electric field (which could be penetrated from the magnetosphere or ionospheric dynamo generated) may not have been responsible for the observed TEC enhancements, but that a strong westward current may have been present during the time of the observed TEC enhancements. This supports the argument that neutral winds are the primary cause of the TEC enhancement.

However, since there is not enough data to fully explain these observations, it is possible that several different mechanisms could have been responsible for the observed ionospheric response. Therefore, further investigations are needed to isolate the various mechanisms associated with these observations.

5.6 Summary

The effects of the intense magnetic storm event on 15 May 2005 on the TEC and ionosonde measurements for mid-latitude locations were analysed. There are indications that ionospheric perturbations observed during this storm were associated with equatorward neutral winds and the passage of TIDs. The first and second TIDs propagated with velocities of $\sim$438 and $\sim$515 m/s respectively. An essential feature of these TIDs appears to be that they associated with equatorward-directed meridional winds of moderate magnitude, which are believed to be responsible for the generation of positive ionospheric storms at daytime mid-latitudes.

The foF2 response was characterised by a dissimilarity (i.e. different response pattern) which is likely due to the competing effects of the westward electric field and equatorward neutral wind. The F2-layer uplift as evidenced by ionosonde measurements and subsequent TEC enhancement have been ascribed to the equatorward neutral winds. In addition, this study has shown that ionospheric disturbances can result in a highly variable TEC response over the mid-latitude regions, as seen at several locations across South Africa.

This study has also shown that the observed TEC enhancement was not due to the expansion of the EIA into the mid-latitude regions, as there was a strong westward current observed in the African sector. Therefore, the equatorial electric field could not be responsible for the TEC enhancements. This supports the argument that neutral winds are the primary cause of the enhancement of the TEC.

In the next chapter, the long-duration ionospheric storm response to the severe geomagnetic storms of July 2004 are discussed. Long-duration storms are considered as one of the major unresolved problems in ionospheric storm studies.

Chapter 6

Long-duration positive ionospheric storms

6.1 Introduction

Energy injection at high latitudes, which is associated with geomagnetic storms, can result in a significant modification of the quiet-time ionospheric F-region electron density. The global electric field and atmospheric changes produced by these disturbances can cause an increase or decrease in the electron density (Fuller-Rowell *et al.*, 1994; Prölss, 1995; Buonsanto, 1999; Mendillo, 2006).

As discussed in Section 4.4, positive ionospheric storms display a wide range of characteristics. The purpose of this chapter is to report on the investigation into some of the observed characteristics of the ionosphere in response to the geomagnetic storm events of 24 to 27 July 2004. Using a multi-instrument approach the interplanetary conditions and the global ionospheric TEC response were investigated, before closely examining the response over South Africa. This report particularly focuses on the long-duration (more than 6 hours of enhancement) positive storm effects observed on 25 and 27 July 2004.

6.2 The 24-27 July 2004 geomagnetic storm events

The period prior to the geomagnetic storm event was characterised by a series of weak CMEs. The first geomagnetic storm began hours after a weak CME hit the

Earth's magnetic field on 24 July and continued, fitfully, for more than 12 hours. Figure 6.1 illustrates the interplanetary conditions during the storm period. The top three panels display the interplanetary parameters observed by the ACE satellite. The panels display, from top to bottom, the solar wind speed (Vsw), proton density (Np) and the IMF Bz-component in GSM coordinates. The corresponding ring current activity as manifested by the symmetric ring current index SYM-H (blue curve, one-minute equivalent of the Dst index) and the three-hourly Kp index (bars) are plotted in the bottom panel of Figure 6.1. The SYM-H data, which are promptly provided by the World Data Centre in Kyoto, Japan, show that the geomagnetic storm events started on 24 July and had two extended main phases on 25 and 27 July. The first SSC, as indicated by the vertical dashed line in Figure 6.1, occurred just after 05:35 UT on 24 July, when the SYM-H gradually decreased as the storm developed. The storm reached its long-lasting main phase

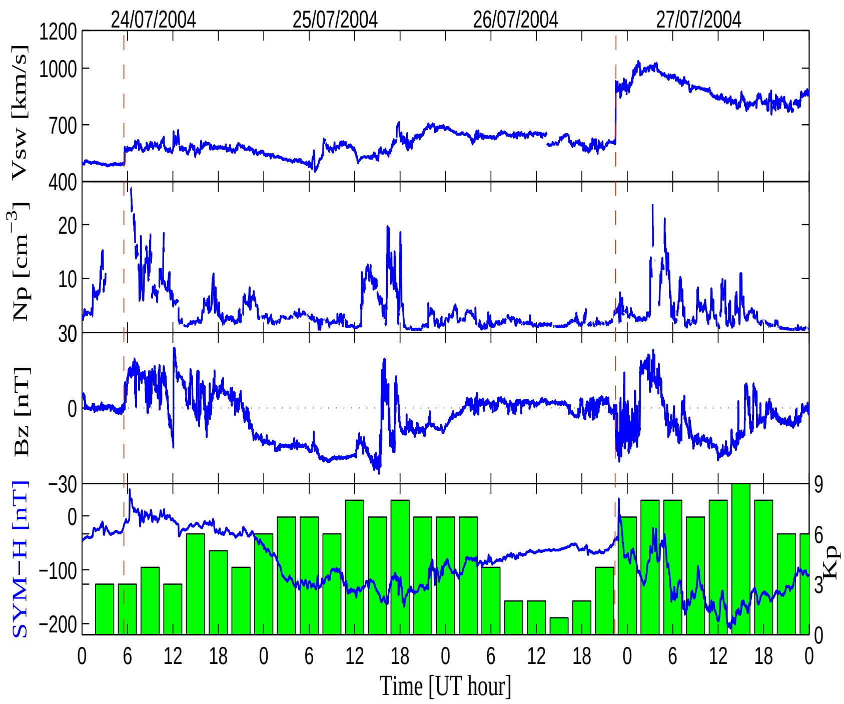

Figure 6.1: The interplanetary and geomagnetic variations on 24-27 July 2004. From top to bottom, the panels display the solar wind speed (Vsw), proton density (Np) and the IMF Bz-component. The SYM-H (blue curve) and Kp indices are displayed in the bottom panel as overlay plots. The vertical dashed lines (red) indicate the times of the two SSCs.

with a minimum $SYM\text{-}H$ of -171 nT occurring around 16:00 UT on 25 July. The second SSC occurred at ∼22:45 UT on 26 July during the recovery phase of the first storm. The $SYM\text{-}H$ steadily decreased to -120 nT at around 02:00 UT on 27 July, and then increased to the pre-storm levels, before steadily decreasing again. A minimum $SYM\text{-}H$ of -215 nT was reached at ∼13:30 UT on 27 July.

The first shock arrival, identified by the abrupt increase of the solar wind speed from ∼500 km/s to ∼600 km/s, occurred at 05:35 UT on 24 July. The IMF Bz-component turned northward and stayed predominately northward until about 11:00 UT when it turned southward for an hour and then turned sharply northward again (turning from about -15 to $+24$ nT in less than 25 minutes). The Bz-component then fluctuated between south and north for the next 8 hours. At 21:00 UT on 24 July, Bz turned southward and remained southward with a major negative excursion for over fifteen hours. Other solar wind parameters also responded to the shock with notable increases. The second shock arrived at 21:27 UT on 26 July, with the solar wind speed initially increasing from ∼600 km/s to ∼920 km/s, before reaching its maximum observed value of 1027 km/s almost 3 hours later. The IMF Bz turned southward and fluctuated between north and south for nearly 4 hours, before turning sharply northward. At about 04:30 UT on 27 July, Bz turned southward and remained southward for most of the following eleven hours. The solar wind proton density only increased slightly in response to the second shock arrival. However, the proton density eventually increased to ∼20 cm^{-3} about six hours after the shock arrival.

6.3 Data and methods

Nowadays, GPS satellite signals are not only used for navigation, but also offer opportunities for ionospheric research. The global availability of GPS signals creates a unique opportunity for the ionospheric community to monitor the TEC at any dual-frequency GPS ground station on the globe. To get a clear picture of the global evolution of the storm, global GPS TEC maps readily provided by the MIT Haystack Observatory via the Madrigal database were employed. Detailed information about the data processing methods used to obtain the observations by ground-based GPS TEC is provided by Rideout and Coster (2006). The variation of the ionospheric electron density as inferred from the vertical TEC values is discussed by Coster *et al.* (2003).

Differential TEC (ΔTEC) values were used in this investigation for all GPS-derived TEC measurements (including TEC maps), because the main interest was the level of the storm-induced perturbations. These values were obtained by taking the difference between the observed TEC on the storm-day and the quiet-time mean for 18-21 July. This process is defined by equation (5.1). However, it is important to note that in this case, the mean values are used instead of the median values as defined in the equation. This is in-line with the madrigal practice. For the regional TEC data over South Africa, three stations were used: Langebaan (LGBN), Kimberley (KLEY), and Graaff Reinet (GRNT). It should be mentioned here that during the period under investigation (2004) only a small number of GPS receiver stations had been installed, and that data were not available from some of these stations. Also, most of the stations were only operational between 03:00 and 18:00 UT.

6.4 Results

Figure 6.2 displays the global differential GPS-derived TEC response to the geomagnetic storm on 25 July. The TEC was plotted for a fixed local time (at each station) to see how the storm produces the same signature at the same local time across the globe. Both positive and negative storm effects can be seen at low to mid-latitudes. However, this study is confined to the observation of storm-time enhancement in TEC during daytime, because the focus is on establishing the mechanisms responsible for the development of daytime positive storm effects. Enhancement in excess of 50 TECU was observed with respect to the quiet-time reference. The colour code was saturated at 6 TECU for better visualisation of the storm response. The enhancement was first observed over the eastern coast of Australia, the Pacific Ocean and American regions in the early morning. The enhancement was later seen over the Indian Ocean and Africa as these regions rotated into the daytime sector. Strong TEC enhancement was seen in the southern hemisphere in the Australian, Indian Ocean and African sectors during most of the day. The TEC observations revealed a hemispherical asymmetry with much of

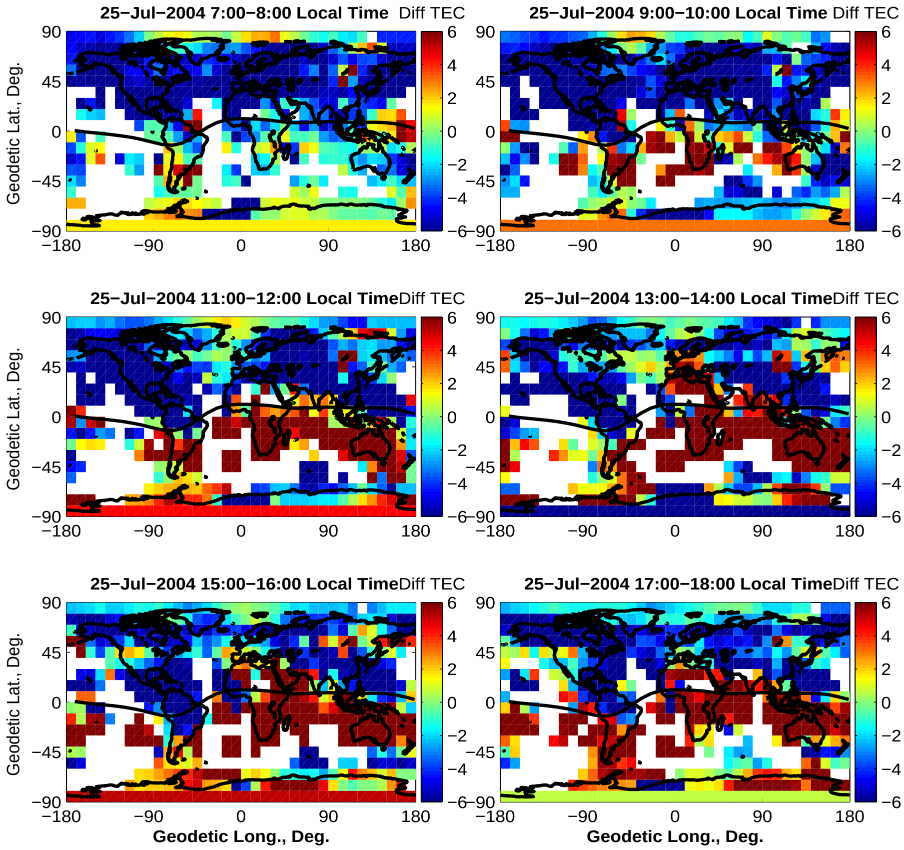

Figure 6.2: Differential ground-based GPS TEC between the storm day on 25 July and the quiet-time mean on 18-21 July from 07:00-18:00 local time. The maximum TEC enhancement exceeded 50 TECU during this period; the colour code was saturated at 6 TECU in order to better visualise the storm response.

the increase in TEC extending to higher mid-latitudes in the southern hemisphere. TEC enhancement in the northern hemisphere over Europe and Asia was only seen after 09:00 UT (apart from a few patches of enhancement). Figure 6.3 displays the ionospheric TEC response during the disturbance on 27 July. The response is similar to that observed on 25 July in that much of the TEC enhancement is concentrated in the southern hemisphere. Also, the enhancement rotates into the daytime sectors. It is important to note that the daytime TEC enhancement persisted for over 7 hours on both days, and can thus be classified as long-duration positive storm effects, according to Prölss (1997).

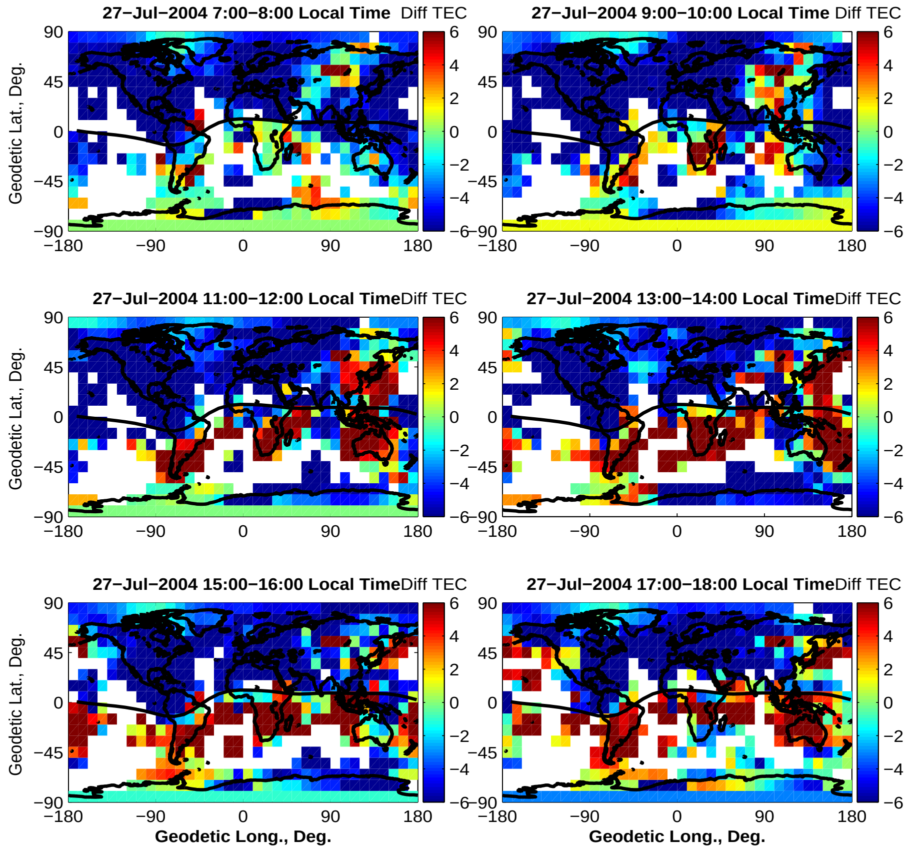

Figure 6.3: Same as Figure 6.2, but for the storm response on 27 July.

To further examine the large ionospheric TEC enhancements, Figure 6.4 shows the DMSP F15 ion drift observations during the orbits on (a) July 25 and (b) July 20. The top three panels show the DMSP F15 drift velocities and the bottom panels show the ion density. Figure 6.4a shows a sharp rise in density between 79.79 - 63.13°S MLAT and 159.78 - 141.83 GLON, while Figure 6.4b shows the quiet-day DMSP F15 observations, which do not reveal any similar sharp density enhancement. The drift measurements during the disturbed period (Figure 6.4a) show strong upward velocities in the mid-latitude region with a maximum at about 65°S geographic latitude.

Figure 6.5 displays the vertical TEC measurements obtained from the TOPEX and JASON-1 altimeters. It is evident from this figure that the TEC was in excess of 60 TECU, with the density being higher in the southern hemisphere than in

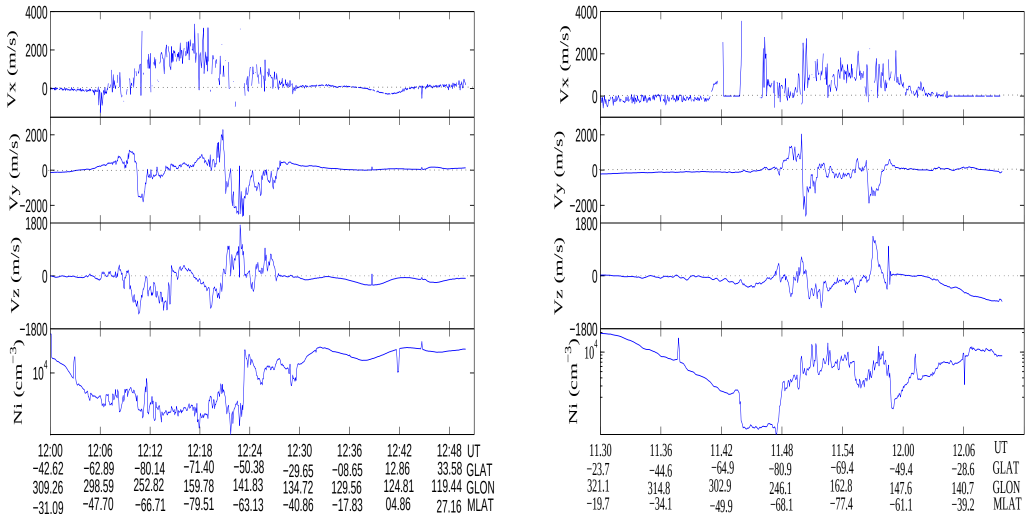

(a) (b)

Figure 6.4: (a) DMSP F15 measurements during the storm on 25 July 2004 and (b) the quiet-day values on 20 July 2004. The top three panels show the DMSP drift velocities and the bottom panels show the ion densities.

the northern hemisphere. The altimeter TEC measurements also show that the EIA extended into the lower mid-latitudes on 25 July, but was restricted to within ±15° GLAT on 27 July. Furthermore, it is worth noting that there was some TEC increase within the 40 - 60°S GLAT. A comparison of the TOPEX/JASON-1 altimeter TEC readings for the quiet-day is provided in Figure 6.6.

The variation of ionospheric vertical TEC at selected ground-based GPS receiver stations across South Africa on 25 and 27 July is shown in Figure 6.7 (top panels). The temporal differential TEC values, which allow for a better visualisation of the accompanying storm-time deviation of the TEC from the background values, are shown in the bottom panels. All three stations exhibit significant positive storm effects. As is evident, the enhancement on 25 July (40 TECU) was much larger than that observed on 27 July (about 22 TECU). However, the positive storm enhancement on 25 and 27 July lasted over 9 and 7 hours respectively.

Ionospheric perturbations driven by disturbance winds and electric fields cause changes in the F-region electron density distribution. In addition to the regional TEC observations, Figure 6.8a displays the ionospheric F2-layer response as mea-

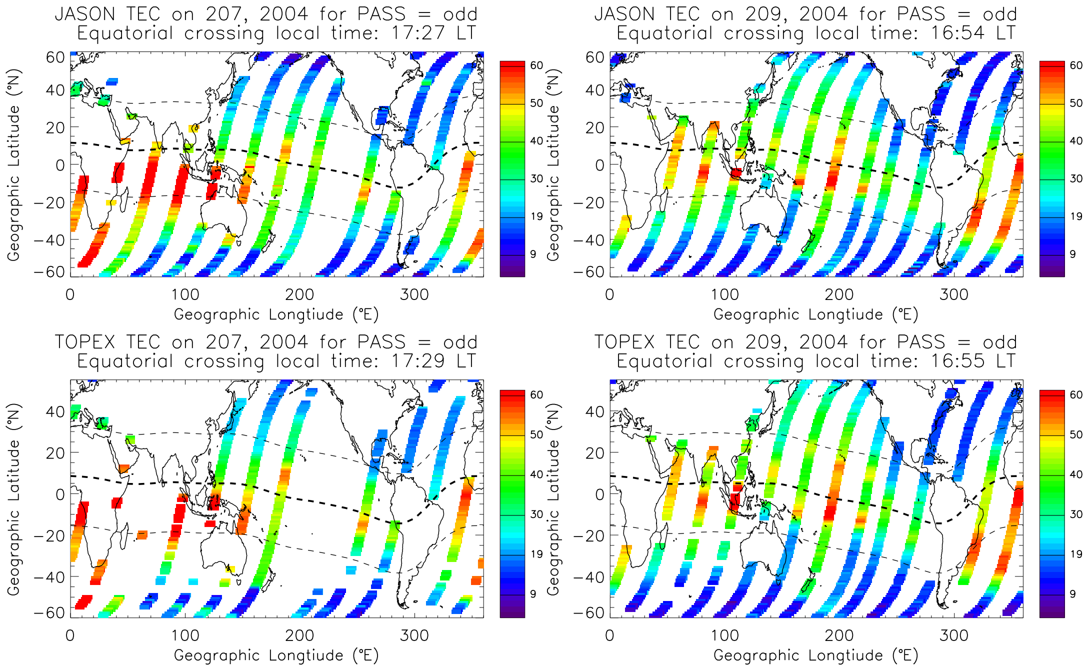

Figure 6.5: TOPEX/JASON-1 altimeter TEC on 25 (left) and 27 (right) July 2004. Ionospheric TEC measurements in excess of 60 TECU were observed, with much of the increase observed in the southern hemisphere.

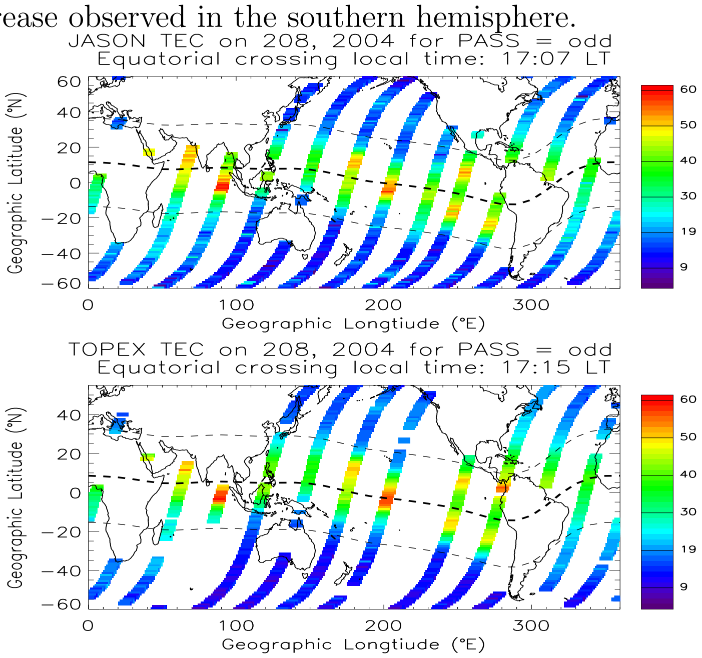

Figure 6.6: TOPEX/JASON-1 altimeter TEC for a quiet-day on 26 July 2004 showing no large mid-latitude TEC increase. Images courtesy of E. Yizengaw.

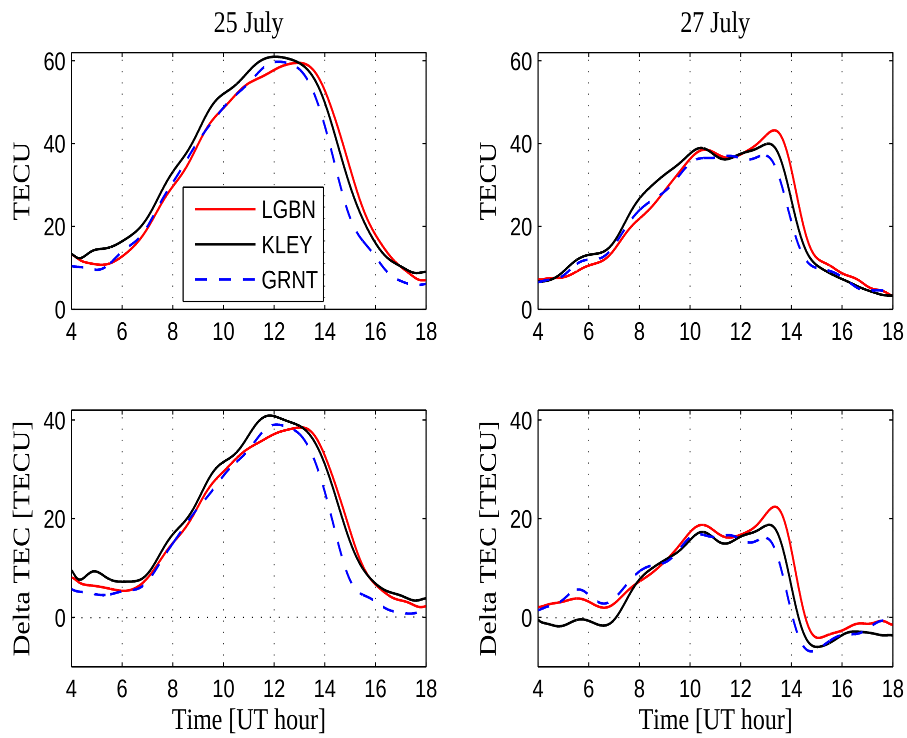

Figure 6.7: Ionospheric vertical TEC variations over selected ground-based GPS receiver stations in South Africa on 25 and 27 July. The top two panels display the observed TEC and the bottom panels display the TEC with the quiet-day subtracted. The mean values were determined for the geomagnetically quiet-days on 18-21 July 2004.

sured by ionosondes at Grahamstown and Madimbo, South Africa. The top panel shows the auroral electrojet index (AE), and the middle and bottom panels show the foF2 and hmF2 values at the two ionosonde stations. Figure 6.8b shows the differential foF2 and hmF2 values. The AE index, a useful proxy for the solar wind energy input into the magnetosphere, reveals that there appeared to be magnetic activity continuously on 25 and 27 July, with the most severe activity being registered on 27 July when the AE exceeded 3500 nT. The SYM-H index (Figure 6.1) identified a +60 nT SSC at 22:45 UT on 26 July followed by a rapid main phase decrease to about -130 nT. These changes were accompanied by a sudden increase in the AE index which denotes the onset of a substorm. This is indicative of a strong compression of the magnetopause, followed by a rapid increase in the strength of the magnetospheric ring current. Unlike the values on 24-26 July, on 27 July the foF2 increase to above the quiet-day reference was seen only at Madimbo and not at Grahamstown even though the largest ionospheric F2-layer peak height (hmF2) increase was measured over Grahamstown. The hmF2 parameter on 24 and 26 July did not show significant increase compared to the other two days.

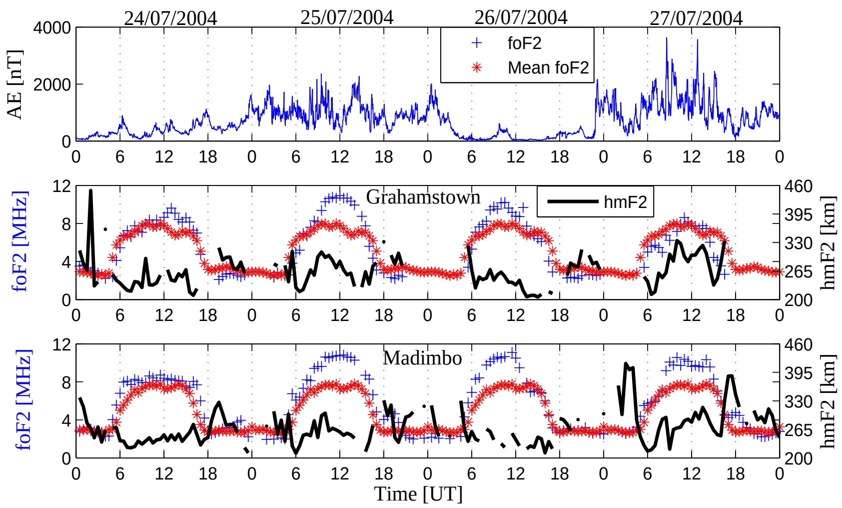

(a)

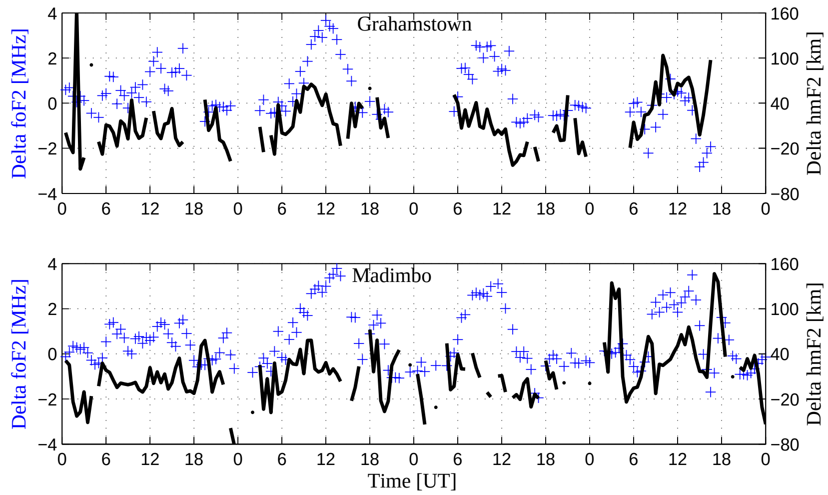

(b)

Figure 6.8: (a) The *AE* index (top panel), ionospheric foF2 (blue +) and hmF2 (overlay black solid line) variations (middle and bottom panels) at Grahamstown and Madimbo ionosonde stations on 24-27 July 2004. The average foF2 and hmF2 values for 18-21 July were used for the quiet-day reference values (red $*$ curves). (b) The relative deviation in foF2 and hmF2 was determined by calculating the difference between the observed values and quiet-day mean values.

6.5 Discussion

Enhanced dissipation of solar wind energy identified by the rise in magnetic activity can lead to large-scale (global) perturbation of the ionosphere. Figures 6.2, 6.3 and 6.5 illustrate that the morphology of this perturbation is not uniform. Both global TEC maps and TEC measurements by the TOPEX/JASON-1 altimeter show that the positive storm effects extended into the mid-latitudes, but that the largest enhancement was restricted to the EIA crest regions. The observations also indicate that the EIA asymmetry was broader and of higher density in the southern (winter) hemisphere than in the northern (summer) hemisphere. According to current understanding (Yizengaw *et al.*, 2005b, and references therein), the EIA peak is expected to be higher in the winter hemisphere due to the summer-to-winter trans-equatorial neutral winds that drive the plasma to the winter hemisphere across the equator. However, during severe magnetic storms, this expected pattern is sometimes over-turned and the unusual response of an EIA of a much higher density in the summer hemisphere than in the winter hemisphere is observed (Yizengaw *et al.*, 2005b). Such occurrences emphasise the complex nature of ionospheric dynamics and their variability from one storm event to another. In addition, the TOPEX/JASON-1 altimeter measurements reveal that the EIA moved into the lower mid-latitudes on 25 July, but was restricted to the $\pm 15°$ geomagnetic latitude on 27 July. The efficiency of energy transfer at high latitudes cannot be ruled out as a possible cause for these differences. This will be discussed below.

The TOPEX/JASON-1 altimeter TEC also indicates that the southern mid-latitudes had formed an enhanced daytime plasma density peak between 40 - 60°S geographic latitudes. The TEC enhancement feature could be attributed to mid-latitude particle precipitation. This argument is supported by DMSP F13 observations shown in Figure 6.9. The DMSP F13 spectrograph plot (Figure 6.9a) confirms the presence of particle precipitation over the mid-latitude regions extending equatorwards to 40°S geographic latitude on 25 July. Figure 6.9b is the quiet-time comparison over the same region and time pertaining to 20 July showing no precipitation activity. Auroral energetic particle intensity may increase

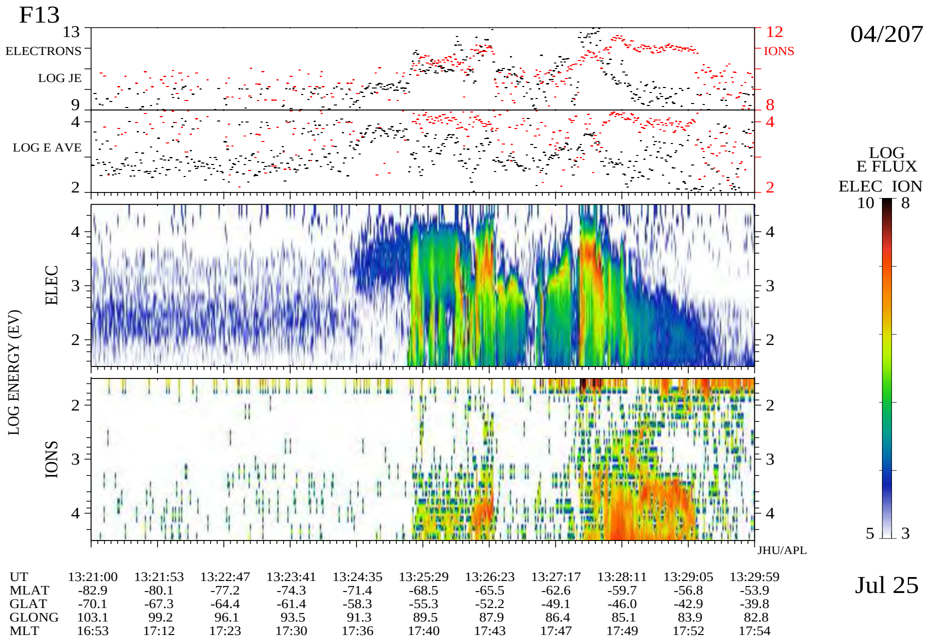

(a)

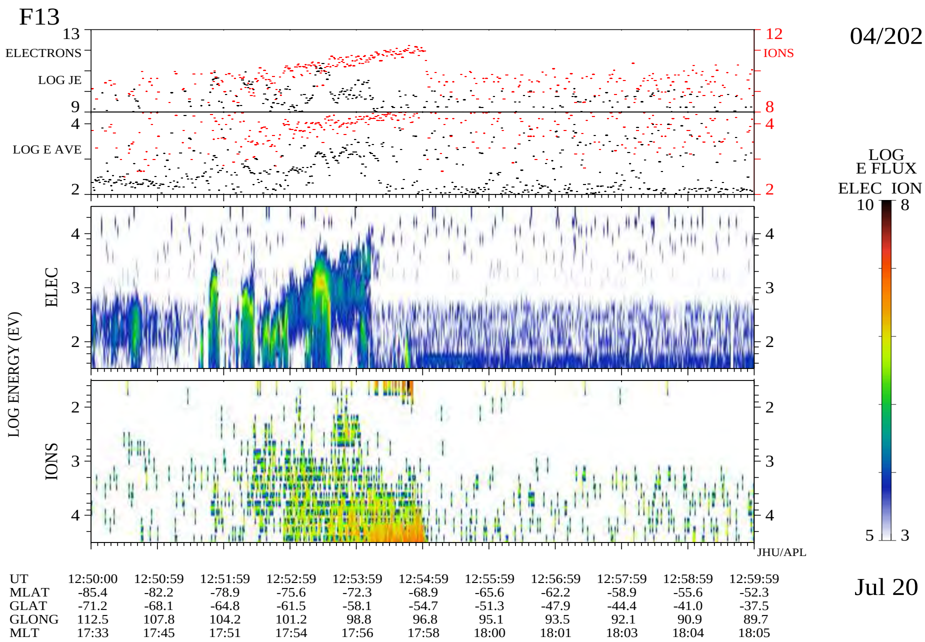

(b)

Figure 6.9: (a) DMSP F13 spectrograph for July 25 showing particle precipitation within the mid-latitudes between 40 - 60°S geographic latitude; (b) quiet-time spectrograph for July 20 showing no precipitation. For the same region.

by several orders of magnitude during geomagnetic storms and substorms, a case which may result in an increase of electron concentration in the region engulfed by the auroral oval (Yizengaw *et al.*, 2005a; Pedatella *et al.*, 2009).

Ionosonde measurements from two stations in South Africa revealed that the rise of the F2-layer (hmF2) was accompanied by an enhancement in foF2. In response to the prolonged high geomagnetic activity in the high latitudes on the two days (see AE index data), the F2-layer critical frequency foF2, which is directly proportional to the electron density according to equation (3.4), remained elevated for more than 7 hours. The electron density increase may be attributed to the increase in the height of the F2-layer. The average height of the maximum electron density increased by more than 60 km on 25 and 27 July, with the largest height increase of $\sim$100 km over Grahamstown on 27 July. The storm-time perturbation in hmF2 and the increase in ionospheric foF2 can be associated with changes in large-scale wind circulation and equatorward neutral winds (Prölss, 1997). It should be recognized that positive storms are dominant in the winter hemisphere, while negative storms prevail in the summer hemisphere. This is attributed to the prevailing summer-to-winter circulation, where the poleward winds restrict the equatorward movement of the composition disturbance in the winter hemisphere (Fuller-Rowell *et al.*, 1996; Buonsanto, 1999). This leads to a decrease of molecular constituents and produces a positive storm effect. The markedly positive foF2 response observed on 24-26 July was different from the foF2 response seen at Grahamstown on 27 July (Figure 6.8b), despite the large increase in hmF2 observed at this station. The 27 July response was without a clear positive storm-type effect. This could be related to the expansion of the EIA into lower mid-latitudes, which would only affect observations at Madimbo, but not at Grahamstown. According to Huang and Foster (2005), an enhanced EIA can give rise to F-region electron density enhancements at lower mid-latitudes (such as Madimbo), but may not be sufficient to cause similar enhancements at higher mid-latitudes like Grahamstown.

Two primary mechanisms have been put forward to explain the long-lasting positive storm effects: downwelling of neutral atomic oxygen (O) or uplifting of the F2-layer due to enhanced winds (see review by Buonsanto, 1999). The downwelling theory suggests that the large-scale changes in thermospheric circulation cause a downwelling (negative vertical velocity) of the neutral species through constant pressure surfaces at low to mid-latitudes equatorward of the composition disturbance zone, thereby increasing the [O] density relative to [N_2] and [O_2], i.e. increasing the [O/N_2] and [O/O_2] ratios (Fuller-Rowell *et al.*, 1997; Rishbeth, 1998; Buonsanto, 1999, and references therein). The consequence of this action is an increase in the daytime F-region electron density. By contrast, the wind mechanism, which is an extension of the TAD theory, proposes that enhanced equatorward winds uplift the ionisation to higher altitudes where the loss rate is low, at a time when production is still prominent, and leads to an increase in the electron density (Prölss, 1997; Bauske and Prölss, 1997). However, both of these mechanisms depend on large-scale changes in thermospheric circulation, accompanied by reduced poleward winds and enhanced equatorward winds to sustain uplifting of the ionospheric F-region (Prölss *et al.*, 1991; Buonsanto, 1999). These processes may in turn be driven by sustained heating in the high-latitude regions.

The present results establish that the most dramatic enhancements were recorded on 25 July during the main phase of the first storm (Figure 6.1) when the IMF Bz-component was southward for an extended time period (more than 15 hours). It is probable that the extended IMF Bz southward orientation on this day could have caused thermospheric and ionospheric disturbance for longer time periods, hence resulting in long-duration storm effects. For sustained high-level magnetic disturbances, the continuing high energy input may lead to prolonged changes in the global wind circulation (Prölss, 1993b, 1997; Bauske and Prölss, 1997, and references therein). These changes are driven by temperature gradients between the auroral region and the lower latitudes (Prölss and Jung, 1978, and references therein). During the daytime, the poleward-directed winds may decrease or even reverse, causing a sustained uplifting of the ionospheric F2-layer, a condition which then leads to the development of long-duration positive storm effects. The total duration of the positive storm phase depends not only on the duration of the magnetic activity, but also on competing processes responsible for negative storm effects (Prölss *et al.*, 1991).

Contrary to the 25 July response, the IMF Bz did not stay predominately southward on 27 July even though observations show that the geomagnetic activity was more disturbed on 27 July, but instead it fluctuated between north and south, then remained southward after 07:00 UT for about 9 hours. The IMF Bz response is consistent with the $SYM\text{-}H$ response on 27 July which experienced three partial recovery phases. The energy transfer from the solar wind to the magnetosphere is more efficient during periods of strong southward IMF Bz (Tsurusani and Gonzalez, 1995; Lopez *et al.*, 2004). This could be the reason for a larger enhancement and broader EIA seen on 25 July when the IMF Bz southward orientation was sustained for a much longer period than on 27 July.

A closer inspection of Figure 6.7 reveals that the TEC response had two peaks on 27 July. These peaks could be related to the two intense isolated bursts of substorm activity observed on the AE index data. The peaks could be associated with TAD events at the high latitudes (considering a propagation delay of ∼2 hours). A major feature of TAD events is their apparent association with equatorward-directed meridional winds of moderate magnitude. These are considered responsible for the generation of positive ionospheric storms at daytime mid-latitudes. In their simulation of long-duration positive storm effects, Bauske and Prölss (1998) show that wind perturbations are more important than composition changes in the generation of these storm effects. According to Prölss (1993a) and Bauske and Prölss (1997), the magnetic activity which follows an initial substorm may temporarily subside, and any new burst of activity may generate another TAD. The second TAD may then be responsible for the development of a second positive storm effect. Equatorward disturbance winds that can uplift the F-region plasma are widely accepted as a cause of the observed upward motion of the F2-layer plasma (Prölss *et al.*, 1991). However, in this case, the time changes in the large-scale wind circulation are still needed to maintain the upward movement of plasma for a long-duration positive storm effect (Prölss *et al.*, 1991; Prölss, 1997). Prölss (1997) explains that the high pressure areas in the polar regions decrease the intensity of the poleward-directed wind in the daytime, a condition which allows for a more 'regular' build-up of plasma density.

Some recent studies consider the action of eastward prompt-penetration electric fields as a possible mechanism to explain the long-duration positive storm effects (see Huang *et al.*, 2005; Pedatella *et al.*, 2009). An enhanced eastward electric field can uplift low-latitude plasma due to $\mathbf{E} \times \mathbf{B}$ drift, so that more plasma is available at higher altitudes where recombination rates are lower, while solar ionisation continues to generate additional plasma. Furthermore, such an electric field also leads to the enhancement of the EIA peaks which may be shifted to the lower mid-latitudes (Tsurutani *et al.*, 2004; Huang and Foster, 2005).

The long-duration positive storm effects presented in this thesis were characterised by enhanced ionospheric densities that persisted only during the daytime. Huang *et al.* (2005) using the Millstone Hill incoherent scatter radar, observed a similar significant daytime mid-latitude F-region electron density increase during the main phase of the storm on 3 April 2004. The electron density increase started immediately after the SSC in the morning sector (09:12 LT at Millstone Hill), and lasted over 10 hours. The cause of the long-duration electron density increase was associated with an enhanced eastward electric field over the entire positive storm phase, and a possible contribution from changes of the neutral circulation. Huang *et al.* (2005) showed that there were no strong equatorward neutral winds during the daytime, and that the associated poleward wind was reduced during the storm. Since the storm-associated atmospheric disturbances are equatorward, they compete with the prevailing poleward circulation (Fuller-Rowell *et al.*, 1994), which acts by moving the mid-latitude ionospheric plasma downward. The higher recombination rates at these lower altitudes then lead to a decrease of plasma. However, a reduced or reversed poleward wind reduces the recombination rates, because the plasma is moved to higher altitudes (Prölss, 1997; Buonsanto, 1999). When these features combine, i.e. an enhanced eastward electric field and reduced or reversed poleward winds, the nett effect is an increase in the electron density of the dayside ionosphere at the time when photoionisation is still prevalent. This creates a condition for the regular build-up of plasma and consequently leads to the long-duration storm effects.

Contrary to the present observations and those reported by Huang *et al.* (2005) in their study of the ionospheric response during the storm on 15 December 2005, Pedatella *et al.* (2009) report electron density enhancement before the dusk hours that persist even beyond midnight. These authors attribute their observation to the effect of an enhanced eastward electric field and equatorward neutral winds.

The difference between the observations by Pedatella *et al.* (2009) and the present observations could probably be explained by the local time dependence of the ionospheric storm effects, which could be related to different driving mechanisms (Prölss, 1993b). It is generally accepted that the effects of a positive storm phase, driven by winds before dusk, may rotate into the nightside (Fuller-Rowell *et al.*, 1994). However, the main phases of the storms discussed here intensified mostly during the dawn hours and persisted during the daytime, as established in Figure 6.1. This ensured that energy was continuously fed into the ionosphere during the daytime when production was still prevalent, leading to the prolonged disturbances.

It is generally expected that the spontaneous action of a penetration electric field should be characterised by a simultaneous response from middle to equatorial latitudes. It can thus be concluded from the observations presented in this chapter that enhanced eastward penetration electric fields may not be the primary mechanism producing the long-duration TEC enhancement. On the other hand, the action of the disturbance dynamo electric field is to oppose the normal diurnal variation with downward plasma drifts, since it is westward on the dayside, thus causing a reduction in the electron density and suppression of the EIA (Fuller-Rowell *et al.*, 2002; Tsurutani *et al.*, 2004). However, the dynamo electric fields can cause an upward plasma drift, which uplifts the F2-layer on the nightside and an enhanced EIA, as reported by Fuller-Rowell *et al.* (2002). In addition, plasma exchange between the ionosphere and the plasmasphere has been put forward as one of the possible explanations for the long-duration positive storm effects (Pedatella *et al.*, 2009, and references therein). It has been argued that enhanced magnetospheric electric fields during geomagnetic disturbances can cause the outer plasmasphere to convect and be refilled due to ionospheric upflow. The resulting vertical distribution of plasma produces a decrease in the rate of loss of plasma, and thereby a relative enhancement in electron density as compared to the quiet-time.

However, since there are no direct observations of the proposed mechanisms for the positive storm effects, it is likely that more than one mechanism could be responsible for the observed density enhancements seen on the two days that were investigated. Therefore, more observations are necessary to distinguish between the various mechanisms that cause long-duration positive storm effects, as suggested by Buonsanto (1999).

6.6 Summary

Ionospheric storms are a manifestation of extreme forms of space weather, and can have a detrimental impact on the reliability of space and ground-based technological systems. In this chapter the ionospheric response to the geomagnetic storm events on 24-27 July 2004 was investigated. It was noted that the positive storm enhancement on 25 and 27 July lasted over 9 and 7 hours respectively, and both have been classified as long-duration positive storm effects.

In addition, both global TEC maps and the TOPEX/JASON-1 altimeter TEC showed that the plasma density enhancement of the EIA asymmetry was larger in the southern (winter) hemisphere than in the northern (summer) hemisphere. This has been attributed to the summer-to-winter trans-equatorial neutral winds that move the plasma density to the winter hemisphere across the equator. Furthermore, the TOPEX/JASON-1 altimeter TEC showed an enhanced daytime plasma density peak between 40-60°S geographic latitude. This enhancement feature could be related to mid-latitude particle precipitation, as was confirmed by the DMSP F13 spectrograph plots.

Ionosonde measurements from two stations in South Africa revealed that the hmF2 height rise was accompanied by an enhancement of foF2. The AE index experienced dramatic sustained enhancement during this geomagnetic storm period. This ensured that a large amount of energy was continuously being injected into the high-latitude region due to Joule heating and particle energy injection. The sustained enhanced energy input to the ionosphere is possibly the cause for the prolonged ionospheric disturbances. It has been suggested that the long-duration positive storm phases observed here could have been caused by large-scale wind circulation and equatorward neutral winds. These processes were in turn probably driven mainly by enhanced and sustained energy input in the high-latitude ionosphere. This is evidenced by the prolonged high-level geomagnetic activity observed on both 25 and 27 July 2004

However, it is probable that other mechanisms may have played a role in producing the observed density enhancements, as there has been no direct observations of the proposed mechanisms. Therefore, more observations are required in order to distinguish between the different mechanisms.

Even more than 80 years after discovery, ionospheric storms are still a fascinating and challenging topic of upper atmospheric physics since many aspects of this striking phenomenon are still not well understood (Prölss, 1995; Burns *et al.*, 2007; Pedatella *et al.*, 2009; Ngwira *et al.*, 2011b). This is especially true for long-duration positive ionospheric storms, which are tabled as one of the major unresolved problems of ionospheric storms in reviews by Prölss (1997) and Buonsanto (1999), and even more recently by Burns *et al.* (2007). This thesis has shown that sustained energy injection in the high latitudes plays an important role in the development of long-duration positive ionospheric storm effects. Therefore, long-lived geomagnetic disturbances are of particular importance to the ionospheric community as they lead to significant modification of the F-region electron density over large scales, which can last for many hours or days (Huang *et al.*, 2005).

An investigation on ionospheric scintillation observed over a high-latitude Antarctic station during solar minimum is presented in the next chapter, and some of the challenges encountered during the initial investigation are also discussed.

Chapter 7

Ionospheric scintillation over Antarctica

7.1 Introduction

This chapter is concerned with the investigation of the occurrence of ionospheric scintillation at the high-latitude South African Antarctic polar research station (SANAE-IV) during the period of the extended solar cycle 23 minimum. In addition, this chapter also highlights some of the challenges that were encountered during the preliminary investigation.

The ionosphere is of practical importance for navigation systems and satellite communication because of its influence on the propagation of trans-ionospheric radio waves. Ionospheric scintillation, which is associated with the presence of plasma density irregularity structures in the ionosphere, can cause fading and phase variation of L-band navigation signals such as those used by GPS. A number of scintillation studies have been conducted in high-latitude regions, particularly at GPS frequencies (Erukhimov *et al.*, 1994; Aarons, 1997; Basu *et al.*, 1998; Doherty *et al.*, 2000; Smith *et al.*, 2008, and references therein). During solar maximum, high-latitude scintillation events are frequently observed in association with increased geomagnetic disturbances, but are rarely observed during solar minimum when geomagnetic activity is low (Basu *et al.*, 1988; Aarons *et al.*, 1995; Basu *et al.*, 1993). The auroral oval expands both equatorwards and polewards under disturbed geomagnetic conditions and contracts under quiet geomagnetic conditions.

It is associated with irregularities in the auroral region (irregularity oval).

7.2 Preliminary investigation

As highlighted in Section 1.2, the principal goal of the initial research project was to investigate the occurrence of ionospheric irregularities in the mid-latitude region using scintillation data recorded by GISTM receivers at Marion and Gough Islands. Scintillation data from a high-latitude station in Antarctica was included for comparison. However, due to unforeseen problems encountered during the preliminary investigation, the primary data recorded on the two mid-latitude instruments could not be used, as will be discussed.

After installation the two mid-latitude receivers recorded data for nearly two years. During the preliminary investigation, at some random time intervals, the receivers (independently) observed moderate to severe phase scintillation which were not consistent with expected scintillation observations. Such observations will be referred to as “false” or “anomalous” scintillation. Figure 7.1 shows an example of such observations recorded at Marion Island on 22 December 2007. Given that satellites are unevenly distributed throughout space, it would be expected that individual satellite signals experience scintillation events at different times as the signal path encounters the irregularity structures. But as highlighted in Figure 7.1b, the anomalous observations on a number of satellite signals appear to have the same profile and level of phase scintillation at the same time. This is irregular and implies that all the affected satellite signals enter the irregularity structures at the same time irrespective of their position in space.

The only logical explanation for observations of this nature is that the scintillation is simultaneously induced by the source mechanism(s). After investigation it turned out that the antennas of the two mid-latitude receivers had been installed on buildings that were subject to vibration. Vibration or antenna movement may be produced by strong winds or by structurally-transmitted movement elsewhere, such as seismic activity. These vibrations in turn can induce the anomalous phase scintillation. According to A. J. Van Dierendonck (personal communication), the

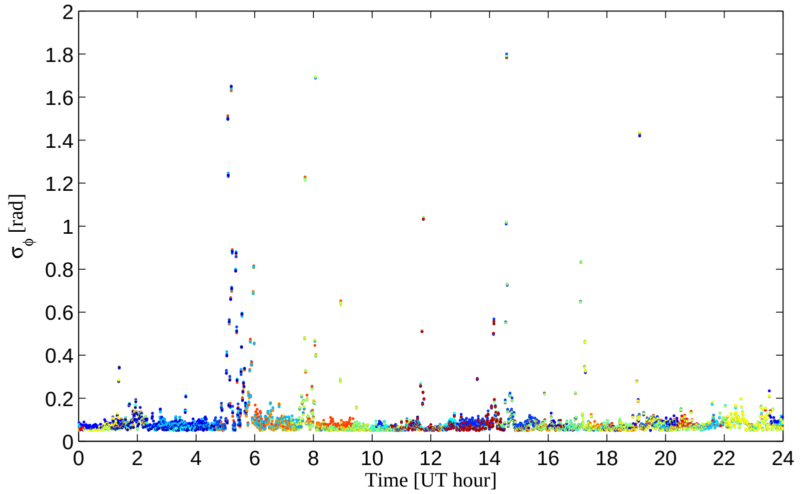

(a)

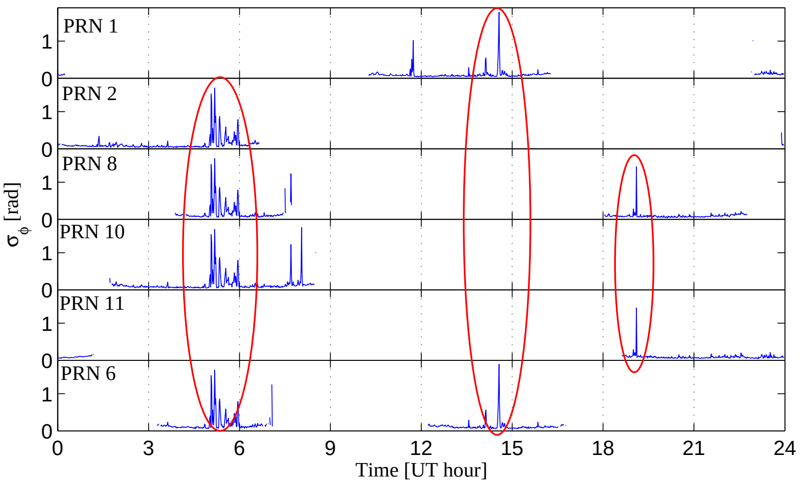

(b)

Figure 7.1: Anomalous scintillation observations recorded at Marion Island on 22 December 2007. (a) All available satellites and (b) selected satellites.

crystal oscillator on the modified GSV4004B GISTM receivers may be affected by vibrations, which can manifest in the form of identical phase scintillations on all channels irrespective of the location of the ray paths of the visible satellites in an absence of accompanying amplitude scintillation (Figure 7.1). In order to address this problem, the two antennas were moved in 2010 and subsequently mounted on solid rock-mounted structures. Improved quality data is now guaranteed.

The scintillation data collected by the Antarctic station receiver, however, proved to be reliable, and scintillation observations for three particular days with fairly low to moderate magnetic activity are presented and discussed in the rest of this chapter. The dates of these events are 28 April 2007, 24 May 2007 and 9 March 2008, with an average *Dst* index of -31, -42 and -12 nT respectively for the hourly periods under consideration. The monthly mean sunspot numbers for the months of these events were typically in the range of 3.4 to 11.7 during the extended solar cycle 23 minimum period. Figure 7.2 shows the location of the SANAE-IV station (MLAT 66°S, L-shell 4.41), relative to other stations in the Antarctic region. It is worth noting that only satellite signals with ray paths above 30° elevation were considered in order to minimise the effects of multipath.

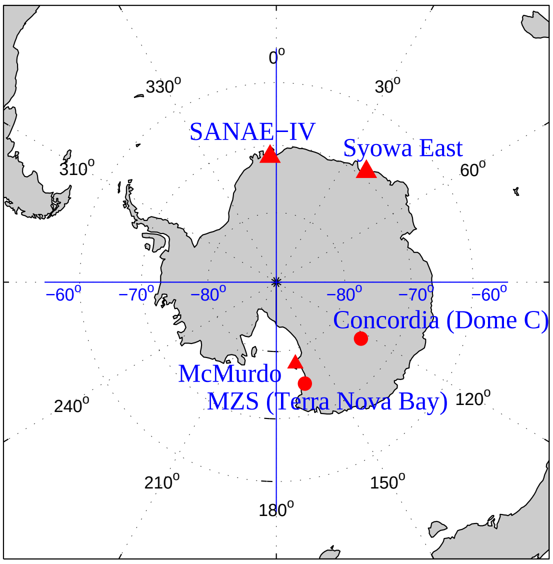

Figure 7.2: Map of Antarctic showing the location of SANAE-IV relative to other stations.

7.3 Results

This section presents observations of phase scintillation (σ_ϕ) at SANAE-IV and focuses only on three days that had significant levels of σ_ϕ during the period from December 2006 to December 2008. In all the cases considered, the S_4 index values did not exceed 0.2. It is commonly accepted that at high latitudes GPS scintillation receivers record high σ_ϕ in the presence of low S_4 (Kersley *et al.*, 1995; Doherty *et al.*, 2000; Forte, 2005). Doherty *et al.* (2000) investigated auroral scintillation over Fairbanks, Alaska, for a near solar maximum period and found that there was frequent phase scintillation activity with negligible amplitude scintillation. The occurrence of phase without amplitude scintillation indicates that most of the scintillation was caused by the presence of large-scale structures, i.e. arising from irregularities above the Fresnel length with scale-sizes of few tens of kilometres at GPS frequencies (Yeh and Liu, 1982; Kersley *et al.*, 1995). On the other hand, observations of amplitude scintillation are dominated by the effect of irregularities with a scale-size approximately near the Fresnel scale length, which are typically of the order of several hundred meters to a kilometre (Aarons *et al.*, 1997).

By contrast, recent works suggest that the occurrence of high σ_ϕ in the presence of low S_4 could be attributed to improper data detrending methods (Forte and Radicella, 2002; Forte, 2005; Beach, 2006). It has been argued that the σ_ϕ index is sensitive to data detrending (Forte and Radicella, 2002). Forte (2005) and Beach (2006) show that failure to adequately take irregularity dynamics into consideration may result in false conclusions, as discussed in Section 3.4.2. However, the full details of these arguments are outside the scope of this thesis work, and interested readers may consult the provided references for more details. Nevertheless, it is necessary to note that the general expectation is that the intensity and frequency of scintillation events decrease during years of low solar flux (solar minimum phase), for both amplitude and phase type events.

Figure 7.3 shows the detrended horizontal magnetic field H-component (ΔH), the 30 MHz riometer absorption and σ_ϕ observations. The σ_ϕ was observed on signals transmitted by three GPS satellites: PRN 9, 18 and 22 during the period 00:00 to 04:00 UT on 28 April 2007 (22:14 to 02:15 corrected magnetic local time, MLT).

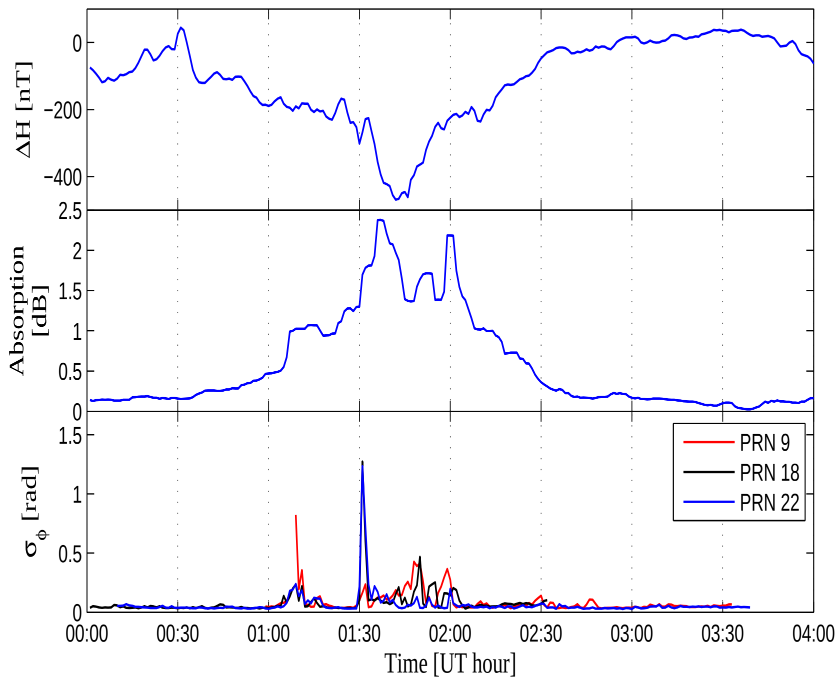

Figure 7.3: Magnetometer horizontal magnetic field ΔH (top) and 30 MHz riometer absorption measurements (middle). The bottom panel shows 1-minute phase scintillation observed on the signals from three GPS satellites 'PRN 9, 18 and 22'. All observations were recorded at SANAE-IV station on April 28, 2007.

These were the only satellites visible with σ_ϕ above 0.4 radians. The first event was observed on PRN 9 and the maximum phase scintillation value of 1.27 radians was recorded on PRN 18. Note that PRN 18 and PRN 22 simultaneously recorded a peak in scintillation activity at 01:30 UT (23:43 MLT on 27 April). With respect to the receiver, these satellites are basically all within an azimuthal range of a 60° degree view of the sky and signals from them could have been affected by the same irregularity structures. This is because the spatial and temporal extent of irregularities can be much greater in the auroral regions than in other regions as discussed by Doherty *et al.* (1994).

Recordings of phase scintillation as depicted in Figure 7.4 (bottom) were observed from 23 May to 24 May, 2007. The affected signals were transmitted by the three GPS satellites PRN 9, 18 and 22 between 23:00 UT on 23 May and 02:00 UT on

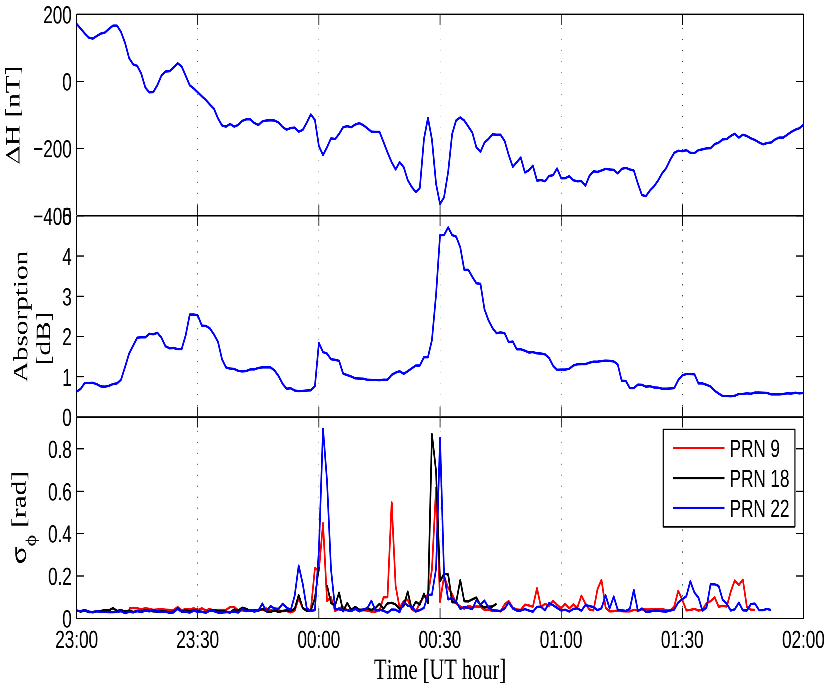

Figure 7.4: Same as Figure 7.3, but showing observations for the period between 23:00 UT on May 23 and 01:30 UT on May 24, 2007.

24 May (21:15 MLT 23 May to 01:30 MLT on 24 May). The highest level of phase scintillation (σ_ϕ = 0.90 radians) was observed on the signal from PRN 22. The σ_ϕ level on the PRN 22 signal peaked just after midnight MLT with another peak about 30 minutes later when the satellite passed from higher to lower elevation angles. Three distinct scintillation peaks were observed during the pass of PRN 9.

On March 9, 2008, significant σ_ϕ activity was recorded on four GPS satellite signals between 04:30 and 07:00 UT (02:45 to 05:17 MLT) as illustrated in Figure 7.5. Peak scintillation activity occurred at different times on the signals of the selected satellites. The first significant event (σ_ϕ = 0.5 radians) on this day was observed on PRN 22 around 04:20 UT (02:35 MLT) and the highest recording of 1.92 radians ocurred about 15 minutes later on the signal from the same satellite. Two scintillation peaks were observed on the signal transmitted by PRN 1 at about 06:25 UT and shortly after 06:30 UT during the recovery phase of the geomagnetic disturbance. In comparison to the other two days, the σ_ϕ levels observed on

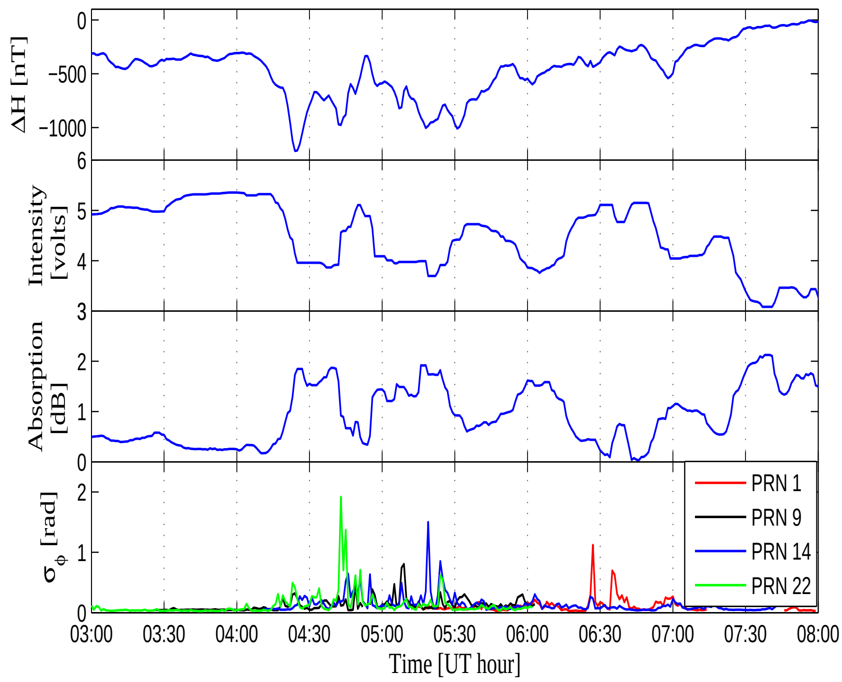

Figure 7.5: Comparison of horizontal magnetic field ΔH (top), 30 MHz riometer absorption and 30 MHz riometer signal intensity measurements (middle) observed on March 9, 2008. The corresponding 1-minute phase scintillation recorded on signals from four GPS satellites are shown in the bottom panel.

March 9 were significantly higher.

7.4 Discussion

At high latitudes scintillation is frequently observed during magnetically disturbed conditions. The response is associated with an influx of high energy particles that gain entry into the Earth's polar cap regions when the solar wind IMF couples with the Earth's magnetic field. This leads to production of the visible aurora and to ionospheric irregularities which are responsible for scintillation (Kersley *et al.*, 1988; Aarons *et al.*, 1995; Doherty *et al.*, 2000).

Figure 7.3 clearly shows that the high riometer absorption, in conjunction with a fall to -500 nT in the H-field, corresponds to the time that scintillation was observed over SANAE-IV on April 28. The scintillation events occurred around midnight MLT and appear to have been triggered by substorm activity before the main phase of the storm. Increased riometer absorption is a manifestation of enhanced ionisation in the D- and E-layers of the high-latitude ionosphere which is associated with auroral electron precipitation. Precipitation is characterised by high energy particles (from ∼500 eV to 20 keV) which produce ionisation at lower heights (D- and E-region) and low energy particles (from ∼50 to few hundred eV) which produce ionisation in the F-region (see Aarons *et al.*, 1997; Kintner *et al.*, 2002, and references therein). In Figure 7.4 the peak in absorption at 00:00 UT (22:22 MLT) is attributed to substorm activity. The peak in absorption at about 00:30 UT (22:50 MLT) is during the main phase of the storm when the H-field decreased to -365 nT. Both these cases confirm the double peak in scintillation noted in Figure 7.4. Note that even though the second absorption event at 00:30 UT exhibited absorption of 2.5 dB more than that at 00:00 UT, the scintillation levels in both cases are approximately the same.

Furthermore, in Figure 7.4 the peak in absorption and scintillation seen around 00:00 UT (22:22 MLT near midnight MLT), was expected due to the explosive discharge of magnetic energy previously stored in the Earth's magnetotail. This is a typical feature of substorm activity leading to enhanced ionisation of particles in the plasma sheet and their injection deeper into the inner magnetosphere and ionosphere. Substorm absorption features are related to the occurrence of dynamic processes in the unstable magnetospheric tail region and are generally a signature of the precipitation of electrons with energies around a few tens of keV in the night sector of the auroral zone (Stauning, 1996, and references therein). Therefore, substorm intensifications play a significant role in the production of irregularities in the auroral zone, as increased energy flows from the solar wind into the magnetosphere (see Skone and Cannon, 1999; Skone and De Jong, 2000; Prikryl *et al.*, 2011, and references therein). In their investigation of the ionospheric range delay, Skone and Cannon (1999) showed that TEC, which is proportional to the ionospheric range delay, varied significantly during auroral substorm events. The work by Skone and De Jong (2000) demonstrated that substorm-induced scintillation can degrade GPS receiver tracking performance. However, these authors emphasise the need to consider both the magnitude of scintillation and the type of

GPS receiver utilised in data collection for the effective assessment of the impact of ionospheric activity on GPS receiver performance.

Figure 7.5 displays a comparison of the horizontal H-field, riometer absorption and riometer signal intensity measurements with the observed σ_ϕ data. The top panel establishes that the horizontal geomagnetic field was highly disturbed as it decreased from about -200 nT to -1100 nT in roughly 30 minutes. During the same period there was an increase in absorption and an accompanying fade in the 30 MHz riometer signal intensity (middle panels). As mentioned earlier, the σ_ϕ levels for this day (March 9) were higher compared to the other two days. This could be attributed to the highly disturbed geomagnetic conditions, which is an indication of enhanced magnetospheric energy input. Two interesting features worth recognising in this figure relate to the two substorm events, one at about 04:45 UT and another just after 05:00 UT. Both corresponded to enhanced σ_ϕ levels observed on the signals of PRN 22 and 9 respectively (Figure 7.5).

Considering that the high-latitude ionosphere is strongly influenced by solar wind dynamics (Kelley, 1989; Carlson Jr. *et al.*, 2004), a knowledge of the solar wind components is essential to understanding the high-latitude ionospheric dynamics. Displayed in Figure 7.6 are the interplanetary and *AE* index conditions corresponding to the case study events on March 9. The IMF Bz-component was directed predominately southward between 02:00 and 04:30 UT, a condition which may have later resulted in multiple magnetospheric substorms with related soft particle precipitation into the auroral zone. Under these conditions, solar wind energy is released into the auroral regions by means of large-scale electric currents carried by high-energy particles along terrestrial magnetic field lines into the high-latitude ionosphere (Tsurutani *et al.*, 2004; Maruyama *et al.*, 2007; Wolf *et al.*, 2007). A significant increase in the *AE* index with a value around 800 nT was observed after the occurrence of both substorm events (see Figure 7.6), a strong indication of the presence of ionospheric currents (auroral electrojet). Precipitating high energy electrons, which are energised by the interaction of the solar wind with the magnetosphere, are responsible for the production of auroral irregularities (Kelley *et al.*, 1982; Kersley *et al.*, 1995; Skone and Cannon, 1999; Doherty *et al.*, 2000).

Additionally, observations by the DMSP F13 satellite shown in Figure 7.7 compare well with magnetometer and riometer measurements in Figure 7.5, during the time that scintillation was observed on the signals from PRN 9 and 14. The DMSP satellites are in sun-synchronous near-polar orbits at an altitude of about 830 km. The top panel of Figure 7.7 shows that the average energy of precipitating ions and electrons increased and then begins to fluctuate in the high-latitude region around 69.1°S. The third panel shows that there was high electron energy flux during the same period at the DMSP F13 orbit height. This is confirmation of the presence of soft electron precipitation in the auroral ionosphere. The time of the electron energy fluctuation corresponded to the point of closest approach of DMSP F13 to the SANAE latitude and longitude, near the time of the substorm (03:14 MLT) and high riometer absorption (Figure 7.5).

The path (blue line) mapped out by the DMSP F13 satellite as it passed over the high latitudes at the DMSP altitude is shown in Figure 7.8. This confirms DMSP

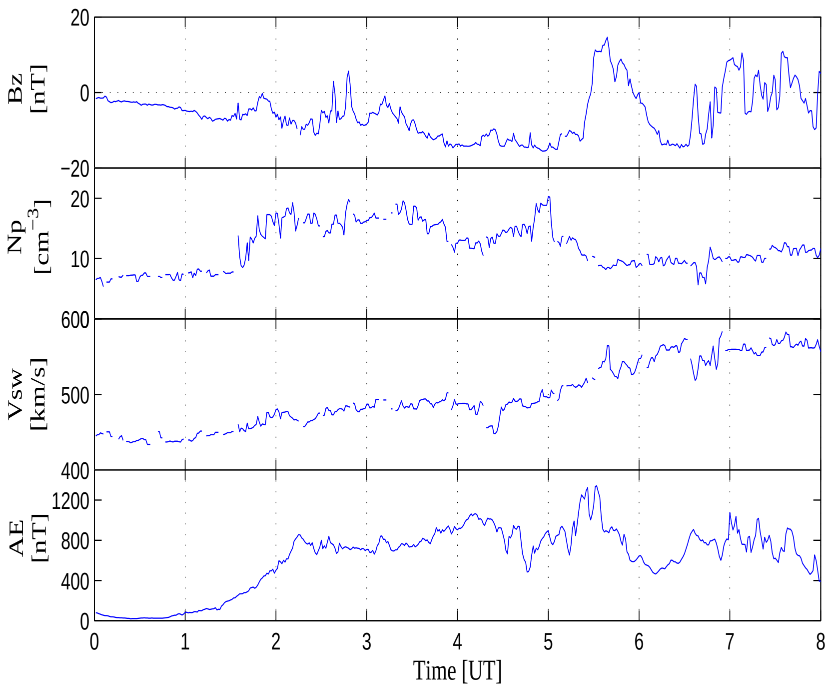

Figure 7.6: OMNI interplanetary conditions (top three panels) and AE index (bottom) for March 9, 2008.

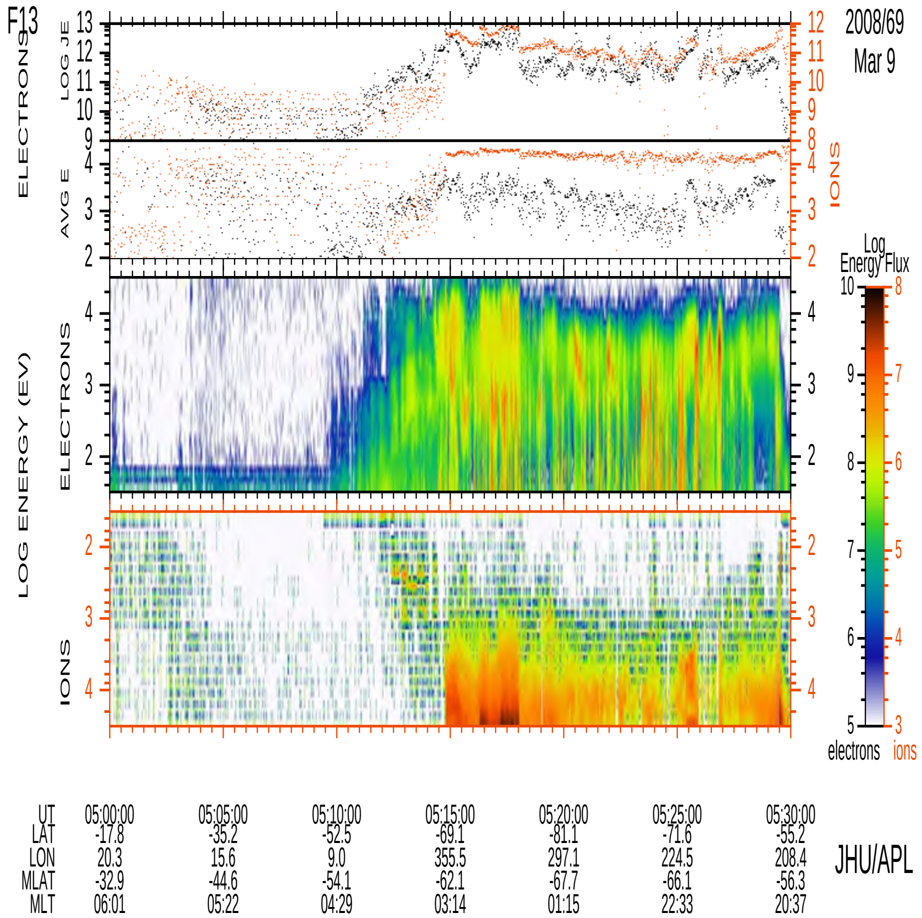

Figure 7.7: DMSP F13 ion and electron energy flux data recorded between 05:00 and 05:30 UT during a flight on March 9, 2008.

precipitation data (Figure 7.7) which suggest that the auroral oval extended over SANAE-IV at the onset of the substorm during this particular passage. The solar wind data above shows that the IMF Bz had a major negative excursion for over two and a half hours, and may have been the means by which energy was continuously fed into the auroral ionosphere, thereby causing the auroral oval to expand equatorward over the SANAE-IV latitude and longitude.

Studies have shown that, particularly during magnetically quiet periods, intense scintillation events are a function of the entrance and exit of an observation site into the expanding auroral oval, the dynamics of the individual storm and the local magnetic time (Kersley *et al.*, 1995; Aarons *et al.*, 1997). The auroral oval is associated with electron density irregularities which are generated by a number of

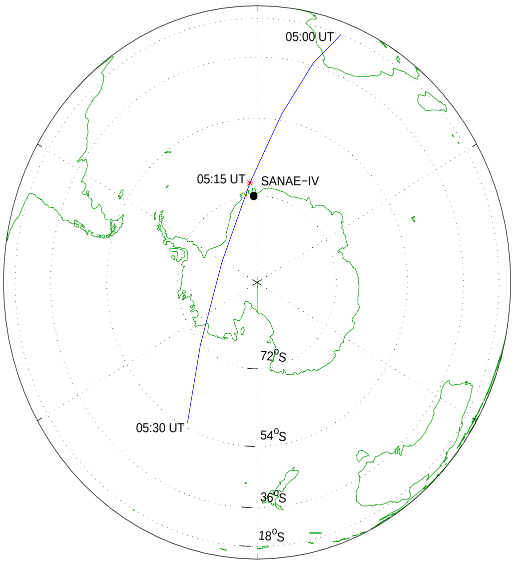

Figure 7.8: As DMSP F13 travelled poleward, it crossed over the point of closest approach just after 05:15 UT on March 9, 2008. The blue line is the track of the satellite at the DMSP height.

plasma instability processes such as velocity shears and precipitation of both high and low energy electrons in the E- and F-regions respectively (Kelley *et al.*, 1982; Kersley *et al.*, 1988; Basu *et al.*, 1998). During magnetic storms, the generation of irregularities is still typically controlled by the entry and exit of the observation station into the auroral oval, however, the storm timing and progression alters the diurnal pattern (Aarons *et al.*, 1997). The discussion by Aarons *et al.* (1997) points out that continuing high magnetic activity may be responsible for continuous energy input to the magnetosphere which in turn controls the development and movement of the auroral oval.

Finally, it is important to examine energy injection into the magnetosphere and its role in the development of irregularities. In their study, Rino and Matthews (1980) investigated the occurrence of scintillation over Poker Flat, Alaska and established that for the most part, scintillation activity followed the general trend of local magnetic conditions. In interpreting the present observations, one important feature to note is that during certain time intervals, high riometer absorption and

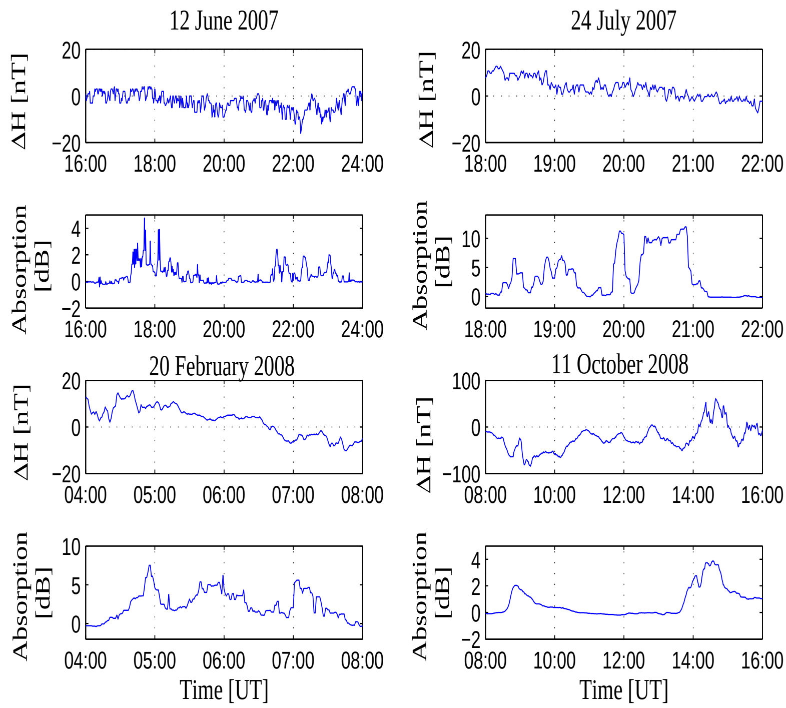

Figure 7.9: Horizontal magnetic field ΔH and 30 MHz riometer absorption comparisons for four selected days which had low magnetic activity and high riometer absorption. No scintillation was observed on these days.

low geomagnetic activity are observed, but no scintillation events, i.e. $\sigma_\phi < 0.2$. Figure 7.9 provides examples of such features. The figure shows plots of the detrended horizontal magnetic field ΔH and 30 MHz riometer absorptions on four selected days. By contrast, when scintillation is observed, both high riometer absorption and enhanced magnetic activity are present. Riometer absorption is typically at the D- and E-layer altitudes. It is argued here that perhaps these features establish the significant contribution that F-region irregularities play in the production of auroral scintillation around solar minimum. The cases cited above may be evidence of the absence of F-region irregularities. In their studies, Aarons *et al.* (1995) and Aarons *et al.* (1997) found that during quiet magnetic conditions and particularly for years of low solar flux, F-region irregularities were more dominant than E-layer irregularities in the production of scintillation. In any case, such events emphasise the need for external energy injection into the ionosphere in order to create unstable conditions which induce the generation of irregularities responsible for the production of scintillation in the auroral ionosphere.

The results presented in this study are generally in agreement with findings by Prikryl *et al.* (2011) who conducted a climatology study of GPS phase scintillation in the northern high latitudes by using data from the Canadian high Arctic ionospheric network during the 2008-2009 solar minimum period. Prikryl *et al.* (2011) found that the strongest phase scintillation events occurred in association with auroral arc brightening and substorms. The study also found a defined statistical agreement between geomagnetic activity and phase scintillation occurrence.

7.5 Summary

Severe ionospheric scintillation is known to have a detrimental impact on the reliability of GPS navigation systems and satellite communication. The focus of this study was the occurrence of phase scintillation events based on the high-latitude auroral station receiver measurements during a solar minimum period.

Using a multi-instrument approach to diagnose the ionosphere, it was shown that the occurrence of scintillation at the SANAE-IV polar research station can be associated with auroral electron precipitation. Observations confirm that scintillation events are strongly dependent on magnetic activity. This dependence has been recognised for a long time and is in agreement with other studies (Aarons *et al.*, 1997; Prikryl *et al.*, 2010, 2011). Also it has been shown that intense scintillation events are a function of the entrance and exit of an observing site into the expanding auroral oval particularly during magnetically quiet periods.

This study demonstrated that substorms play an essential role in the production of scintillation in the high-latitude ionosphere. Furthermore, the investigation revealed that external energy input into the ionosphere plays a leading role in the development of irregularities which produce scintillation.

Chapter 8

Summary and conclusions

In this thesis the effects of intense geomagnetic storms on the upper atmosphere was investigated for the storm events on 15 May 2005 and 24-27 July 2004. The emphasis was on mid-latitude locations over South Africa. In addition, high-latitude ionospheric irregularities were investigated by using ionospheric scintillation data recorded at the South African Antarctic polar research station during a solar minimum period. This chapter summarises the investigation and the major challenges encountered.

8.1 The thesis work

Currently, major challenges face the ionospheric community, such as understanding the development of geomagnetic storms and the impact of storms on ionospheric behaviour, the development and evolution of ionospheric irregularities, and the development of methods for predicting the ionosphere. Findings of the investigation presented in this thesis include the following:

The F2-layer uplift, as determined by the use of ionosonde measurements and the subsequent TEC enhancement, observed during the 15 May 2005 storm event was associated with equatorward neutral winds and the passage of TIDs. The two TIDs propagated with average velocities of $\sim$438 and $\sim$515 m/s during the first and second event respectively. The velocity of the first TID (438 m/s) was consistent with velocities calculated in other studies for the same storm event. The ionospheric response on May 15 was characterised by a dissimilarity between the foF2 and the TEC. This could be related to the competing effects of the westward electric field and equatorward neutral wind. Furthermore, the observed TEC enhancements were not due to the expansion of the EIA into the mid-latitude regions, because a strong westward current was observed in the African sector. Therefore, the equatorial electric field could not be responsible for the TEC enhancements. This supports the argument that neutral winds could be the primary cause of the observed TEC enhancements.

Research for this thesis demonstrated that the positive storm enhancement on both 25 and 27 July 2004 lasted for more than 7 hours and were classified as long-duration positive ionospheric storm effects. Both global TEC maps and the TOPEX/JASON-1 altimeter TEC showed that the EIA asymmetry was broader and of higher density in the winter hemisphere than in the summer hemisphere. This was attributed to the summer-to-winter trans-equatorial neutral winds that move the ionospheric plasma to the winter hemisphere across the equator. Ionosonde measurements from stations in South Africa revealed that the rise of the peak height (hmF2) was accompanied by an enhancement of peak electron density (foF2). It has been suggested that the long-duration positive storm effects could have been caused by large-scale thermospheric wind circulation and enhanced equatorward neutral winds. These processes were in turn probably driven mainly by enhanced and sustained energy input in the high-latitude ionosphere. This is evident by the prolonged high-level geomagnetic activity observed on both 25 and 27 July 2004.

It has been shown that the occurrence of scintillation at the SANAE-IV polar research station was associated with auroral electron precipitation. Observations showed that intense scintillation events were strongly dependent upon magnetic activity, and upon the entrance and exit of the observing site into the expanding auroral oval. In addition, it was demonstrated that substorms play an essential role in the production of scintillation in the high-latitude ionosphere, and that external energy input into the ionosphere is necessary for the generation of irregularities that produce scintillation.

Finally, it was established that there are not enough data sources to fully investigate the ionospheric storm responses presented in this thesis. More data is required for a complete understanding of the storm-driving mechanisms. Therefore, due to the absence of any direct observations of proposed mechanisms responsible for positive storm effects, it is likely that more than one mechanism could be responsible for the observed density enhancements. This implies that more observations are necessary to distinguish between the various mechanisms responsible for positive storm effects.

8.2 Challenges

This thesis marks the first attempt to investigate the mechanisms responsible for the generation of positive storm effects over mid-latitude South Africa. The study revealed a number of challenges that need to be addressed in future studies. One of the key factors is the need to expand the existing infrastructure, such as the implementation of new instruments and projects, in order to fully develop our understanding of ionospheric storms. This would enable us to distinguish between the various storm drivers over the Southern African mid-latitude region.

Since the two case studies on ionospheric storms date back to the era when part of the existing infrastructure was unavailable or insufficient, some of the concerns may have been addressed or are in the process of being addressed. For example, the setting up of a Doppler radar system in the Western Cape region is an important development for TID studies.

8.3 Future work

The goal for future studies should be to conduct an analysis of the occurrence of scintillation at Marion and Gough Islands. Since the GISTM antennas at the two sites were moved to more suitable and stable locations, there is need to perform a quality check on the data and to also perform a climatology study of the occurrence of scintillation in order to advance our understanding of irregularities over the two stations.

In conclusion, this thesis has highlighted some of the major challenges that need to be addressed in order to fully understand the ionospheric storm drivers over the Southern Africa mid-latitudes region. In addition, a successful ionospheric scintillation study was performed for a high-latitude Antarctic polar research station during solar minimum conditions. Therefore, the results presented in this thesis on the ionospheric response to geomagnetic disturbances at middle and high latitudes will provide essential information to direct further investigation aimed at developing these emerging fields of study in South Africa.

References

Aarons J. “The role of the ring current in the generation or inhibition of equatorial F layer irregularities during magnetic storms”. Radio Science, vol. 26(4), pp. 1131–1149, 1991.

Aarons J. “The longitudinal morphology of equatorial F-layer irregularities relevant to their occurrence”. Space Science Reviews, vol. 63, pp. 209–243, 1993.

Aarons J. “Global positioning system phase fluctuations at auroral latitudes”. Journal of Geophysical Research, vol. 102(A8), pp. 17,219–17,231, 1997.

Aarons J., Kersley L. and Rodger A.S. “The sunspot cycle and “auroral” F layer irregularities”. Radio Science, vol. 30(3), pp. 631–638, 1995.

Aarons J. and Lin B. “Development of high latitude phase fluctuations during the January 10, April 10-11, and May 15, 1997 magnetic storms”. Journal of Atmospheric and Solar-Terrestrial Physics, vol. 61, pp. 309–327, 1999.

Aarons J., Mendillo M. and Yantosca R. “GPS phase fluctuations in the equatorial region during the MISETA 1994 campaign”. Journal of Geophysical Research, vol. 101(A12), pp. 26,851–26,862, 1996.

Aarons J., Mendillo M. and Yantosca R. “GPS phase fluctuations in the equatorial region during sunspot minimum”. Radio Science, vol. 32, pp. 1535–1550, 1997.

Abdu M.A. “Major phenomena of equatorial ionosphere-thermosphere system under disturbed conditions”. Journal of Atmospheric and Solar-Terrestrial Physics, vol. 59(13), pp. 1507–1519, 1997.

Alfonsi L., Kavanagh A.J., Amata E., Cilliers P., Correia E., Freeman M., Kauristie K., Liu R., Luntama J.P., Mitchell C.N. and Zherebtsov G.A. “Probing the high latitude ionosphere from ground-based observations: The state of current knowledge and capabilities during IPY (2007-2009)". Journal of Atmospheric and Solar-Terrestrial Physics, vol. 70, pp. 2293–2308, 2008.

Anderson D., Anghel A., Chau J. and Veliz O. "Daytime vertical $\mathbf{E} \times \mathbf{B}$ drift velocities inferred from ground-based magnetometer observations at low latitudes". Space Weather, vol. 2, S11001, 2004. doi:10.1029/2004SW000095.

Bagiya M.S., Iyer K.N., Joshi H.P., Thamp S.V., Tsugawa T., Ravindran S., Sridharan R. and Pathan B.M. "Low-latitude ionospheric-thermospheric response to storm time electrodynamical coupling between high and low latitudes". Journal of Geophysical Research, vol. 116, A01303, 2011. doi:10.1029/2010JA015845.

Basu S., Basu Sa., Eastes R., Huffman R.E., Daniell R.E., Chaturvedi P.K., Valladares C.E. and Livingston R.E. "Remote sensing of Auroral E region plasma structure by radio, radar, and UV techniques at solar minimum". Journal of Geophysical Research, vol. 98(A2), pp. 1589–1602, 1993.

Basu S., Basu Sa., Makela J.J., Sheehan R.E., MacKenzie E., Doherty P., Wright J.W., Keskinen M.J., Pallamraju D., Paxton L.J. and Berkey F.T. "Two components of ionospheric plasma structuring at midlatitudes observed during the large magnetic storm of October 30, 2003". Geophysical Research Letters, vol. 32, L12S06, 2005a. doi:10.1029/2004GL021669.

Basu S., Basu Sa., Valladares C.E., Yeh H.C., Su S.Y., MacKenzie E., Sultan P.J., Aarons J., Rich F.J., Doherty P., Groves K.M. and Bullett T.W. "Ionospheric effects of major magnetic storms during the International Space Weather Period of September and October 1999: GPS observations, VHF/UHF scintillations, and in situ density structures at middle and equatorial latitudes". Geophysical Research Letters, vol. 106(A12), pp. 30,389–30,413, 2001.

Basu S., Basu Sa., Weber E.J. and Coley W.R. "Study of polar cap scintillation modeling using DE 2 irregularity measurements at 800 km". Radio Science, vol. 23(4), pp. 545–553, 1988.

Basu S. and Basu Su. "Equatorial scintillations−a review". Journal of Atmospheric and Terrestrial Physics, vol. 43(5/6), pp. 473–489, 1981.

Basu S., Basu Su., Groves K.M., MacKenzie E., Keskinen M.J. and Rich F.J. “Near-simultaneous plasma structuring in the midlatitude and equatorial ionosphere during magnetic superstorms”. Geophysical Research Letters, vol. 32, LI2S05, 2005b.

Basu S., Groves K.M., Basu Su. and Sultan P.J. “Specifcation and forecasting of scintillations in communication/navigation links: current status and future plans”. Journal of Atmospheric and Solar-Terrestrial Physics, vol. 64, pp. 1745–1754, 2002.

Basu S., Weber E.J., Bullet T.W., Keskinen M.J., MacKenzie E., Doherty P., Sheehan R., Kuenzler H., Ning P. and Bongiolatti J. “Characteristics of plasma structuring in the cusp/cleft region at Svalbard”. Radio Science, vol. 33(6), pp. 1885–1899, 1998.

Bauske R. and Prölss G.W. “Modeling the ionospheric response to traveling atmospheric disturbances”. Journal of Geophysical Research, vol. 102(A7), pp. 14,555–14,562, 1997.

Bauske R. and Prölss G.W. “Numerical simulation of long-duration positive ionospheric storm effects”. Advances in Space Research, vol. 22(1), pp. 117–121, 1998.

Beach T.L. “Perils of the GPS phase scintillation index (σ_ϕ)”. Radio Science, vol. 41, RS5S31, 2006. doi:10.1029/2005RS003356.

Blanc M. and Richmond A.D. “The ionospheric disturbance dynamo”. Journal of Geophysical Research, vol. 85(A4), pp. 1669–1686, 1980.

Boteler D.H. “Space weather effects on power systems”. In *Space Weather*, Song D. et al. (eds.), American Geophysical Union, Washington, D.C., pp. 347–352, 2001.

Bowman G.G. “Small-scale ionospheric troughs detected over a range of midlatitude locations”. Annales Geophysicae, vol. 9(7), pp. 470–475, 1991.

Buonsanto M.J. “Millstone Hill incoherent scatter F region observations during the disturbances of June 1991”. Journal of Geophysical Research, vol. 100(A4), pp. 5743–5755, 1995.

Buonsanto M.J. “Ionospheric storms−a review”. Space Science Reviews, vol. 88, pp. 563–601, 1999.

Burns A.G., Killeen T.L. and Roble R.G. “A theoretical study of thermospheric composition perturbations during an impulsive geomagnetic storm”. Journal of Geophysical Research, vol. 96(A8), pp. 14,153–14,167, 1991.

Burns A.G., Solomon S.C., Wang W. and Kileen T.L. “The ionospheric and thermospheric response to CMEs: Challenges and successes”. Journal of Atmospheric and Solar-Terrestrial Physics, vol. 69, pp. 77–85, 2007.

Campbell W.H. *Introduction to geomagnetic fields*. Cambridge University Press, Cambridge, 1997.

Carlson Jr. H.C., Oksavik K., Moen J. and Pedersen T. “Ionospheric patch formation: Direct measurements of the origin of a polar cap patch”. Geophysical Research Letters, vol. 31, L08806, 2004. doi:10.1029/2003GL018166.

Cervera M.A. and Thomas R.M. “Latitudinal and temporal variation of the equatorial ionospheric irregularities determined from GPS scintillation observations”. Annales Geophysicae, vol. 24, pp. 3329–3341, 2006.

Christensen A.B., Paxton L.J., Avery S., Craven J., Crowley G., Humm D.C., Kil H., Meier R.R., Meng C.I., Morrison D., Ogorzalek B.S., Straus P., Strickland D.J., Swenson R.M., Walterscheid R.L., Wolven B. and Zhang Y. “Initial observations with the Global Ultraviolet Imager (GUVI) in the NASA TIMED satellite mission”. Journal of Geophysical Research, vol. 108(A12), pp. 1451–1466, 2003.

Cilliers P.J., Opperman B.D.L., Mitchell C.N. and Spencer P.J. “Electron density profiles determined from tomographic reconstruction of total electron content obtained from GPS dual frequency data; first results from the South African network of dual frequency GPS receiver stations”. Advances in Space Research, vol. 34, pp. 2049–2055, 2004.

Coster A.J., Foster J.C. and Erickson P. “Monitoring the ionosphere with GPS: Space weather”. GPS World, (14), pp. 42–49, 2003.

Crowley G. and Meier R.R. "Disturbed O/N_2 ratios and their transport to middle and low latitudes". In *Midlatitude ionospheric dynamics and disturbances*, Kintner P. M. et al. (eds.), American Geophysical Union, Washington, D.C., pp. 221–234, 2008.

Dashora N., Sharma S., Dabas R.S., Alex S. and Pandey R. "Large enhancements in low latitude total electron content during 15 May 2005 geomagnetic storm in Indian zone". Annales Geophysicae, vol. 27, pp. 1802–1820, 2009.

Davies K. *Ionospheric Radio.* Peter Peregrinus, London, 1990.

De Franceschi G., Alfonsi L., Romano V., Aquino M., Dodson A., Mitchell C.N., Spencer P. and Wernik A.W. "Dynamics of high-latitude patches and associated small-scale irregularities during the October and November 2003 storms". Journal of Atmospheric and Solar-Terrestrial Physics, vol. 70, pp. 879–888, 2008.

De Paula E.R., Kantor I.J. and De Rezende L.F.C. "Characteristics of the GPS signal scintillations during ionospheric irregularities and their effects over GPS systems". In *Proceedings of the 4th Brazilian Symposium on the Inertial Engineering (SBEIN'04), São José dos Campos, Brazil.* 2004.

De Paula E.R., Rodrigues F.S., Iyer K.N., Kantor I.J., Kintner P.M., Ladvina B.M. and Kil H. "Equatorial anomaly effects on GPS scintillations in Brazil". Advances in Space Research, vol. 31(3), pp. 749–754, 2003.

De Rezende L.F.C., De Paula E.R., Batista I.S., Kantor I.J. and De Assis Honorato Muella M.T. "Study of ionospheric irregularities during intense magnetic storms". Brazilian Journal of Geophysics, vol. 25(Suppl. 2), pp. 151–158, 2007.

De Santis A., De Franceschi G., Zolesi B., Pau S. and Cander L.R. "Regional mapping of the critical frequency of the F2 layer by spherical cap harmonic expansion". Annales Geophysicae, vol. 9, pp. 401–406, 1991.

Ding F., Wan W., Ning B. and Wang M. "Large-scale traveling ionospheric disturbances observed by GPS total electron content during the magnetic storm of 29-30 October 2003". Journal of Geophysical Research, vol. 112, A06309, 2007. doi:10.1029/2006JA012013.

Doherty P., Coster A.J. and Murtagh W. "Space weather effects of October-November 2003". GPS Solutions, vol. 8, pp. 267–271, 2004.

Doherty P., Delay S.H., Valladares C.E. and Klobuchar J.A. "Ionospheric scintillation effects in the equatorial and auroral regions". In *Proceedings of ION GPS-2000, 19-22 September 2000, Salt Lake City, UT*, pp. 662–671, 2000.

Doherty P., Raffi E., Klobuchar J.A. and El-Arini M.B. "Statistics of time rate of change of ionospheric range delay". In *Proceedings of ION GPS-94, September 1994, Salt Lake City, Utah*, pp. 1589–1598, 1994.

Dubey S., Wahi R. and Gwal A.K. "Effects of ionospheric scintillation on GPS receiver at equatorial anomaly region Bhopal". In *URSI XXVIIIth General Assembly, GP1.57(01238), New Delhi, India*. 2005.

Erukhimov L.M., Myasnikov E.N., Kosolapenko V.I., Cheremnyj V.A. and Evstaf'ev O.V. "Observation of total electron content, amplitude and phase scintillations in the auroral ionosphere". Radio Science, vol. 29(1), pp. 311–315, 1994.

Fejer B.G., Jensen J.W., Kikuchi T., Abdu M.A. and Chau J.L. "Equatorial ionospheric electric fields during the November 2004 magnetic storm". Journal of Geophysical Research, vol. 112, A10304, 2007. doi:10.1029/2007JA012376.

Fejer B.G. and Scherliess L. "Time dependent response of equatorial ionospheric electric fields to magnetospheric disturbances". Geophysical Research Letters, vol. 22, p. 851, 1995.

Fejer B.G. and Scherliess L. "Empirical models of storm time equatorial zonal electric fields". Geophysical Research Letters, vol. 102(A11), pp. 24,047–24,056, 1997.

Fejer B.G., Scherliess L. and De Paula E.R. "Effects of the vertical plasma drift velocity on the generation and evolution of equatorial spread F". Journal of Geophysical Research, vol. 104(A9), pp. 19,859–19,869, 1999.

Forte B. "Optimum detrending of raw GPS data for scintillation measurements at auroral latitudes". Journal of Atmospheric and Solar-Terrestrial Physics, vol. 67(12), pp. 1100–1109, 2005.

Forte B. and Radicella S. “Problems in data treatment for ionospheric scintillation measurements”. Radio Science, vol. 37(6), p. 1096, 2002.

Foster J.C. “Storm time plasma transport at middle and high latitude”. Journal of Geophysical Research, vol. 98(A2), pp. 1675–1689, 1993.

Foster J.C., Coster A.J., Erickson P.J., Holt J.M., Lind F.D., Rideout W., McCready M., Van Eyken A., Barnes R.J., Greenwald R.A. and Rich F.J. “Multiradar observations of the polar tongue of ionization”. Journal of Geophysical Research, vol. 110, A09S31, 2005. doi:10.1029/2004JA010928.

Foster J.C., Erickson P.J., Coster A.J., Goldstein J. and Rich F.J. “Ionospheric signatures of plasmaspheric tails”. Geophysical Research Letters, vol. 29(13), pp. 1623–1626, 2002.

Foster J.C. and Rich F.J. “Prompt midlatitude electric fields effects during severe geomagnetic storms”. Journal of Geophysical Research, vol. 103(A11), pp. 26,367–26372, 1998.

Fuller-Rowell T.J., Codrescu M.V., Moffett R.J. and Quegan S. “Response of the thermosphere and ionosphere to geomagnetic storms”. Journal of Geophysical Research, vol. 99, p. 3893, 1994.

Fuller-Rowell T.J., Codrescu M.V., Rishbeth H., Moffett R.J. and Quegan S. “Seasonal response of the thermosphere and ionosphere to geomagnetic storms”. Journal of Geophysical Research, vol. 101, pp. 2343–2353, 1996.

Fuller-Rowell T.J., Codrescu M.V., Roble R.G. and Richmond A.D. “How does the thermosphere and ionosphere react to a geomagnetic storm?” In *Magnetic storms*, Tsurutani B. T. et al. (eds.), American Geophysical Union, Washington D.C., pp. 203–225, 1997.

Fuller-Rowell T.J., Richmond A.D. and Maruyama N. “Global modeling of storm-time thermospheric dynamics and electrodynamics”. In *Midlatitude ionospheric dynamics and disturbances*, Kintner P. M. et al. (eds.), American Geophysical Union, Washington D.C., pp. 187–200, 2008.

Fuller-Rowell T.M., Millward G.H., Richmond A.D. and Codrescu M.V. "Storm-time changes in the upper atmosphere at low latitudes". Journal of Atmospheric and Solar-Terrestrial Physics, vol. 64, pp. 1383–1391, 2002.

Gaunt C.T. and Coetzee G. "Transformer failure in regions incorrectly considered to have low GIC-risks". In *Power Tech, 2007 IEEE, Lausanne, July 2007*, pp. 807–812, 2007.

Goodman J.M. "Operational communication systems and relationships to the ionosphere and space weather". Advances in Space Research, vol. 36(12), pp. 2241–2252, 2005.

Gopalswamy N., Yashiro S., Michalek G., Xie H., Lepping R.P. and Howard R.A. "Solar source of the largest geomagnetic storm of cycle 23". Geophysical Research Letters, vol. 32, L12S09, 2005.

Habarulema J.B., McKinnell L.A., Cilliers P.J. and Opperman B.D.L. "Application of neural networks to South African GPS TEC modelling". Advances in Space Research, vol. 43, pp. 1711–1720, 2009.

Habarulema J.B., McKinnell L.A. and Opperman B.D.L. "TEC measurements and modelling over Southern Africa during magnetic storms; a comparative analysis". Journal of Atmospheric and Solar-Terrestrial Physics, vol. 72, pp. 509–520, 2010.

Hardy D., Gussenhoven M. and Holeman E. "A statistical model of auroral electron precipitation". Journal of Geophysical Research, vol. 90(A5), pp. 4229–4248, 1985.

Heelis R.A., Sojka J.J., David M. and Schunk R.W. "Storm time density enhancements in the middle-latitude dayside ionosphere". Journal of Geophysical Research, vol. 144, A033315, 2009. doi:10.1029/2008JA013690.

Hines C.O. "Internal atmospheric gravity waves at ionospheric heights". Canadian Journal of Physics, vol. 38, pp. 1441–1481, 1960.

Ho C.M., Mannucci A.J., Sparks L., Pi X. and Lindqwister U.J. "Ionospheric total electron content perturbations monitored by the GPS global network during two northern hemisphere winter storms". Journal of Geophysical Research, vol. 103(A11), pp. 26,409–26,420, 1998.

Hocke K. and Schlegel K. "A review of atmospheric gravity waves and traveling ionospheric disturbances". Annales Geophysicae, vol. 14, pp. 917–940, 1996.

Hofmann-Wellenhof B., Lichtenegger H. and Collins J. *Global Positioning System: Theory and practice*. Springer-Verlag, Vienna, 1992.

Huang C.S. and Foster J.C. "Long-duration penetration of the interplanetary electric field to the low-latitude ionosphere during the main phase of magnetic storms". Journal of Geophysical Research, vol. 110, A11309, 2005. doi: 10.1029/2005JA011202.

Huang C.S., Foster J.C., Goncharenko L.P., Erickson P.J., Rideout W. and Coster A.J. "A strong positive phase of ionospheric storms observed by the Millstone Hill incoherent scatter radar and global GPS network". Journal of Geophysical Research, vol. 110, A06303, 2005. doi:10.1029/2004JA010865.

Hunsucker R.D. "Atmospheric gravity waves generated in the highlatitude ionosphere: A review". Reviews of Geophysics, vol. 20, pp. 293–315, 1982.

Hunsucker R.D. *Radio techniques for probing the terrestrial ionosphere*. Springer-Verlag, New York, 1990.

Imel D.A. "Evaluation of TOPEX/Poseidon dual frequency ionospheric correction". Journal of Geophysical Research, vol. 99(24), pp. 24,895–24,906, 1994.

Jakowski N., Schlüter S. and Sardón E. "Total electron content of the ionosphere during the geomagnetic storm on 10 January 1997". Journal of Atmospheric and Solar-Terrestrial Physics, vol. 61, pp. 299–307, 1999.

Jones K.L. and Rishbeth H. "The origin of storm increases of mid-latitude F-layer electron concentration". Journal of Atmospheric and Terrestrial Physics, vol. 33, pp. 391–401, 1971.

Kelley M.C. *The Earth's ionosphere*. Academic Press, San Diego, 1989.

Kelley M.C. *The Earth's ionosphere: Plasma physics and electrodynamics*. Academic Press, Amsterdam, 2nd edn., 2009.

Kelley M.C., Makela J.J., Chau J.L. and Nicolls M.J. “Penetration of the solar wind electric field into the magnetosphere/ionosphere system”. Geophysical Research Letters, vol. 30(4), pp. 1158–1160, 2003.

Kelley M.C., Vickrey J.F., Carlson C.W. and Torbert R. “On the origin and spatial extent of high-latitude F region irregularities”. Journal of Geophysical Research, vol. 87(A6), pp. 4469–4475, 1982.

Kelley M.J., Garcia F., Makela J., Fan T., Mak E., Sia C. and Alcocer D. “Highly structured tropical airglow and TEC signatures during strong geomagnetic activity”. Geophysical Research Letters, vol. 27(4), pp. 465–468, 2000.

Kersley L., Pryse S.E. and Wheadon N.S. “Amplitude and phase scintillation at high latitudes over northern Europe”. Radio Science, vol. 23(3), pp. 320–330, 1988.

Kersley L., Russell C.D. and Rice D.L. “Phase scintillation and irregularities in the northern polar ionosphere”. Radio Science, vol. 30(3), pp. 619–629, 1995.

Keskinen M.J. and Ossakow S.L. “Theories of high-latitude ionospheric irregularities: A review”. Radio Science, vol. 18(6), pp. 1077–1091, 1983.

Kintner P.M., Kil H., Beach T.L. and De Paula E.R. “Fading timescales associated with GPS signals and potential consequences”. Radio Science, vol. 36, pp. 731–743, 2001.

Kintner P.M., Kil H., Deehr C. and Schuck P. “Simultaneous total electron content and all-sky camera measurements of an auroral arc”. Journal of Geophysical Research, vol. 107(A7), pp. 1127–1132, 2002.

Kintner P.M. and Ledvina B.M. “The ionosphere, radio navigation, and global navigation satellite systems”. Advances in Space Research, vol. 35, pp. 788–811, 2005.

Kintner P.M., Ledvina B.M. and De Paula E.R. “GPS and ionospheric scintillations”. Space Weather, vol. 5, S09003, 2007. doi:10.1029/2006SW000260.

Kivelson M.G. and Russell C.T. *Introduction to space physics.* Cambridge University Press, Cambridge, 1995.

Klobuchar J.A. "Ionospheric effects on GPS". In *Global positioning system: Theory and application, vol. I*, Parkinson B. et al. (eds), American Institute of Aeronautic and Astronautic, pp. 485–515, 1996.

Lanzerotti L.J. "Space weather effects on technologies". In *Space Weather*, Song D. et al. (eds.), American Geophysical Union, Washington D.C., pp. 11–22, 2001.

Ledvina B.M. and Kintner P.M. "Temporal properties of intense GPS L1 amplitude scintillations at midlatitudes". Radio Science, vol. 39, RS1S18, 2004. doi:10.1029/2002RS002832.

Ledvina B.M., Makela J.J. and Kintner P.M. "First observations of intense GPS L1 amplitude scintillations at midlatitudes". Geophysical Research Letters, vol. 29(14), pp. 1659–1662, 2002.

Lin C.H., Richmond A.D., Heelis R.A., Bailey G.J., Lu G., Liu J.Y., Yeh H.C. and Su S.Y. "Theoretical study of the low- and midlatitude ionospheric electron density enhancement during the October 2003 superstorm: Relative importance of the neutral wind and electric field". Journal of Geophysical Research, vol. 110, A12312, 2005. doi:10.1029/2005JA011304.

Lockwood M. and Carlson Jr. H.C. "Production of polar cap electron density patches by transient magnetopause reconnection". Geophysical Research Letters, vol. 19, pp. 1731–1734, 1992.

Lopez R.E., Wiltberger M., Hernandez S. and Lyon J.G. "Solar wind density control of energy transfer to the magnetosphere". Geophysical Research Letters, vol. 31, L08804, 2004. doi:10.1029/2003GL018780.

Lynn K.J.W., Gardiner-Garden R., Sjarifudin M., Terkildsen M., Shi J. and Harris T.J. "Large-scale travelling atmospheric disturbances in the night ionosphere during the solar-terrestrial event of 23 May 2002". Journal of Atmospheric and Solar-Terrestrial Physics, vol. 70, pp. 2184–2195, 2008.

Malik R., Sarkar S., Mukherjee S. and Gwal A.K. "Study of ionospheric variability during geomagnetic storms". Journal of the Indian Geophysical Union, vol. 14(1), pp. 47–56, 2010.

Mannucci A.J., Tsurutani B.T., Iijima B.A., Komjathy A., Saito A., Gonzalez W.D., Guarnieri F.L., Kozyra J.U. and Skoug R. "Dayside global ionospheric response to the major interplanetary events of October 29-30, 2003 "Halloween Storms"". Geophysical Research Letters, vol. 32, L12S02, 2005. doi:10.1029/2004GL021467.

Maruyama N., Sazykin S., Spiro R.W., Anderson D., Anghel A., Wolf R.A., Toffoletto F.R., Fuller-Rowell T.J., Codrescu M.V., Richmond A.D. and Millward G.H. "Modeling storm-time electrodynamics of the low-latitude ionosphere-thermosphere system: Can long lasting disturbance electric fields be accounted for?" Journal of Atmospheric and Solar-Terrestrial Physics, vol. 69, pp. 1182–1199, 2007.

Maruyama T. "The formation of the inosphere". 2001.

Maruyama T. and Nakamura M. "Conditions for intense ionospheric storms expanding to lower midlatitudes". Journal of Geophysical Research, vol. 112, A05310, 2007. doi:10.1029/2006JA012226.

Matsushita S. and Campbell W.H. *Physics of geomagnetic phenomena*. Academic Press, New York, 1967.

Mazaudier C. and Venkateswaran S.V. "Delayed ionospheric effects of the geomagnetic storms of March 22, 1979 studied by the six co-ordinated data analysis workshop (CDAW-6)". Annales Geophysicae, vol. 8(7-8), pp. 511–518, 1990.

McKinnell L.A. "The progress of the South African Ionosonde network". American Institute of Physics Conference Proceedings, vol. 974(1), Lowell, MA, ISBN 978-0-7354-0493-9, pp. 47–52. 2008.

McKinnell L.A., Opperman B. and Cilliers P.J. "GPS TEC and ionosonde TEC over Grahamstown, South Africa: First comparisons". Advances in Space Research, vol. 39, pp. 816–820, 2007.

McPherron R.L. "Magnetospheric substorms". Reviews of Geophysics and Space Physics, vol. 17, p. 657, 1979.

Meggs R.W., Mitchell C.N. and Smith A.M. "An investigation into the relationship between ionospheric scintillation and loss of lock in GNSS receivers". In

Characterising the ionosphere. Meeting Proceeding RTO-MP-IST-056, Paper 5, Neuilly-sur-Seine, France, pp. 5–1−−5–10, 2006.

Meier R.R., Crowley G., Strickland D.J., Christensen A.B., Paxton L.J., Morrison D. and Hackert C.L. "First look at the 20 November 2003 superstorm with TIMED/GUVI: Comparisons with a thermospheric global circulation model". Journal of Geophysical Research, vol. 110, A09S41, 2005. doi: 10.1029/2004JA010990.

Mendillo M. "Storms in the ionosphere: Patterns and processes for total electron content". Reviews of Geophysics, vol. 44, RG4001, 2005RG000193, 2006.

Mikhailov A.V., Skoblin M.G. and Förster M. "Daytime F2-layer positive storm effect at middle and lower latitudes". Annales Geophysicae, vol. 13, pp. 532–540, 1995.

Misra P. and Enge P. *Global Positioning System: Signals measurements, and performance*. Ganga-Jamuna Press, Lincoln, Massachusetts, 2nd edn., 2007.

Mitchell C.N., Alfonsi L., Franceshi G.D., Lester M., Romano V. and Wernik A.W. "GPS TEC and scintillation measurements from the polar ionospheric during the October 2003 storm". Geophysical Research Letters, vol. 32(12), L12S03, 2005. doi:10.1029/2004GR021644.

Moeketsi D.M., Combrinck W.L., McKinnell L. and Fedrizzi M. "Mapping GPS-derived total electron content over Southern Africa during different epochs of solar cycle 23". Advances in Space Research, vol. 39, pp. 821–829, 2007.

Moldwin M. *An introduction to space weather*. Cambridge University Press, New York, 2008.

Ngwira C.M., McKinnell L.A. and Cilliers P.J. "GPS phase scintillation observed over a high-latitude Antarctic station during solar minimum". Journal of Atmospheric and Solar-Terrestrial Physics, vol. 72(9-10), pp. 718–725, 2010.

Ngwira C.M., McKinnell L.A., Cilliers P.J. and Coster A.J. "Ionospheric observations during the geomagnetic storm events on 24-27 July 2004: Long-duration positive storm effects". Journal of Geophysical Research, in press, 2011a. doi: 10.1029/2011JA016990.

Ngwira C.M., McKinnell L.A., Cilliers P.J. and Yizengaw E. "An investigation of ionospheric disturbances over South Africa during the magnetic storm on 15 May 2005". Advances in Space Research, in press, 2011b. doi: 10.1016/j.asr.2011.09.035.

Nicolls M., Kelley M.C., Coster A.J., González S.A. and Makela J.J. "Imaging the structure of a large-scale TID using ISR and TEC data". Geophysical Research Letters, vol. 31, L09812, 2004. doi:10.1029/2004GL019797.

Nishioka M., Saito A. and Tsugawa T. "Occurrence characteristics of plasma bubble derived from global ground-based GPS receiver networks". Journal of Geophysical Research, vol. 113, A05301, 2008. doi:10.1029/2007JA012605.

Opperman B.D.L., Cilliers P.J., McKinnell L.A. and Haggard R. "Development of a regional GPS-based ionospheric TEC model for South Africa". Advances in Space Research, vol. 39, pp. 808–815, 2007.

Pedatella N.M., Lei J., Larson K.M. and Forbes J.M. "Observations of the ionospheric response to the 15 December 2006 geomagnetic storm: Long-duration positive storm effect". Geophysical Research Letters, vol. 114, A12313, 2009. doi:10.1029/2009JA014568.

Pi X., Mannucci A.J., Lindqwister U.J. and Ho C.M. "Monitoring of global ionospheric irregularities using the wordwide GPS network". Geophysical Research Letters, vol. 24(18), pp. 2283–2286, 1997.

Pi X., Mendillo M. and Fox M.W. "Diurnal Double Maxima patterns in the F region ionosphere: Substorm-related aspects". Journal of Geophysical Research, vol. 98(A8), pp. 13,677–13,691, 1993.

Pirjola R. "Effects of space weather on high-latitude ground systems". Advances in Space Research, vol. 36, pp. 2231–2240, 2005.

Prikryl P., Jayachanrandran P.T., Mushini S.C. and Chadwick R. "Climatology of GPS phase scintillation and HF radar backscatter for the high-latitude ionosphere under solar minimum conditions". Annales Geophysicae, vol. 29, pp. 377–392, 2011.

Prikryl P., Jayachanrandran P.T., Mushini S.C., Pokhotelov D., MacDougall J., Donovan E., Spanswick E. and St.-Maurice J. "GPS TEC, scintillation and cycle slips observed at high latitudes during solar minimum". Annales Geophysicae, vol. 28, pp. 1307–1316, 2010.

Prölss G.W. "Common origin of positive ionospheric storms at middle latitudes and the geomagnetic activity effect at low latitudes". Journal of Geophysical Research, vol. 98(A4), pp. 5981–5991, 1993a.

Prölss G.W. "On explaining the local time variation of ionospheric storm effects". Annales Geophysicae, vol. 11, pp. 1–9, 1993b.

Prölss G.W. "Ionospheric F region storms". In *Handbook of atmospheric electrodynamics*, Volland H. (ed.), CRC Press, Boca Raton, Fla, p. 195, 1995.

Prölss G.W. "Magnetic storm associated perturbations of the upper atmosphere". In *Magnetic storms*, Tsurutani B. T. et al. (eds.), American Geophysical Union, Washington D.C., pp. 227–241, 1997.

Prölss G.W., Brace L.H., Mayr H.G., Carignan G.R., Killeen W.L. and Klobuchar J.A. "Ionospheric storm effects at subauroral latitudes: A case study". Journal of Geophysical Research, vol. 96(A2), pp. 1275–1288, 1991.

Prölss G.W. and Jung M.J. "Travelling atmospheric disturbances as a possible explanation of the daytime positive storm effects of moderate duration at middle latitudes". Journal of Atmospheric and Terrestrial Physics, vol. 40, pp. 1351–1354, 1978.

Richardson I.G., Cliver E.W. and Cane H.V. "Sources of geomagnetic storms over the solar cycle: Relative importance of coronal mass ejections, high-speed streams, and slow solar wind". Journal of Geophysical Research, vol. 105, pp. 18,203, 2000.

Richardson I.G., Cliver E.W. and Cane H.V. "Sources of geomagnetic storms for solar minimum and maximum conditions during 1972-2000". Geophysical Research Letters, vol. 28(13), pp. 2569–2572, 2001.

Richmond A.D., Peymirat C. and Roble R.G. "Long-lasting disturbances in the equatorial ionospheric electric field simulated with a coupled magnetosphere-ionosphere-thermosphere model". Journal of Geophysical Research, vol. 108(A3), pp. 1118–1129, 2003.

Rideout W. and Coster A. "Automated GPS processing for global total electron content data". GPS Solutions, vol. 10(3), pp. 219–228, 2006.

Rino C.L. "A power law phase screen model for ionospheric scintillation. 1. Weak scatter". Radio Science, vol. 14(6), pp. 1135–1145, 1979a.

Rino C.L. "A power law phase screen model for ionospheric scintillation. 2. Strong scatter". Radio Science, vol. 14(6), pp. 1147–1155, 1979b.

Rino C.L. and Matthews S.J. "On the morphology of auroral zone radio wave scintillation". Journal of Geophysical Research, vol. 85(A8), pp. 4139–4151, 1980.

Rishbeth H. "Ionospheric dynamics 1945-1970". Journal of Atmospheric and Terrestrial Physics, vol. 34, pp. 2309–2319, 1974.

Rishbeth H. "On the F2-layer continuity equation". Journal of Atmospheric and Terrestrial Physics, vol. 48(6), pp. 511–519, 1986.

Rishbeth H. "F-region storms and thermospheric dynamics". Journal of Geomagnetism and Geoelectricity, vol. 43, Suppl., pp. 513–524, 1991.

Rishbeth H. "How the thermospheric circulation affects the ionospheric F1-layer". Journal of Atmospheric and Terrestrial Physics, vol. 60, pp. 1385–1402, 1998.

Rishbeth H. and Barron D.W. "Equilibrium electron distributions in the ionospheric F2-layer". Journal of Atmospheric and Terrestrial Physics, vol. 18, pp. 234–252, 1960.

Rishbeth H. and Garriott O.K. *Introduction to ionosphere.* Academic Press, New York, 1969.

Rodger A.S. and Jarvis M.J. "Ionospheric research 50 year ago, today and tomorrow". Journal of Atmospheric and Solar-Terrestrial Physics, vol. 62, pp. 1629–1645, 2000.

Rosenqvist L., Opgenoorth H., Buchert S., McCrea I., Amm O. and Lathuillere C. "Extreme solar-terrestrial events of October 2003: High-latitude and cluster observations of the large geomagnetic disturbances on 30 October". Journal of Geophysical Research, vol. 110, A09S23, 2005. doi:10.1029/2004JA01927.

Schaer S. *Mapping and predicting the Earth's ionosphere using the Global Positioning System*. Ph.D. thesis, Astronomical Institute, University of Berne, 1999.

Scherliess L. and Fejer B.G. "Storm time dependence of equatorial disturbance dynamo zonal electric fields". Journal of Geophysical Research, vol. 102(A12), pp. 24,037–24,046, 1997.

Skone S. and Cannon M.E. "Ionospheric effects on differential GPS applications during auroral substorm activity". ISPRS Journal of Photogrammetry and Remote Sensing, vol. 54(4), pp. 279–288, 1999.

Skone S., Coster A.J., Hoyle V. and Laurin C. "WAAS availability and performance at high latitudes". In *Proceedings of the ION GPS/GNSS-2003, Portland, 9-12 September 2003*, pp. 1279–1287, 2003.

Skone S. and De Jong M. "The impact of geomagnetic substorms on GPS receiver performance". Earth Planets Space, vol. 52, pp. 1067–1071, 2000.

Smith A.M., Mitchell C.N., Watson R.J., Meggs R.W., Kintner P.M., Kauristie K. and Honary F. "GPS scintillation in the high Arctic associated with an auroral arc". Space Weather, vol. 6, S03D01, 2008. doi:10.1029/2007SW000349.

Srivastava N. and Venkatakrishnan P. "Solar and interplanetary sources of major geomagnetic storms during 1996-2002". Journal of Geophysical Research, vol. 109(A10103), 2004. doi:10.1029/2003JA010175.

Stauning P. "High-latitude D- and E-region investigations using imaging riometer observations". Journal of Atmospheric and Solar-Terrestrial Physics, vol. 58(6), pp. 765–783, 1996.

Stone E.C., Frandsen A.M., Mewaldt R.A., Christian E.R., Margolies D., Ormes J.F. and Snow F. "The Advanced Composition Explorer". Space Science Reviews, vol. 86(1-4), 1998.

Su Y.J., Thomsen M.F., Borovsky J.E. and Foster J.C. "A linkage between polar patches and plasmaspheric drainage plumes". Geophysical Research Letters, vol. 28(1), pp. 111–113, 2001.

Trimble. *GPS the first Global Navigation Satellite System.* Trimble Navigation, Sunnyvale, CA, 2007.

Tsugawa T., Otsuka Y., Coster A.J. and Saito A. "Medium-scale traveling ionospheric disturbances detected with dense and wide TEC maps over North America". Geophysical Research Letters, vol. 34, L22101, 2007. doi: 10.1029/2007GL031663.

Tsugawa T., Shiokawa K., Otsuka Y., Ogawa T., Saito A. and Nishioka M. "Geomagnetic conjugate observations of large-scale traveling ionospheric disturbances using GPS networks in Japan and Australia". Journal of Geophysical Research, vol. 111, A02302, 2006. doi:10.1029/2005JA011300.

Tsunoda R.T. "High-latitude F region irregularities: A review and synthesis". Reviews of Geophysics, vol. 26, p. 719, 1988.

Tsurusani T.B. and Gonzalez W.D. "The efficiency of "viscous interaction" between the solar wind and the magnetosphere during intense northward IMI events". Geophysical Research Letters, vol. 22, p. 663, 1995.

Tsurutani B., Mannucci A., Iijima B., Abdu M.A., Humberto J., Sobral A., Gonzalez W., Guarnieri F., Tsuda T., Saito A., Yumoto K., Fejer B., Fuller-Rowell T.J., Kozyra J., Foster J.C., Coster A., and Vasyliunas V.M. "Global dayside ionospheric uplift and enhancement associated with interplanetary electric fields". Journal of Geophysical Research, vol. 109, A08302, 2004. doi: 10.1029/2003JA010342.

Van Dierendonck A.J., Hua Q., Fenton P. and Klobuchar J. "Commercial Ionospheric Scintillation Monitoring Receiver Development and Test Results". In *Proceedings of the 52nd Annual Meeting of the ION GPS, Cambridge, MA, June 1996*, pp. 1333–1342, 1996.

Vlasov M., Kelley M.C. and Kil H. "Analysis of ground-based and satellite observations of F-region behavior during the great magnetic storm of July 15, 2000".

Journal of Atmospheric and Solar-Terrestrial Physics, vol. 65, pp. 1223–1234, 2003.

Walker A.D.M. *Magnetohydrodynamic waves in geospace.* IOP Publishing, Bristol, 2005.

Warnant R., Lejeune S. and Bavier M. "Space weather influence on satellite-based navigation and precise positioning". In *Space Weather*, Lilensten J. (ed.), Springer, Dordrecht, pp. 129–146, 2007.

Werner S., Bauske R. and Prölss G.W. "On the origins of positive ionospheric storms". Advances in Space Research, vol. 24(11), pp. 1485–1489, 1999.

Wernik A.W., Alfonsi L. and Materassi M. "Ionospheric irregularities, scintillation and its effects on systems". ACTA Geophysica Polonica, vol. 52(2), pp. 237–249, 2004.

Wernik A.W., Secan J.A. and Fremouw E.J. "Ionospheric irregularities and scintillation". Advances in Space Research, vol. 31(4), pp. 971–981, 2003.

White R.S. *Space physics.* Gordon and Breach, New York, 1970.

Wilson A. *Imaging riometer observations on energetic electron precipitation at SANAE IV, Antarctica.* Ph.D. thesis, Potchefstroom University, 2000.

Wolf R.A., Spiro R.W., Sazykin S. and Toffoletto F.R. "How the Earth's inner magnetosphere works: An evolving picture". Journal of Atmospheric and Solar-Terrestrial Physics, vol. 69, pp. 288–302, 2007.

Yeh K.C. and Liu C.H. "Radio wave scintillations in the ionosphere". In *Proceedings of the IEEE vol. 70(4)*, pp. 324–360, 1982.

Yizengaw E., Dewar J., MacNeil J., Moldwin M.B., Galvan D., Sanny J., Berube D. and Sandel B. "The occurrence of Ionospheric Signatures of Plasmaspheric Plumes over different longitudinal sectors". Journal of Geophysical Research, vol. 113, A08318, 2008. doi:10.1029/2007JA012925.

Yizengaw E., Dyson P.L., Essex E.A. and Moldwin M.B. "Ionosphere dynamics over the southern hemisphere during the 31 March 2001 severe magnetic storm using multi-instrument measurement data". Annales Geophysicae, (23), pp. 707–721, 2005a.

Yizengaw E., Moldwin M.B., and Galvan D.A. "Ionospheric signatures of a plasmaspheric plume over Europe". Geophysical Research Letters, vol. 33, L17103, 2006a. doi:10.1029/2006GL026597.

Yizengaw E., Moldwin M.B., Dyson P.L. and Immel T.J. "Southern hemisphere ionosphere and plasmasphere response to the interplanetary shock event of 29-31 October 2003". Journal of Geophysical Research, vol. 110, A09S30, 2005b. doi:10.1029/2004JA010920.

Yizengaw E., Moldwin M.B., Komjathy A. and Mannucci A.J. "Unusual topside ionospheric density response to the November 2003 superstorm". Journal of Geophysical Research, vol. 111, A02308, 2006b. doi:10.1029/2005JA01143365.

Yizengaw E., Moldwin M.B., Mebrahtu A., Damtie B., Zesta E., Valladares C.E. and Doherty P. "Comparison of storm time equatorial ionospheric electrodynamics in the African and American sectors". Journal of Atmospheric and Solar-Terrestrial Physics, vol. 73, pp. 156–163, 2011.